LOCAL VOID FRACTION MEASUREMENTS

IN LARGE VERTICAL PIPES

AN EXPERIMENTAL STUDY ON THE LOCAL VOID FRACTION MEASUREMENTS IN LARGE-DIAMETER VERTICAL PIPES USING OPTICAL FIBER PROBES

by

BRANKO STANKOVIC, B.Sc.

A Thesis

Submitted to the School of Graduate Studies

in Partial Fulfilment of the Requirements

for the Degree

Master of Engineering

McMaster University

MASTER OF ENGINEERING (1997) McMASTER UNIVERSITY

(Mechanical Engineering) Hamilton, Ontario

TITLE: An Experimental Study on the Local Void Fraction Measurements in Large-Diameter Vertical Pipes using Optical Fiber Probes

AUTHOR: Branko Stankovic, B.Sc. (University of Belgrade)

SUPERVISOR: Professor M. Shoukri

NUMBER OF PAGES: xviii, 145

ABSTRACT

This thesis contains the details of an experimental study on the local void fraction measurements in large-diameter vertical pipes using optical fiber probes. The experiments were conducted in vertical transparent acrylic pipe of a 20-cm diameter. An experimental test facility used for performing of experiments, was designed as a low-pressure air-water loop, which can operate in either a natural circulation mode or a forced circulation mode. Radial void fraction profiles were measured using an optical fiber probe. An average cross-sectional void fraction was calculated by integration of the data obtained by the optical fiber probe. The average void fraction was also calculated using two-phase pressure-drop measurements . The results were compared and the resulting good accuracy of the optical fiber probe was determined. The flow regime results were plotted in terms of superficial gas and liquid velocities using flow regime maps of several researchers. Absence of the slug flow regime in large-diameter pipes was observed during the experiments. The data were correlated using the drift-flux model. A near unity distribution parameter showed that nearly uniform radial distribution of the void fraction dominates in two-phase flow through large-diameter vertical pipes.

ACKNOWLEDGEMENTS

The author wishes to express his sincere gratitude to Professor M. Shoukri, his research supervisor, for his guidance, valuable suggestions and constant encouragement during the preparation of this thesis.

The author is also very grateful to Dr. A. Abdul-Razzak for very successful design of the experimental loop and his suggestions and advices at the beginning of the research. Thanks are also due to S.M. Nada, who was a visiting scholar and a research assistant, for his help in performing of the experiments and collecting of the experimental data.

The author gratefully acknowledges his gratitude to technicians R. Lodewyks, D. Schick, J. McLaren and J. Verhaeghe for their valuable professional advices, technical guidance and generous help in construction of the experimental loop.

The author thanks Atomic Energy of Canada Limited for supplying of the optical fiber probe. The financial support provided by Atomic Energy of Canada Limited and the Mechanical Engineering Department is gratefully acknowledged.

Most of all, the author expresses his deep appreciation to his parents Nikola and Dobrila, without whose love, understanding and encouragement he could not finish this work.

TABLE OF CONTENTS

LIST OF FIGURES

NOMENCLATURE

SYMBOL	DESCRIPTION	UNITS
A	cross-sectional area of a pipe	m^2
A_L	cross-sectional pipe area occupied by liquid	m^2
A_G	cross-sectional pipe area occupied by gas	m^2
c_p	specific heat at constant pressure	J/kg*K
c_v	specific heat at constant volume	J/kg*K
C_0	distribution parameter	
C_L	liquid-phase distribution parameter	
C_G	gas-phase distribution parameter	
d_{crit}	critical bubble diameter	m
D	diameter of the pipe	m
f	friction factor	
g	gravitational acceleration	m/s^2
G	mass flux	kg/m^2*s
H or h	height	m
H_{gas}	height of the riser pipe occupied by gas	m

SYMBOL	DESCRIPTION	UNITS
H_{pt}	test-section pressure transducer liquid height	m
H_{ts}	test-section height	m
I	integer	
i_1 or i_0	angle of beam incidence at fiber tip	°
i_2	angle of beam refraction from fiber tip into a medium	°
j	integer	
J	superficial velocity (volumetric flux)	m/s
J_L or j_L	superficial velocity of liquid	m/s
J_G or j_G	superficial velocity of gas	m/s
k	ratio of specific heats	
K	flow coefficient	
l_E	entry length of a pipe to establish stable slug flow	m
L	length of a pipe	m
m	mass flow rate	kg/s
n_1 or n_g	index of refraction of fiber glass	
n_2	index of refraction of a surrounding medium	
n_W	index of refraction of water	
n_a	index of refraction of air	

SYMBOL	DESCRIPTION	UNITS
N	number of equal periods of sampling time	
p	pressure	N/m^2
p_a	atmospheric pressure	N/m^2
Q	volumetric flow rate	m^3/s
r	pressure ratio, or pipe radius	- , m
R	gas constant	J/kg*K
	or pipe radius	m
Re	Reynolds number	
T	sampling time	s
T_G	probe residence time in void	s
U	velocity	m/s
$<U_L>$	average cross-sectional liquid velocity	m/s
$<U_G>$	average cross-sectional gas velocity	m/s
U_0	rise velocity of large bubbles	m/s
U_{Gj}	average local drift velocity	m/s
V	volume	m^3
V_L	volume occupied by liquid	m^3
V_G	volume occupied by gas	m^3

SYMBOL	DESCRIPTION	UNITS
x	flow quality, or length	-, m
Y	compressibility (expansion) factor	

GREEK SYMBOL	DESCRIPTION	UNITS
α	local void fraction	
α_T	local void fraction within sampling time T	
$<\alpha>$	average void fraction	
β	diameter ratio	
Δp_{FR}	frictional pressure drop	N/m^2
Δp_G	gas-phase frictional pressure drop	N/m^2
Δp_L	liquid-phase frictional pressure drop	N/m^2
Δp_{op}	pressure drop at orifice plate	N/m^2
Δp_{pt}	pressure drop in the test section	N/m^2
θ	inclination angle from horizontal line	°
μ	dynamic viscosity	$N*s/m^2$
ν	kinematic viscosity	m^2/s

GREEK SYMBOL	DESCRIPTION	UNITS
ρ	density	kg/m^3
$\rho_{2\phi}$	density of a two-phase mixture	kg/m^3
σ	surface tension	N/m
ΣH_{eq}	equivalent riser length	m
ϕ_1	correction function for superficial gas velocity	
ϕ_2	correction function for superficial liquid velocity	
Φ^2	Two-phase friction multiplier	
Φ_L^2	Two-phase friction multiplier for liquid-phase pressure drop	
Φ_G^2	Two-phase friction multiplier for gas-phase pressure drop	
X^2	Lockhart-Martinelli parameter	

SUBSCRIPT	DESCRIPTION
air,inl	air inlet line
eq	equivalent
FR	frictional
G or *g*	gas phase

SUBSCRIPT	DESCRIPTION
$_L$ or $_l$	liquid phase
op	orifice plate
PH	phase
pt	pressure transducer
s	standard
ts	test section
2ϕ	two-phase

CHAPTER ONE

INTRODUCTION

There is a continuous need to enhance current knowledge of the mechanics of two--phase flow in large vertical pipes as related to many industrial applications: boiler and nuclear reactor industry, refrigeration industry and chemical industry, to mention some of them. A typical example is the design and analysis of emergency core cooling systems (ECCS) in light- and heavy-water-cooled nuclear reactors, as a way of improving the safety and reliability of them. Atomic Energy of Canada Ltd. (AECL) at Chalk River Nuclear Laboratories (CRNL) has been investigating the design of a **passive moderator cooling system** (PMCS) as a part of an integrated emergency heat-rejection concept being developed for CANDU reactors (Canadian heavy-water cooled and moderated reactors, using natural uranium as a fissile fuel). While CANDU moderator heat-rejection systems normally use pumps (forced circulation) to circulate the heavy water to heat exchangers cooled by pumped service water, the PMCS design is based on passive heat rejection using a **flashing-driven natural circulation** at low pressure. The flow in this case is buoyancy driven due to vapor generation caused by decreasing moderator hot-leg pressure.

The flashing-driven PMCS concept is depicted in Figure 1.1 on page 3. A flashing--driven natural-circulation loop works best if the calandria vessel runs at a temperature near the boiling point. For this reason, in the PMCS design, the moderator is maintained close to saturation temperature at the calandria pressure. Heat is transported from the calandria to an elevated passive heat exchanger (external heat sink) in a natural-circulation loop, where two-phase flow occurs in the vertical hot-leg pipe due to flashing. Since the moderator temperature is very close to saturation temperature, flashing occurs close to the calandria exit, which provides a large driving force, because of the large density difference between the cold-leg subcooled liquid (returning to the bottom of the calandria) and the hot-leg two-phase mixture. This design feature makes it possible to remove moderator heat under both normal and accident conditions using buoyancy-driven flow and, therefore, the moderator system can serve as the ultimate heat sink (ECCS) in CANDU reactors. Having the moderator temperature close to saturation also provides a very attractive option of utilizing (recovering) the moderator heat for feedwater heating (instead of the heat rejection to ambient), which improves plant thermal efficiency. Finally, an obvious advantage of a natural-circulation system over a forced-circulation one is that the pumps can be eliminated with cost savings and improvements in reliability.

According to current PMCS designs, flashing and, accordingly, two-phase flow will

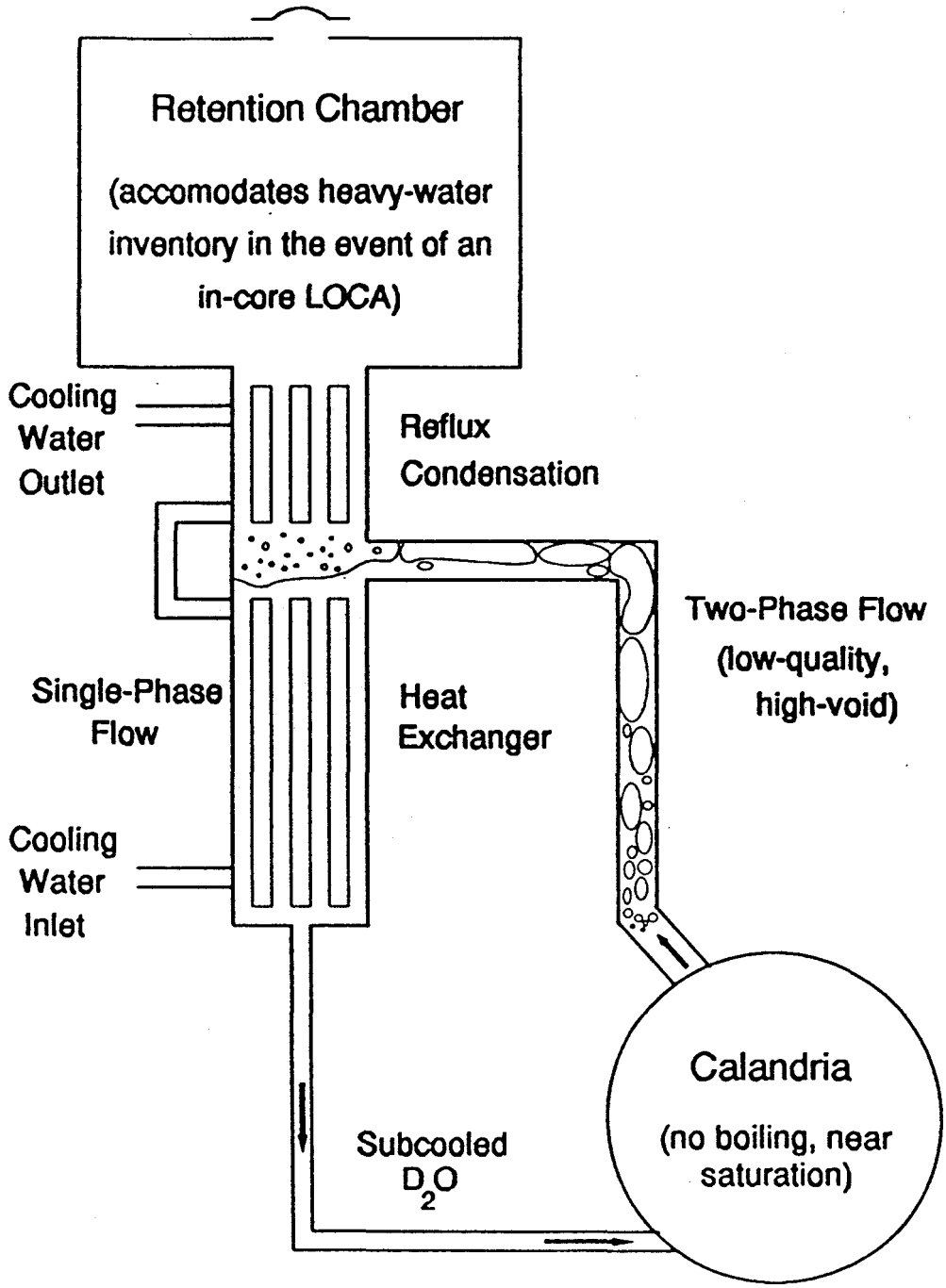

Figure 1.1: Flashing-Driven Passive Moderator Cooling System Concept

occur in one or more large-diameter vertical pipes (hot legs), with a diameter of up to 45 cm. There is a lack of knowledge of flow regimes and the associated void fraction and slip ratio relations in low-pressure low-quality two-phase flow in large--diameter vertical pipes. Most available data and correlations were developed based on experimental data obtained in pipes of a diameter smaller than 10 cm. Since, in the designing of the advanced CANDU passive moderator cooling system, AECL-CRNL uses thermal-hydraulic code CATHENA to simulate the system, it needs the information about two-phase flow structure in large-diameter pipes to incorporate them in the computer code. Furthermore, although AECL-CRNL uses a flashing-driven natural-circulation water loop to simulate the basic features of the PMCS and thus support its design, the pipe diameters are scaled down, with a maximum riser (hot-leg) diameter of 10 cm.

The main objective of this experimental research work was to bridge the gap in knowledge of two-phase flow regimes in large-diameter vertical pipes and to provide information that could help the designers of the PMCS. This objective was achieved through the following phases:

(a) Design, construction and commission of a test facility for investigating two--phase flow regimes and flow structure in large-diameter vertical pipes;

(b) Obtaining detailed experimental data on two-phase flow with progressively increasing pipe sizes. The work was initially carried out in a 10-cm diameter vertical pipe to provide the basis for comparisons with the test loop at AECL. This was followed by extensive experiments in a 20-cm diameter vertical pipe to investigate the effect of the pipe diameter;

(c) Developing of flow regime maps for low-pressure two-phase flow in large--diameter vertical pipes and developing of appropriate void-fraction correlations in large pipes using the results;

(d) Generating detailed data on the local void fraction in vertical two-phase flow in large pipes.

It is also important to emphasize that phases (b) and (d) were fulfilled using an **optical fiber probe** for measuring of the void fraction. In addition, the objectives of the phase (c) were achieved using the results of the probe measurements. In this context, the reason for devoting significant part of this thesis to evaluation of the accuracy of optical fiber probes becomes understandable.

CHAPTER TWO

LITERATURE REVIEW

2.1. TWO-PHASE FLOW PATTERNS IN VERTICAL PIPES

The two-phase flow patterns influence most of the typical two-phase quantities, such as: pressure drop, void fraction and heat transfer coefficient. Also, a good knowledge of flow regimes is required to quantify the interfacial transport of mass, momentum and energy. Such interfacial transport is key to the application of various two-phase flow models used in nuclear power plant safety analysis.

In the case of upward co-current two-phase flow in a vertical tube, the two phases of a gas-liquid mixture may be distributed in a number of patterns, each characterizing the radial and/or axial distribution of liquid and gas. Although two--phase flow is usually quite chaotic causing difficulties in describing these phase distributions, the two-phase flow regimes identified in vertical flow are classified into the four basic patterns, depicted in Figure 2.1 on page 7, as follows:

(1) **Bubbly Flow Regime** is distinguished by the presence of vapor bubbles that

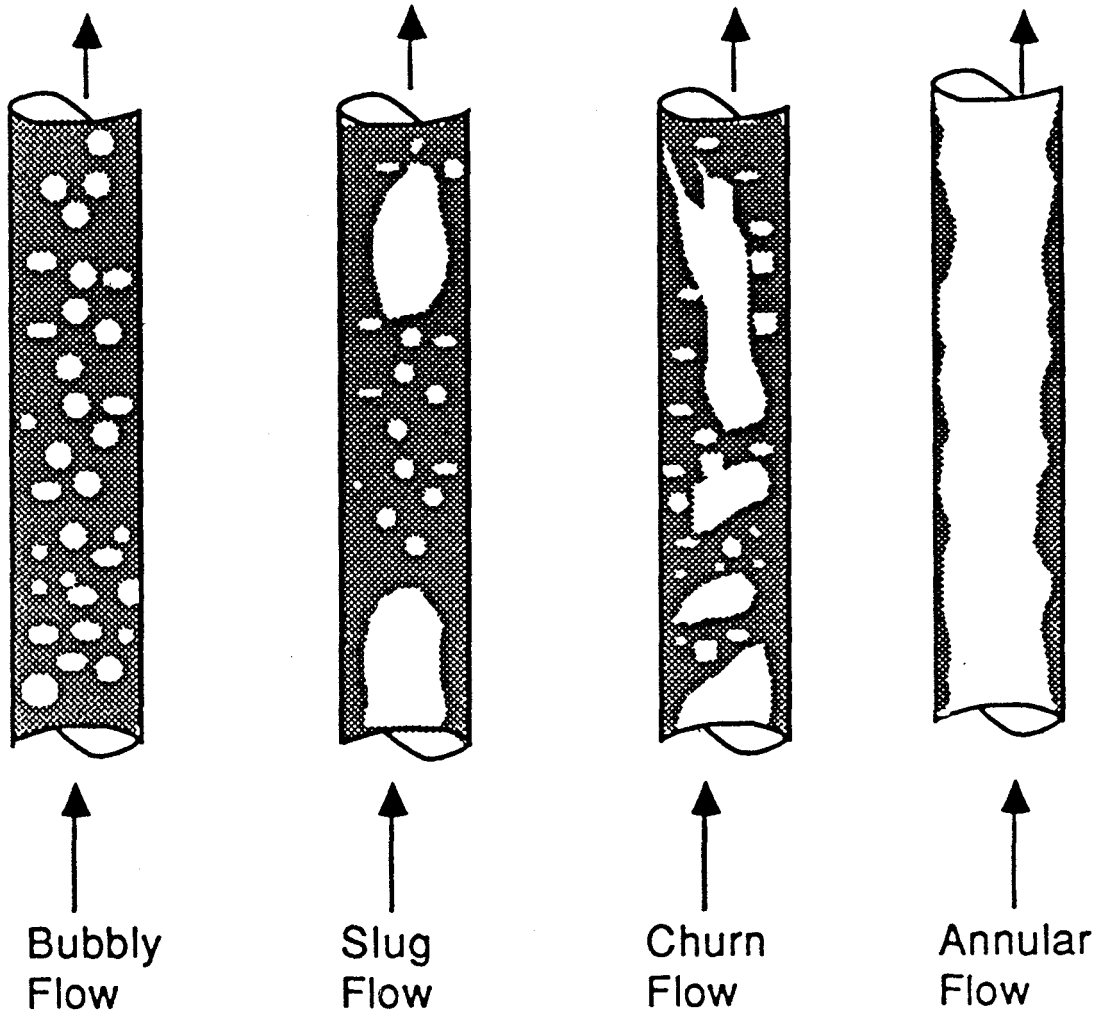

Figure 2.1: Two-Phase Flow Patterns in Vertical Upward Co-current Flow

are approximately uniformly dispersed in a continuous liquid phase. When the bubbles are smaller than a critical size, they remain spherical and perform a rectilinear vertical motion in a static liquid medium, but when they are larger than the critical size, they move in a 'zigzag' fashion. The critical bubble diameter is given by the following equation:

$$d_{crit} = \left[\frac{0.4*\sigma}{(\rho_L-\rho_G)*g}\right]^{1/2} \qquad (2.1)$$

where "σ" is the surface tension and "*g*" is the gravitational acceleration. Depending on the size of bubbles present, a bubbly flow is classified either as **dispersed bubbly flow** or bubbly flow. In a dispersed bubbly flow, which occurs at high liquid flow rates and velocities, bubble diameters never exceed this critical value. **Taitel *et al.*** (1980) have shown that bubbly flow cannot occur in a pipe if its diameter D satisfies the following inequality:

$$\left[\frac{\rho_L^{\,2}*g*D^2}{(\rho_L-\rho_G)*\sigma}\right]^{1/4} \leq 4.36 \qquad (2.2)$$

For an air-water flow near atmospheric pressure, equation 2.2 is satisfied up to a pipe diameter of about 50 mm. In pipes of smaller diameters only the dispersed bubbly flow can accordingly occur;

(2) **Slug Flow Regime** is characterized by the presence of large bullet-shaped bubbles (plugs), which have a diameter nearly equal to or larger than the pipe diameter and move uniformly upward. They are usually designated as "Taylor bubbles". Taylor bubbles are separated by slugs of a continuous liquid phase that bridge the pipe and contain small gas bubbles. Between the Taylor bubbles and the pipe wall, liquid may flow downward as a thin liquid film. This flow pattern has been designated by some observers as plug (piston) flow at lower flow rates with well-defined gas-liquid boundaries, or as slug flow at higher flow rates where the phasic boundaries are less clear;

(3) **Churn Flow Regime** is of the same basic character as the slug flow regime, but it is much more chaotic, frothy and disordered. It is characterized by unstable and frothy liquid slugs and occurs at a higher gas flow rate compared with that of the slug flow. The bullet-shaped Taylor bubble becomes narrow and its shape is distorted. The continuity of the liquid slug between successive Taylor bubbles is repeatedly destroyed by a high local gas concentration in the slug, which then falls. Then, this liquid accumulates, forms a bridge and is again lifted by the gas. This oscillatory or alternating direction of the liquid motion is typical for churn flow. Some observers refer to a froth flow pattern at higher liquid flow rates, for more finely dispersed churn flow;

(4) **Annular Flow Regime** is characterized by the presence of a continuous core of gas along the pipe, surrounded by an annulus of the liquid phase. The liquid phase moves upwards partly as a wavy liquid film and partially in the form of droplets entrained in the gas core at a sufficiently high gas velocity. In this case an annular-dispersed flow regime is said to exist. When the entrained liquid phase is in the form of large lumps or wisps, annular flow has been described as a wispy--annular flow pattern.

2.2. FLOW REGIME MAPS

The use of correct flow regime maps is necessary for simulation and scaling of real thermal-hydraulic loops and components, in order to extend the experimental results to the actual situations. Since most of the flow regimes have been defined in one-dimensional channels, many one-dimensional flow regime transition boundaries (or flow regime maps) have been developed and they have generally been related to the average flow properties in the channel. It is important to say that these maps usually propose transition boundaries in a two-dimensional coordinate system (sometimes with dimensionless coordinates), determined from experiments.

Among the several flow regime maps available for upward two-phase flow, the maps of **Hewitt and Roberts** (1969) and **Taitel *et al.*** (1980) are the most widely known and used. It is also interesting to mention the flow regime maps of **Weisman and Kang** (1981), **Mishima and Ishii** (1984) and recently **Ohnuki *et al.*** (1995).

The one-dimensional flow regime map of **Hewitt and Roberts** (1969) was developed from air-water data obtained in a 3.12-cm diameter vertical pipe and at pressure varying from 0.14 to 0.54 MPa. It was found suitable for steam-water data in a 1.27-cm diameter pipe at pressures of 3.45 to 6.90 MPa. It is based on relating the superficial liquid and vapor momentum fluxes.

Recently **Ohnuki *et al.*** (1995) experimentally investigated transitions between flow patterns in air-water two-phase flow in a large vertical pipe (D = 0.48 m). It is interesting that slug flow was not observed over their range of test conditions.

The one-dimensional flow regime maps of **Taitel *et al.***, **Mishima and Ishii** and **Weisman and Kang** will be discussed in more details, including their mathematical formulations, since an objective of this research was to develop a flow regime map for low-pressure two-phase flow in large-diameter vertical pipes.

Before proceeding with the mathematical formulations of the flow regime maps, the definitions of some common basic two-phase flow parameters will be given. Before all, the void fraction is essential in determining the state of a mixture flow. The average void fraction is defined as volume, or area, occupied by the gas phase in the total volume, or area, of the two-phase mixture:

$$<\alpha> \equiv \frac{V_G}{V_L+V_G} \qquad (2.3) \qquad\qquad <\alpha> \equiv \frac{A_G}{A_L+A_G} \qquad (2.3')$$

The average cross-sectional gas velocity is by definition a ratio of the volumetric gas flow rate and the area occupied by gas (equation 2.4), whereas the average cross-sectional liquid velocity is similarly defined as a ratio of the volumetric liquid flow rate and the area occupied by liquid (equation 2.5):

$$<U_G> \equiv \frac{\dot{Q}_G}{A_G} = \frac{\dot{Q}_G}{<\alpha> * A} \qquad (2.4)$$

$$<U_L> \equiv \frac{\dot{Q}_L}{A_L} = \frac{\dot{Q}_L}{(1-<\alpha>) * A} \qquad (2.5)$$

where "A" is the total flow area (pipe cross-sectional area), equal to the summation of the areas occupied by gas and liquid.

Finally, the average cross-sectional superficial gas velocity (volumetric gas flux) is by definition a ratio of the volumetric gas flow rate and the total flow area A (equation 2.6), and the average cross-sectional superficial liquid velocity (volumetric liquid flux) is similarly defined as a ratio of the volumetric liquid flow rate and the total flow area (equation 2.7):

$$<J_G> \equiv \frac{\dot{Q}_G}{A} = <\alpha> * <U_G> \tag{2.6}$$

$$<J_L> \equiv \frac{\dot{Q}_L}{A} = (1 - <\alpha>) * <U_L> \tag{2.7}$$

In the equations from 2.3 to 2.7, and in all further corresponding equations, the symbol "< >" represents the averaging over the pipe cross-sectional area.

2.2.1. Taitel *et al.*'s Flow Regime Map

Undoubtedly, the most important and the most popular flow regime map is the one of **Taitel *et al.*** (1980). This flow regime map was developed based on a theoretical analysis of the mechanisms contributing to the transition boundaries between the

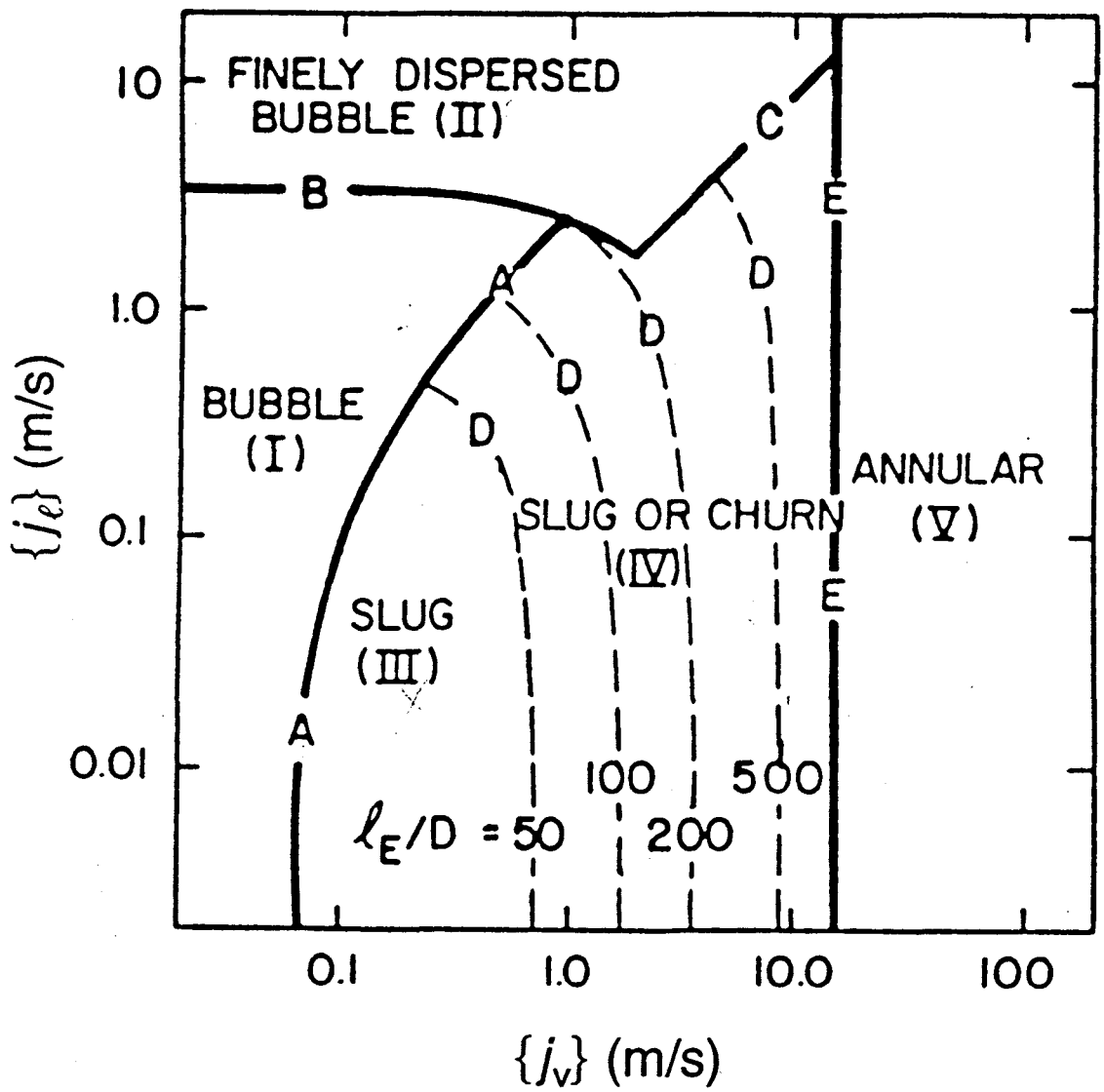

Figure 2.2: Flow Regime Map of **Taitel *et al.*** (1980) for Air-Water at 25°C and 0.1 MPa in 50-mm Diameter Vertical Pipes

various flow regimes. The predictions of this flow map were found to agree well with air-water data in vertical pipes having diameters of 25 mm and 51 mm. It is based on relating of the superficial gas and liquid velocities. A flow regime map of Taitel and co-workers for air-water at 25°C and 0.1 MPa in 50-mm diameter vertical pipes is depicted in Figure 2.2 on page 14. It can be noted that five lines (A, B, C, D and E) represent the transition boundaries between the following 5 flow regimes: (I) bubbly; (II) finely-dispersed bubbly; (III) slug; (IV) churn and (V) annular.

Taitel and co-workers related the transition from bubbly to slug or churn flow to a maximum possible void fraction of 0.25 (or 25%) at which bubble coalescence occurs to form slugs. They introduced the rise velocity of large bubbles, which has been shown to be quite insensitive to the bubble size, given by the following equation:

$$U_0 = 1.53 * [\frac{\sigma * (\rho_L - \rho_G) * g}{\rho_L^2}]^{1/4} \qquad (2.8)$$

From the relation between the average liquid and gas velocities and the rise velocity of large bubbles, the following equation may be derived with respect to equations 2.6 and 2.7:

$$<J_L> = <J_G> * \frac{(1 - <\alpha>)}{<\alpha>} - (1 - <\alpha>) * U_0 \qquad (2.9)$$

Substituting equation 2.8 into equation 2.9, considering that transition from bubbly to slug (or churn) flow occurs at the average void fraction of 0.25, results in an equation of the line A in the flow regime map (Figure 2.2):

$$<J_L> = 3.0*<J_G> - 1.15*[\frac{\sigma*(\rho_L-\rho_G)*g}{\rho_L^2}]^{1/4} \qquad (2.10)$$

In small pipes the rising bubbles can catch up to form a slug. Thus in narrow pipes the bubbly flow regime may not exist, in which case only slug flow would exist at low liquid and gas superficial velocities. The criterion for eliminating of bubbly flow in a narrow pipe of a diameter D is given with inequality 2.2 on page 8.

For high liquid volumetric fluxes, a bubble breakup would occur due to turbulent forces, so that coalescence of bubbles into Taylor bubbles would be prevented above a limit on the sum of superficial liquid and gas velocities given by the following equation:

$$<J_L> + <J_G> = 4.0*[\frac{D^{0.429}*(\sigma/\rho_L)^{0.089}}{v_L^{0.072}}]*[\frac{g*(\rho_L-\rho_G)}{\rho_L}]^{0.446} \qquad (2.11)$$

Equation 2.11 is represented by the line B in the Taitel et al.'s flow regime map (Figure 2.2) and it denotes transition from finely dispersed bubbly flow to bubbly

and/or slug (or churn) flow.

When small bubbles (of spherical shape, arranged in a cubic lattice) are packed together, the maximum allowable void fraction (which occurs when they touch each other) is equal to 0.52, according to Taitel and co-workers. At high liquid velocities the slip velocity can be neglected and the gas holdup can be calculated from a simple equation:

$$\langle\alpha\rangle = 0.52 = \frac{\langle J_G \rangle}{\langle J_G \rangle + \langle J_L \rangle} \qquad (2.12)$$

Equation 2.12 is represented by the line C in the Taitel et al.'s flow regime map (Figure 2.2) and it denotes transition from finely dispersed bubbly flow to churn and/or slug flow.

The slug flow pattern develops from a bubbly flow pattern if enough small bubbles can coalesce to form Taylor bubbles. If the liquid slug between two Taylor bubbles is too small to be stable, the churn flow regime develops. Taitel et al. presented a view that the churn flow regime is essentially a developing length region for slug flow. They observed that, as the gas flow rate increased, the length of the entrance region (churn flow) also increased, until it occupied the entire length of any test section. Thus they derived the entry length of a pipe required to establish stable

slug flow and, therefore, the region one would observe churning. It is represented by the line D in the flow regime map (Figure 2.2), denoting transition from slug to churn flow, and given by the following equation:

$$\frac{l_E}{D} = 40.6 * [\frac{<J_G> + <J_L>}{(g*D)^{1/2}} + 0.22] \qquad (2.13)$$

Figure 2.2 shows that region of slug flow decreases with an increase of the pipe diameter or with a decrease of the pipe length. If a position along the pipe length is shorter than the developing length, churn or slug flow may exist. If the developing length is short compared with the position of interest along the pipe, slug flow alone exists.

For transition from slug/churn flow to annular flow, Taitel et al. suggested that stable annular flow can only exist if the gas velocity in the gas core is sufficient to lift the entrained liquid droplets, thus preventing them from falling and bridging between the liquid film. After determining the minimum gas velocity required for stable annular flow from a balance between the gravity and drag forces, they have shown that transition to annular flow is independent of the pipe diameter and the liquid flow rate. It is represented by the straight vertical line E in the flow regime map (Figure 2.2) and given by the following simple equation:

$$\langle J_G \rangle = 3.1 * \frac{[\sigma*(\rho_L-\rho_G)*g]^{1/4}}{\rho_G^{1/2}} \qquad (2.14)$$

2.2.2. Mishima and Ishii's Flow Regime Map and Drift-Flux Model

Mishima and Ishii (1984) proposed a flow regime map for upward gas-liquid flow in vertical pipes based on a direct geometrical parameter, such as the void fraction, instead of the superficial gas and liquid velocities. They based their model on the experimental observations, which showed that transition from bubbly to slug flow occurs at $\langle\alpha\rangle = 0.3$. Therefore, they incorporated this criterion for bubbly-to-slug flow transition in their mathematical model of the flow regime map. Other parts of their mathematical interpretation were derived based on the superficial gas and liquid velocities using the **drift-flux model**, which will now be outlined with its most important characteristics.

The well-known **drift-flux model** for predicting of the void fraction in two-phase flow was derived by **Zuber and Findley** in 1965. It implies a linear relationship between the average cross-sectional gas velocity and the average cross-sectional superficial mixture velocity (mixture volumetric flux):

$$<U_G> = \frac{<J_G>}{<\alpha>} = U_{Gj} + C_0 * <J> = U_{Gj} + C_0 * (<J_G> + <J_L>) \qquad (2.15)$$

where "C_0" is the distribution parameter that represents effect of radial non-uniform flow and concentration profiles, whereas "U_{Gj}" is the average local drift velocity that represents the effect of the local relative velocity between the phases. It was shown that $C_0 < 1$ when the void fraction near the wall is higher than the void fraction in the center of a pipe (a "saddle" type radial void profile) and vice versa. When $C_0 > 1$ it was analytically shown that the value of C_0 varies between 1 for flat void profiles, up to 1.5 for parabolic (peaked) void profiles.

Clark and Flemmer (1986) suggested the use of individual flow parameters, C_L and C_G, for the liquid and gas phase respectively, instead of a single parameter C_0:

$$C_0 = C_L * (\frac{<J_L>}{<J>}) + C_G * (\frac{<J_G>}{<J>}) \qquad (2.16)$$

The values of C_L and C_G were experimentally found to be 0.93 and 1.95 respectively. Equation 2.16 was derived based on data obtained from a 10-cm inside diameter pipe for void fraction of up to 0.25.

Hasan (1988) discussed the use of the drift flux model for predicting of the void

fraction in bubbly, slug and churn flow regimes for vertical upward co-current two -phase flow. He suggested that in bubbly flow C_0 should vary between 1.2, for turbulent bubbly flow, and 2.0, for laminar bubbly flow, based on the assumption that the gas phase tends to flow through the central portion of a channel (pipe), where the local mixture velocity is higher than the average mixture velocity. Since in most practical cases the flow is turbulent, the value of 1.2 for C_0 was suggested, especially for pipe diameters less than 10 cm. For large-diameter pipes (with D > 10 cm), the use of the procedure suggested by **Clark and Flemmer** (1986) was recommended. From this relation (2.16) it can be concluded that, for large-diameter pipes with stagnant liquid columns, the value of C_0 is 1.95. For slug flow, a value for C_0 of about 1.2 was recommended, based on experimental studies of several researchers. Similarly, **Hasan** obtained a value for C_0 of about 1.15 for churn flow.

It was suggested that in vertical upward bubbly flow the average local drift velocity U_{Gj} (which accounts for the local velocity difference between the phases) can be taken as the bubble terminal (rise) velocity predicted by **Harmathy's** correlation (1960):

$$U_{Gj} = \langle U_G \rangle - \langle J \rangle = 1.53 * \left[\frac{\sigma * (\rho_L - \rho_G) * g}{\rho_L^2}\right]^{1/4} \qquad (2.17)$$

The above equation 2.17 results in a U_{Gj} value of 0.24 m/s for air bubbles in water near atmospheric conditions. When the presence of other bubbles affects the motion of a given bubble, the local drift velocity depends on the void concentration. This effect was analyzed by **Zuber and Hench** (1962), who obtained a drift velocity correlation for bubbles with diameters between 0.1 and 2 cm as:

$$U_{Gj} = \langle U_G \rangle - \langle J \rangle = 1.53 * \left[\frac{\sigma * (\rho_L - \rho_G) * g}{\rho_L^2}\right]^{1/4} * (1 - \langle \alpha \rangle)^{3/2} \qquad (2.18)$$

Similar to the equations 2.17 and 2.18 are correlations for drift flux velocity U_{Gj} in bubbly (equation 2.19) and slug (equation 2.20) flow derived by **Ishii** (1977) and used in the flow regime map of **Mishima and Ishii** (1984):

$$U_{Gj} = 1.41 * \left[\frac{\sigma * (\rho_L - \rho_G) * g}{\rho_L^2}\right]^{1/4} * (1 - \langle \alpha \rangle)^{7/4} \qquad (2.19)$$

$$U_{Gj} = 0.35 * \left[g * D * \frac{(\rho_L - \rho_G)}{\rho_L}\right]^{1/2} \qquad (2.20)$$

The drift flux velocity given by equation 2.20 is known as the rise velocity of a Taylor bubble, since it is related to slug flow. Also, according to **Ishii** (1977), the distribution parameter C_0 for a circular pipe in the range of moderate Reynolds

numbers is given by the equation:

$$C_0 = 1.2 - 0.2 * \left(\frac{\rho_G}{\rho_L}\right)^{1/2} \qquad (2.21)$$

Substituting equations 2.19 and 2.21 into the drift-flux equation 2.15 and using the value of $<\alpha> = 0.3$, **Mishima and Ishii** obtained relationship between J_G and J_L at the transition from bubbly to slug flow:

$$<J_L> + <J_G> = \frac{3.33 * <J_G> - 0.76 * \left[\frac{\sigma * (\rho_L - \rho_G) * g}{\rho_L^2}\right]^{1/4}}{1.2 - 0.2 * \left(\frac{\rho_G}{\rho_L}\right)^{1/2}} \qquad (2.22)$$

Also, substituting equations 2.20 and 2.21 into the drift-flux equation 2.15, they obtained relationship between J_G and J_L at the transition from slug to churn flow:

$$<J_L> + <J_G> = \frac{\frac{<J_G>}{<\alpha>} - 0.35 * \left[g * D * \frac{(\rho_L - \rho_G)}{\rho_L}\right]^{1/2}}{1.2 - 0.2 * \left(\frac{\rho_G}{\rho_L}\right)^{1/2}} \qquad (2.23)$$

The average void fraction for the transition from slug to churn flow, for weakly viscous fluids (such as water) at standard conditions, is given by the equations:

$$a = \left[\frac{g * D^3 * (\rho_L - \rho_G)}{\rho_L * v_L^2}\right]^{1/18} \qquad (2.24')$$

$$\langle\alpha\rangle \geq 1 - 0.813 * \left[\frac{(C_0 - 1) * \langle J\rangle + 0.35 * \left[g * D * \frac{(\rho_L - \rho_G)}{\rho_L}\right]^{1/2}}{\langle J\rangle + 0.75 * a * \left[g * D * \frac{(\rho_L - \rho_G)}{\rho_L}\right]^{1/2}}\right]^{3/4} \qquad (2.24)$$

where C_0 is given by equation 2.21, and $\langle J\rangle = \langle J_L\rangle + \langle J_G\rangle$.

Transition from churn (or slug) to annular flow in this flow regime map is described with two criteria. The first criterion assumes the flow reversal in the liquid film section along large bubbles (condition $\langle J_L\rangle = 0$). It uses the annular drift-velocity correlation and can be approximated by the equation:

$$\langle J_G\rangle = (\langle\alpha\rangle - 0.11) * \left[g * D * \frac{(\rho_L - \rho_G)}{\rho_G}\right]^{1/2} \qquad (2.25)$$

where the average void fraction $\langle\alpha\rangle$ satisfies equation 2.24. The second criterion was obtained from the onset of droplet entrainment and it is applicable for predicting the transition from churn to annular flow in large-diameter pipes:

$$\langle J_G \rangle = \left[\frac{\sigma*(\rho_L-\rho_G)*g}{\rho_G^2}\right]^{1/4} * \left[\frac{(\rho_L*\sigma)^{1/2}}{\mu_L} * \left[\frac{\sigma}{g*(\rho_L-\rho_G)}\right]^{1/4}\right]^{1/5} \qquad (2.26)$$

2.2.3. Weisman and Kang's Flow Regime Map

The one-dimensional flow regime map of **Weisman and Kang** (1981) was developed for upward flow in vertical and sharply inclined pipes. It was based on Freon-113 data obtained in a 2.5-cm diameter vertical pipe. In this map the suggested churn-to-annular transition boundary depends on the pipe diameter, unlike the flow regime map of **Taitel *et al.***. According to **Weisman and Kang**, there are three main transition boundaries between two-phase flow patterns in vertical and sharply inclined lines (pipes): transition to dispersed flow, transition to annular flow and transition between intermittent and bubbly flow, whereas the intermittent flow includes both slug and churn flow. They recommended their previously developed flow regime map for horizontal and slightly inclined lines to be adopted for transitions to annular and dispersed flow in vertical and sharply inclined lines. This flow regime map was developed in terms of average superficial velocities of gas $\langle J_G \rangle/\phi_1$ and liquid $\langle J_L \rangle/\phi_2$, where the functions ϕ_1 and ϕ_2 include the corrections needed to account for the effects of physical fluid properties and diameter variations from the standard values used in constructing the map. These

standard values are: standard pipe diameter D_s = 2.54 cm, standard densities of the gas phase ρ_{sG} = 1.3 kg/m^3 and of the liquid phase ρ_{sL} = 1000 kg/m^3, standard average superficial liquid velocity $\langle J_{sL} \rangle$ = 0.305 m/s, standard dynamic viscosity of the liquid phase $\mu_{sL} = 10^{-3}$ Pa*s and standard surface tension σ_{sL} = 0.07 N/m.

Based on the above considerations, transition from intermittent (slug and churn) flow to bubbly flow, for vertical and sharply inclined pipes, is given by equation:

$$\frac{\langle J_G \rangle}{(g * D)^{1/2}} = 0.45 * \left[\frac{\langle J_G \rangle + \langle J_L \rangle}{(g * D)^{1/2}}\right]^{0.78} * (1 - 0.65 * \cos\theta) \qquad (2.27)$$

where "θ" is the inclination angle from horizontal line; θ = 90° for vertical pipes.

The corresponding correction functions for bubbly-to-intermittent transition in vertical and sharply inclined pipes are ϕ_2 = 1.0 and:

$$\phi_1 = \left(\frac{D}{D_s}\right)^{\left[0.26 * \exp^{-0.17 * \left(\frac{\langle J_L \rangle}{\langle J_{sL} \rangle}\right)}\right]} * (1 - 0.65 * \cos\theta) \qquad (2.28)$$

Transition from intermittent (slug and churn) flow to annular flow, for vertical, sharply and slightly inclined, as well as horizontal pipes, is given by the equation:

$$1.9 * \left(\frac{<J_G>}{<J_L>}\right)^{1/8} = \left[\frac{<J_G> * \rho_G^{1/2}}{[g*\sigma*(\rho_L-\rho_G)]^{1/4}}\right]^{0.2} * \left[\frac{<J_G>^2}{g*D}\right]^{0.18} \quad (2.29)$$

The corresponding correction functions for intermittent-to-annular transition in vertical, sharply and slightly inclined and horizontal pipes are $\phi_2 = 1.0$ and:

$$\phi_1 = \left(\frac{D}{D_s}\right)^{0.415} * \left(\frac{\rho_{sG}}{\rho_G}\right)^{0.23} * \left[\frac{(\rho_L-\rho_G)}{(\rho_{sL}-\rho_{sG})}\right]^{0.11} * \left(\frac{\sigma}{\sigma_s}\right)^{0.11} \quad (2.30)$$

Finally, transition from all other flow regimes to dispersed flow, for vertical, sharply and slightly inclined, as well as horizontal pipes, is given by the equation:

$$\left[\frac{|(dp/dx)|_{L,s}}{g*(\rho_L-\rho_G)}\right]^{1/2} * \left[\frac{\sigma}{g*D^2*(\rho_L-\rho_G)}\right]^{-1/4} = 1.7 \quad (2.31)$$

where $|(dp/dx)|_{L,s}$ represents absolute value of the pressure drop per unit length due to single liquid phase. Equation 2.31 applies only to low and moderate quality two-phase flows. At high quality two-phase flows a revised formulation applies, which depends on the pressure drop due to total flow rather than liquid flow. For hydraulically smooth pipes and Reynolds numbers of liquid between 3000 and 100,000 the pressure drop per unit length due to liquid flow can be expressed as:

$$\left(\frac{dp}{dx}\right)_{L,s} = \frac{f}{2} * \left(\frac{\rho_L * <J_L>^2}{D}\right) = \frac{0.158 * \mu_L^{1/4}}{(\rho_L * D * <J_L>)^{1/4}} * \left(\frac{\rho_L * <J_L>^2}{D}\right) \quad (2.32)$$

where "f" is the friction factor and it can be estimated from the equation of Blasius:

$$f = \frac{0.316}{Re_L^{1/4}} = 0.316 * \left(\frac{\mu_L}{\rho_L * D * \langle J_L \rangle}\right)^{1/4} \qquad (2.33)$$

where Re_L is the Reynolds number of liquid.

Connecting equations 2.31 and 2.32, it can be noted that, for a given fluid and a pipe diameter, the transition to dispersed flow occurs at a constant superficial liquid velocity (liquid mass flow rate), according to **Weisman and Kang**.

The corresponding correction functions for transition to dispersed flow in vertical, sharply and slightly inclined and horizontal pipes are $\phi_1 = 1.0$ and:

$$\phi_2 = \left(\frac{D}{D_s}\right)^{0.16} * \left(\frac{\rho_{sL}}{\rho_L}\right)^{0.33} * \left(\frac{\mu_{sL}}{\mu_L}\right)^{0.09} * \left(\frac{\sigma}{\sigma_s}\right)^{0.24} \qquad (2.34)$$

2.3. LOCAL VOID FRACTION MEASURING TECHNIQUES

Two-phase flow modelling requires information such as local instantaneous measurements of phase densities, liquid and gas velocities, interfacial passage frequencies, liquid and vapor temperatures and their statistical characteristic (probability density functions and spectral densities). The purpose of these measurements is to obtain data regarding interfacial area densities, correlation coefficients between void fraction and velocity or void fraction and energy, and to verify hypotheses regarding the shape of the void, velocity and temperature profiles, their interrelations and their statistical variations. Among several types of local measuring techniques for transient and statistical diagnosis, the most successful and nowadays used ones are the two techniques that use **electrical resistivity probes** and **optical fiber probes** as the instruments. Both types of probes can be used as **single-sensor** probes to obtain local measurements of the void fraction, or as **dual-sensor** probes to provide information on phase velocities.

2.3.1. Electrical Resistivity Probes

Electrical resistivity probes are suitable for local measurements when one phase

has a significantly different electrical conductivity (or resistivity) from the other. These variations in conductance enable the measurements of the local void fraction and the arrival frequency of the bubbles, at a given point in a continuous conducting fluid. Electrical impedance changes due to the passage of bubbles at the probe tip produce a fluctuation in the output signal. By using a double (dual-sensor) probe, a transit velocity of bubbles can be measured.

The electrical resistivity probe (or any other local probe) signal is processed and electronically integrated for a certain sampling time T, in order to determine the fraction of time during which the gas is in contact with the probe tip T_G (the probe residence time in void). Thus, the local void fraction is determined as a ratio of the probe residence (dwell) time in void during N equal periods of the sampling time T and the sampling time itself:

$$\alpha_T = \frac{\sum_{i=1}^{i=N} (T_{Gi})}{T} \tag{2.35}$$

The electrical resistivity probe method, as well as any other local probe method, is accurate provided the sampling time is sufficiently long to allow sampling of a large number of bubbles. Thus, the sampling time has to be increased as bubble population decreases (a bubbly or dispersed bubbly flow regime).

Electrical probes are usually more accurate than optical probes, since they can be made with smaller sizes, that is, thinner sensors. Figure 2.3 on page 32 displays a typical geometry of an electrical resistivity probe. It can be noted that the thickness of the sensor, made of tungsten wire, is very small (20 μm). The electrical probe as the one depicted in Figure 2.3 does not work in dispersed droplet flow (annular-dispersed flow regime) because of the impossibility of having a continuous electrical path in the liquid phase between two electrodes.

When a direct current supply is used as the type of electrical supply, low voltages are required in order to reduce electrochemical deposits on the sensor. Still, some electrochemical depositing may occur at low flows. With an alternating current supply, phase changes are detected by amplitude modulation of the alternating output signal. When high-speed flows are investigated, the required supply frequency can be very high (~1MHz) and significant electrochemical depositing occurs. To eliminate electrochemical effects and ensure pseudo direct-current operation, a supply frequency much lower than the frequency of the observed physical phenomenon should be used.

The potential sources of error related to use of electrical probes (and local probes in general) were described in details by **Tawfik** (1979) and classified into the following four groups: the bubble deformation, the bubble deflection, the trigger

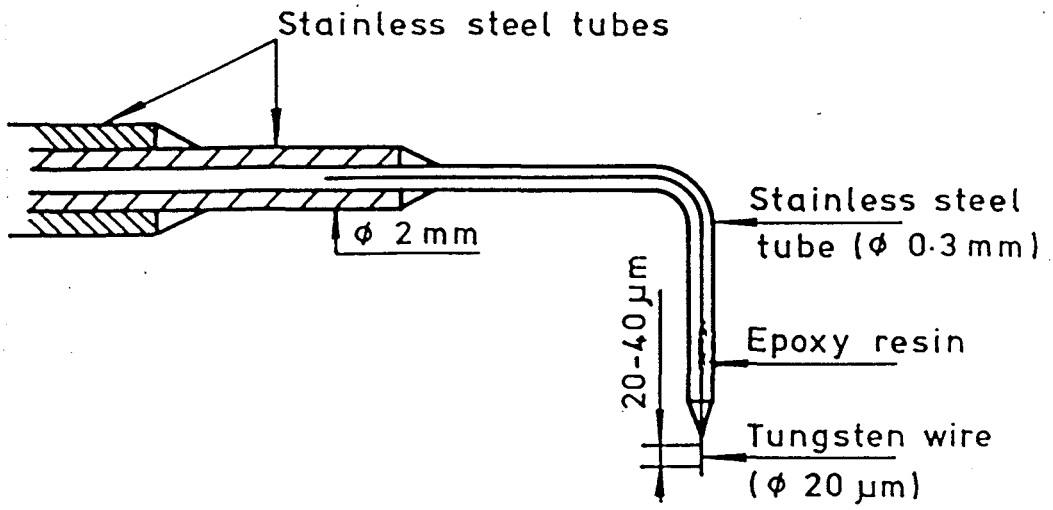

Figure 2.3: Typical Electrical Resistivity Probe Geometry from **Delhaye** (1981)

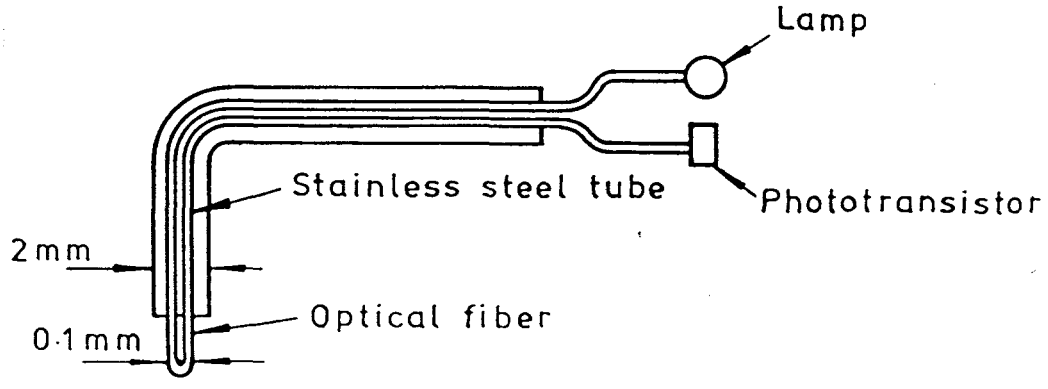

Figure 2.4: U-Shaped Optical Fiber Sensor Probe from **Delhaye** (1981)

voltage level, and the electrical field distortion. The change in shape of the bubble interface (bubble deformation) due to surface tension force increases the probe penetrating time into the bubble, resulting in an underestimation of the probe residence time in the voids, and consequently the measured void fraction. Deflecting of bubbles from their paths during their approach to the stationary probe tip, reduces the probe sensitivity to the existence of some bubbles and also results in an underestimation of the measured void fraction. The electrical field distortion due to the entrance of a bubble before it touches the probe tip, changes the desirable rectangular shape of the probe output voltage signal and, therefore, results in inaccurate void measurements. Finally, setting the **trigger voltage level** at different levels of the nominal probe signal amplitude, can significantly affect the accuracy of the probe measurements, underestimating or overestimating it if the trigger level is, respectively, relatively high or low compared with the signal amplitude. For lower trigger voltage levels it is expected that the probe electrical field distortion, as an overestimating source of error, will be the most predominant. For higher trigger voltage levels the probe measurements may be more sensitive to the underestimating sources of error, such as bubble deflection and bubble deformation.

2.3.2. Optical Fiber Probes

One of the most successful techniques for local void fraction measurements, employed in air-water and Freon systems, has been the **optical fiber probe**. While an electrical probe can be used only in aqueous systems, using the liquid phase conductivity to register the presence or absence of liquid (water), an optical fiber probe can be applied to non-aqueous systems, which are so important to chemical industry based largely on hydrocarbons. An optical fiber probe is sensitive to change in the refractive index of the surrounding medium and is thus responsive to interfacial passages, enabling measurements of the local void fraction and interface passage frequencies even in a non-conducting fluid.

Several types of optical probes have been investigated in the past (**Delhaye**, 1981):

- The **Glass Rod System** consisting of a 0.3-mm diameter glass rod, ground and polished to form a right-angled cone;
- The **Fiber Bundle System** consisting of several hundred glass fibers tied together and sealed at its end with a glass rod;
- The **'U'-Shaped Fiber System** (Figure 2.4 on page 32 and Figure 2.5 on page 35) consisting of a 40-μm single optical fiber, bent into a 'U'-shape, with an advantage over other methods of faster response due to smaller size;

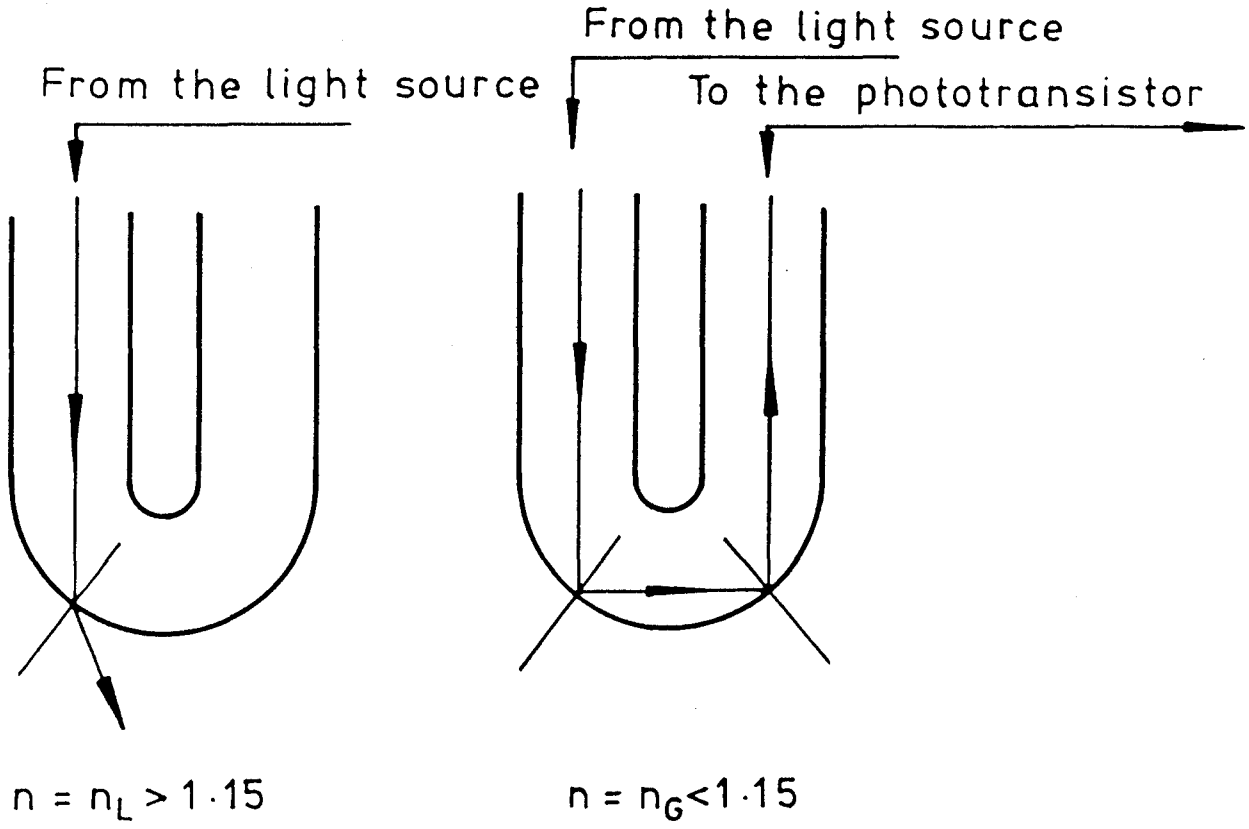

Figure 2.5: Principle of Operation of the U-Shaped Optical Fiber Sensor Probe

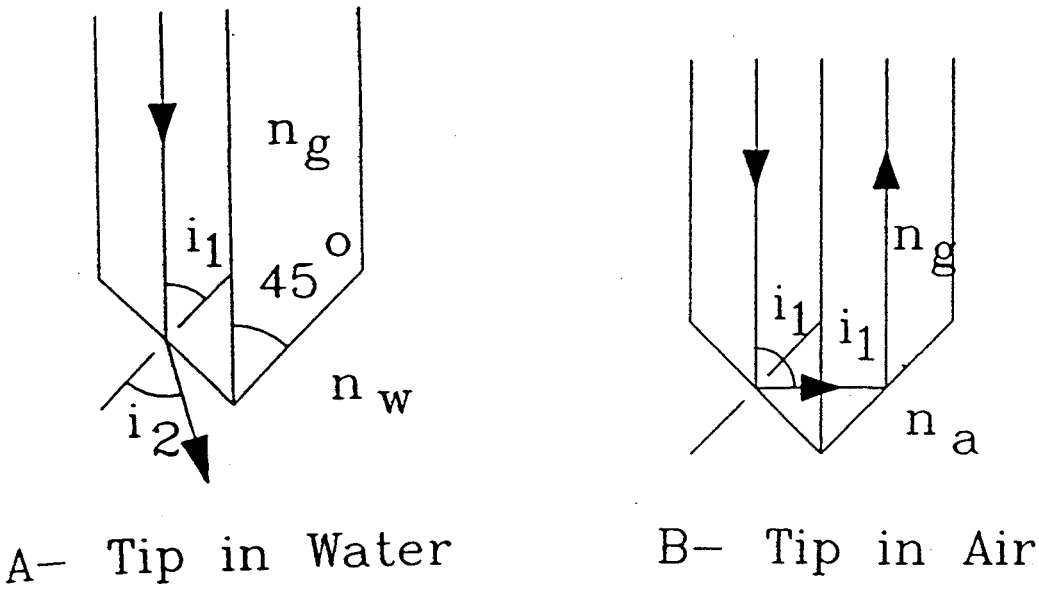

Figure 2. 6:Principle of Operation of the 90°-Chamfered Dual Tip Probe

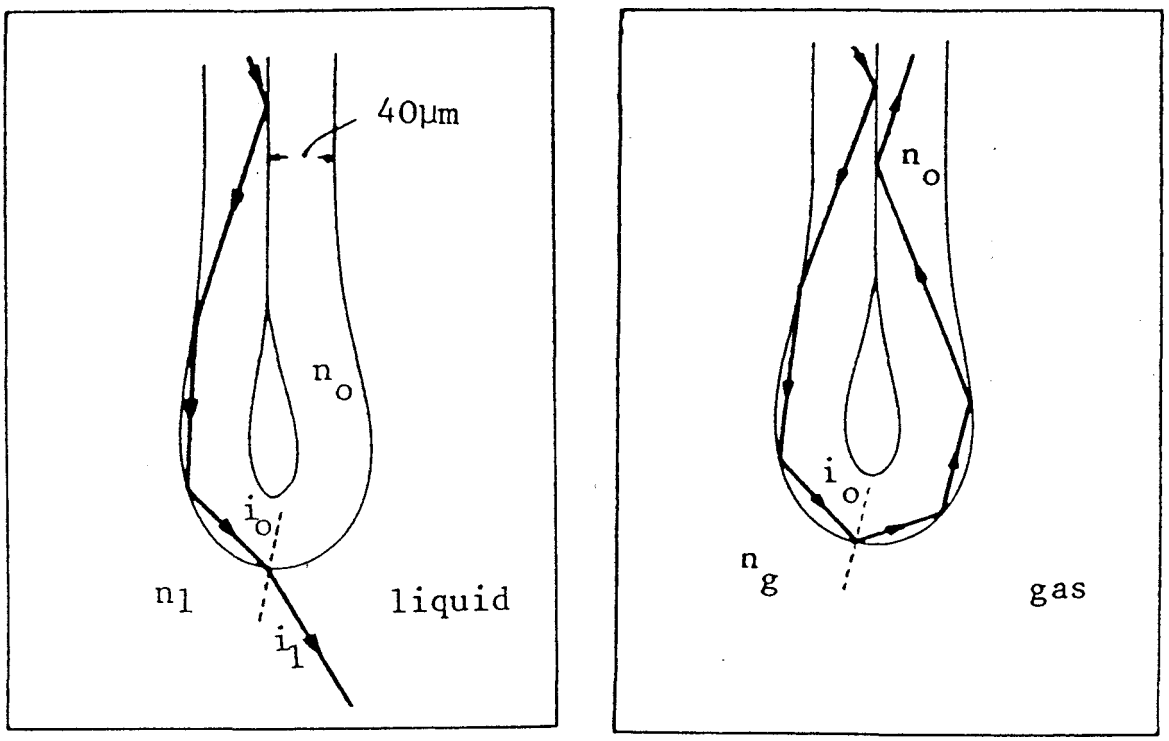

Figure 2.7: Principle of Operation of the Single Sensor Optical Fiber Probe

- The **Dual Sensor Fiber System** (Figure 2.6 on page 36) consisting of single 125-mm fibers fused at one end and ground and polished to a right-angled (90°) cone.

The **U-shaped-sensor optical fiber probe** (Figure 2.4 on page 32) was proposed by Danel and Delhaye in 1971 and developed by Galaup in 1975 (**Delhaye**, 1981). This probe consisted of a single U-shaped optical fiber, 40 μm in diameter. The entire fiber, except the U-shaped bend, was protected inside a stainless steel tube, 2 mm in diameter. The active part of the probe had a characteristic size of 0.1 mm. The light source was a lamp and reflected light was conducted by the optical fiber into the phototransistor. Usually, the light source is a laser filled with an inert gas (Helium, Neon or a mixture) and connected to the fiber via a beam-splitter, which ensures the separation of the forward and backward (reflected) light beams.

The principle of operation of an optical fiber probe for various probe-tip geometries is the same and it is depicted in Figures 2.5, 2.6 and 2.7 on pages 35 and 36. Figure 2.5 on page 35 shows the principle of operation of an **U-shaped-sensor** optical fiber probe, described by **Delhaye** (1981). Figure 2.6 on page 36 shows the principle of operation of a typical **90°-chamfered dual-sensor** optical fiber probe, while figure 2.7 on page 36 shows the principle of operation of a **single-sensor** optical fiber probe, described and used by **Mann and Hackett** (1985) and **Moujaes** (1990). An optical fiber probe is sensitive to change in the refractive index of the

medium at its tip, as it was already explained. If gas is present at the probe tip, the light from the source is reflected and a higher signal is detected by the amplifier. If liquid is present at the tip, the light is refracted giving a lower signal. The principle of the optical fiber probe (Figure 2.6, page 36) operation is based on the **Snell's law of diffraction** and mathematically depicted by the following equation:

$$n_1 * \sin(i_1) = n_2 * \sin(i_2) \qquad (2.36)$$

where: "i_1" is the angle of the incidence at the fiber tip, "i_2" is the angle of refraction from the fiber tip into the medium 2 (a liquid or a gas), "n_1" (or "n_g") is the index of refraction of fiber glass and "n_2" is the index of refraction of the medium 2 ("n_w" for water or "n_a" for air). Rearranging the equation 2.2, we can obtain:

$$\sin(i_2) = \frac{n_1}{n_2} * \sin(i_1) \qquad (2.37)$$

For a coherent ray of light travelling parallel to the axis of the probe, intercepting the 45°-chamfered tip (Figure 2.6), it means that $\sin(i_1) = 0.7071$ (since $i_1 = 45°$). Since the ray refraction into the liquid occurs if $\sin(i_2) < 1$, from the equation 2.37 it can be calculated that, for a given refractive index of the fiber optic silica glass of $n_1 = 1.62$, the refractive index of liquid (water) should be $n_2 = 1.15$ or $n_2 > 1.15$.

Thus, for the successful operation of an optical fiber probe, the refractive index of liquid must be greater than 1.15 (in Figure 2.5 on page 35 this is designated as n_L > 1.15), which is the condition for total refraction, and that of the gas must be less than 1.15 (n_G < 1.15 in Figure 2.5), which is the condition for total reflection. This means that medium 2 can be steam, air or Freon vapor. In Figure 2.7 the designations are different, meaning that "i_0" is the angle of the incidence at the fiber tip, "i_1" is the angle of refraction from the fiber tip into the medium 1 (a liquid or a gas), "n_0" is the index of refraction of fiber glass and "n_1 " is the index of refraction of the medium 1 ("n_g" for gas). However, the principle of operation of the single-sensor optical fiber probe is essentially the same as already described one. Similarly as in the case of an electrical probe, the local void fraction is determined from the optical fiber probe signal as a ratio of the probe residence (dwell) time in void during N equal periods of a certain sampling time T and the sampling time itself, given by equation 2.35 on the page 30.

The major potential sources of error related to use of optical fiber probes are: the trigger voltage level, the bubble deformation and the bubble deflection (page 33). The problem with trigger voltage level can be overcome with a signal of an essentially rectangular shape. By using two optical fiber sensors (dual-sensor probes) and a cross-correlation method, the local interface velocity can be measured.

2.4. PREVIOUS WORK ON THE VOID FRACTION MEASUREMENTS USING LOCAL PROBES

The following experimental studies include local measurements of the void fraction and radial void fraction distribution in bubbly two-phase flow in vertical tubes, using optical fiber probes or electrical resistivity probes. Some of them compare the accuracy of these two techniques with accuracies of other void fraction measuring techniques, or report the estimated range of the measurement error.

Serizawa *et al.* (1975) reported an experimental investigation on the structure of vertical upward air-water bubbly two-phase flow in a 60-mm inside diameter (I.D.) vertical pipe, under nearly atmospheric pressure. The results included radial distribution of the local void fraction. Measurements were taken from three axial positions, at Z/D=10, 20 and 30. The local void fraction was measured by means of three electrical resistivity probes, which were radially traversed every 1 or 2 mm, from r/R=-0.98 to r/R=+0.98. The ranges of the flow variables covered in this experimental study were: superficial water velocity 0.30~1.03 m/s, quality 0.0085~ ~0.09%, water temperature 291~295 K, system pressure 0.11 MPa absolute and mean bubble diameter 4 mm. It was shown that fully-developed bubbly flow was attained at Z/D=30, while a shorter entrance length was required to obtain fully developed bubbly-to-slug transition flow and slug flow. The results indicated that,

over a large portion of fully-developed bubbly flow, the phases, the velocities of bubbles, and water and the ratio between the velocities of the phases, have flat radial profiles. It was shown that the void fraction distribution was a strong function of the flow pattern and that it changed from a saddle-shaped distribution, which corresponded to bubbly flow, to a parabolic-shaped distribution, which corresponded to slug flow, as the gas flow rate or the quality increased at constant water velocity. The peaking phenomenon of the local void fraction was observed near the pipe wall commonly in the low-quality region. The void peak of the saddle shape profile was observed at a position of about 2~2.5 mm away from the wall, that is, at a distance of nearly one mean bubble radius away from the wall, or at r/R=0.92~ 0.94 (that is, at a distance of 92~94% of the tube radius) measured from the pipe center. Increasing quality at constant water velocity resulted in decreasing the peak value of the void fraction near the wall, compared with the value at the pipe center.

Sekoguchi *et al.* (1981) reported an experimental investigation on vertical upward air-water bubbly two-phase flow with various bubble concentrations. The purpose of the study was to explain the interrelationship between the phase distribution and the heat transfer in bubbly flow and to determine radial profiles of the void fraction, number of bubbles per unit volume and the relation of these parameters to bubble size. The experiments were performed on the test section, a 35.3-mm I.D. and 6.5-

m long vertical tube, and the void fraction profiles were measured by an electrical resistivity probe, which was traversed over the length of one radius R of the tube and at a downstream distance of 5 m from the air injection section. Metered air was introduced into a water stream through air-injection holes of a 0.4-mm diameter, drilled on the tube wall. The resistivity probe consisted of a 0.3-mm diameter platinum wire insulated with polyurethane varnish, except its tip. A 1.6-mm diameter stainless steel tube, which covered the wire, acted as the other electrode. The reference voltage level was established at 40% of the maximum voltage difference between both phases, that is, the maximum voltage signal amplitude. Superficial liquid and gas velocities were in the range of 0.5~3.0 and 0.02 ~0.2 m/s, respectively. The experiment showed that the void fraction profiles depended on the experimental conditions, such as superficial velocities of both phases and number of air-injection holes. From these experiments and other similar studies, the authors classified the void fraction profiles for bubbly flow into three following types: (1) **sliding bubbly flow** characterized by a void faction peak very close to the tube wall; (2) **centrally coring bubbly flow** with a void faction peak at the center of the tube; and (3) **intermediately coring bubbly flow** characterized by a void fraction peak appearing at some distance from the tube wall, greater than those of the first type. The void peak of the sliding bubbly-flow profile (that is, the saddle-shape profile) was observed at a distance of about 0.9~2.3 mm away from the wall, or at a distance of r/R=0.87~0.95 measured from the tube center. The void peak of the

intermediately-coring bubbly-flow profile was observed at a distance of about 3.5~4.6 mm away from the wall, or at r/R=0.74~0.80 measured from the tube center. The experimental measurements of the void fraction, done with the electrical resistivity method, were compared with those of the isolating (quick-closing) valve method. It was reported that the cross-sectional mean void fraction, calculated from the measured values of the void fraction, was in very good agreement with the volumetric mean void fraction measured by the quick-closing valves method.

Takamasa (1988) conducted an experimental study of vertical upward air-water bubbly two-phase flow in an attempt to clarify the effects of wall roughness and entry length on the void profile. Experiments were performed under nearly atmospheric pressure and at room temperature in a 25-mm I.D. vertical circular tube with 2.9-m long test section. The void profiles were measured at three measuring positions with an electrical resistivity probe of double void sensor type, traversed in 24 measuring points across the tube diameter. Superficial liquid and gas velocities were in the range of 0.4~1.6 and 0.035 ~0.17 m/s, respectively. The measuring error due to the inserted probe, which affected the bubble motion, was estimated within ±5% at the flow conditions. The void profile changed from a pattern similar in appearance to the saddle shape, which has local void peaks near the tube wall, into the power law (parabolic) shape with increasing wall roughness and/or tube entry length. Two types of power law shape patterns were observed: a pattern

with a sharp center peak and a pattern with an obtuse center peak. The void profile changed from the former pattern to the latter one with increasing wall roughness and/or tube entry length. It was concluded that the change of the void profile should be considered in connection with the wall friction, since it increases with wall roughness and/or entry length, that is, that the void profiles have the tendency to change from the saddle shape into the power law shape with a friction increase, as well as with decreasing liquid flow rate and/or increasing the gas flow rate. It was also observed that, in stagnant water, the void profiles had almost the same uniform profile independent of wall roughness, which revealed that the wall roughness (friction) can affect the void profile not directly but through changing the liquid velocity and/or its fluctuation. It was also noticed that some void profiles were asymmetric to the axis of the tube. The void peak of the saddle-shape profile was observed at a distance of about 2 mm away from the wall, or at a distance of r/R=0.85 measured from the tube center.

In a very useful report, **Hinata *et al.*** (1991) proposed a **miniature optical fiber sensor**, which can be used to measure the distribution of local void fractions. The sensor consisted of two optical fibers glued together and inserted into a stainless steel support tube. To find the most suitable position of their contact, a light beam was sent through one of the fibers and the intensity of the refracted light beam was observed through another. The fibers were glued together when the position of the

two ends was detected, at which the intensity of the refractive light was the strongest. The tip of the probe was ground and polished to reflect the incident light. In this study, three kinds of probes were constructed with optical fibers of a 20-μm, 40-μm and 125-μm diameter, respectively, to measure the void fraction in the bubble boundary layer near the heating surface, where comparatively small bubbles existed. In the first part of the experiment, the effectiveness of the optical fiber probes was examined by comparing the void signals obtained by the optical fiber probe and an electrical resistivity probe in air-water two-phase flow. The electrical probe consisted of two platinum needles, each with a 25.4-μm diameter, covered with glass tubes of a 40-μm outside diameter; the distance between the two electrodes was 2.885 mm. It was located 50 μm from the tip of the optical fiber probe, so that the void fraction could be detected using the both probes simultaneously. The experimental apparatus was an air-water two-phase flow system, with a vertical 20-mm I.D. transparent acrylic pipe and a bubble generator that could reportedly produce bubbles of almost constant diameter. The optical fiber probe and the electrical probe were inserted through a hole located 5 cm downstream from (above) the tip of the bubble generator. The bubble size was determined from photographs taken by a camera. A halogen lamp was used as the light source. From the results, it was concluded that the measurement accuracy of bubble size was considerably affected by the thickness of the optical fiber probe tip. Thus, it was reportedly difficult to measure bubble size with the probe of 125-μm-

-diameter optical fiber accurately under the conditions of small bubble sizes and high void fractions. The electrical probe with the most miniaturized tip was reportedly excellent in measuring bubble size, followed by the probe of 40-μm-diameter optical fiber. It was reported that the minimum accurately measurable bubble size was about 0.7 mm with the electrical probe, about 0.8 mm with the probe of 40-μm-diameter optical fiber within a relative error of 15%, and about 2 mm with the probe of 125-μm-diameter optical fiber within a relative error of 30%. It was found that a further miniaturized probe of 20-μm-diameter optical fiber could produce more accurate measurements of bubble sizes, if a source (a laser tube) of sufficient light intensity was used. In the second part of the experiment, a test of the applicability of the optical fiber probe to the electrical nonconductive liquids was performed by measuring of the void fraction during nucleate pool boiling of Freon--11 in a horizontal cylindrical container with a concentric heating pipe. The reported measurements of the void fraction distribution around a heating pipe suggested a good applicability of the optical fiber probe to electrical nonconductive fluids.

Liu and Bankoff (1993) reported measurements of the radial profiles of void fraction, bubble velocity and bubble size in air-water bubbly two-phase co-current upflow in a circular 38-mm I.D. pipe, using a miniature dual-sensor electrical resistivity probe. The experiments were conducted with six different superficial liquid velocities, ranging from 0.376 to 1.391 m/s, with seven superficial gas

velocities, ranging from 0.027 to 0.347 m/s, thus employing a total of 42 combinations of two-phase flow conditions. The measured local void fractions were up to 50% and average void fractions up to 42%. Local mean bubble sizes ranged from 2 to 4 mm. The sensing element of the miniature dual-needle electrical resistivity probe was made from a 0.1-mm O.D. (outside diameter) stainless steel drill, welded into a 0.2-mm O.D., 0.1-mm I.D. stainless-steel hypodermic tube, which was insulated by a hot shrinkable tube to serve as a signal conductor. Two separate identical sensors were encased in a 30-mm long, 3-mm O.D. stainless--steel tube to form a dual-sensor resistivity probe for gas-phase local-parameters measurements. It is interesting that the authors observed that the void-fraction, bubble-frequency and bubble-size profiles all showed distinct peaks near the pipe wall, becoming flat at the core (r/R<=0.8). The experiments showed that increasing the gas flow rate at a constant liquid flow rate resulted in an increased void fraction, both in the core region and in its peaking region near the wall. Wall peaking became more pronounced for high liquid flow rates, with a relatively sharp peak near the wall (at r/R=0.88~0.90) and a small amount of bubbles nearly uniformly--distributed in the core region. At lower liquid flow rates, a more uniform void distribution was observed at all gas flow rates, with a relatively lower peak near the wall (at r/R= 0.92). Similarly, it was observed that increasing the liquid flow rate at a constant gas flow rate resulted in a decreased void fraction, both in the core region and in the peaking region near the wall (at r/R=0.88~0.90). The bubble

frequency also decreased in the core region, but reportedly increased near the wall, and, consequently, the authors concluded that the bubble frequency near the pipe wall becomes larger for higher liquid flow rates. The experimental data of the void fraction were compared with the above reported data of **Serizawa *et al.*** (1975). While a similarity of the void fraction profiles existed for lower gas flow rates, large discrepancies were noted for higher gas flow rates, which were probably caused by the different entrance geometry and gas injection method, causing different size and configuration of bubbles. The authors concluded that the different bubble size distributions may even result in different flow regimes at the same liquid and gas flow rates.

Leung *et al.* (1995) studied the local geometric and statistical characteristics of upward co-current dispersed bubbly two-phase flow in a vertical pipe, both at the entrance (L/D=8) and at a region far away from the entrance (L/D=60). The test section was made of a 50.8-mm I.D. and 3750-mm long Lucite pipe. The experiments were conducted with four superficial liquid velocities, ranging from 0.1 to 1.0 m/s, in combination with four superficial gas velocities, ranging from 0.02 to 0.1 m/s. With these experimental conditions, the void fraction ranged from 2.4 to 27%, which was in the bubbly flow regime. A dual-sensor electrical resistivity probe was employed to measure the radial profiles of void fraction, interfacial area concentration, bubble velocity and bubble frequency. The first error of the void

fraction measurement, due to the sensor tip wetting characteristics, was reduced by choosing a proper threshold level on the probe signal and was reportedly less than 4%. The second error, due to the electronic circuit response and the data acquisition system, was reportedly about 2.5%. Consequently, the total error of the void fraction measurement of about 7% was reported. A two-phase pressure drop measurement was used for the void fraction comparison and the frictional pressure drop was calculated by the homogeneous model. The comparison of the cross-sectional average void fraction showed that most of the probe-method data were within a ±20% error range compared with the data from the pressure drop measurements. The authors recognized that the overall error of the local measurements, including the void fraction measurements, was much larger than the estimated one, mainly because the void fraction distribution was not axially symmetric and measurements were taken in one azimuthal direction only. It was observed that at the entrance region (L/D=8) of the test section all the radial void fraction profiles showed a bubbly flow distribution with the void fraction peaking near the pipe wall, at r/R=0.86~0.89, or about 2.8~3.5 mm from the pipe wall. The local void fraction began to rise at roughly r/R=0.78, or about 5.6 mm from the pipe wall and this spacing was roughly 1.5 times the reportedly typical bubble size (3.7 mm). In the fully developed region (L/D=60) of the test section, it was observed that the near-wall void peak (at r/R=0.89~0.91, or about 2.3~2.8 mm from the pipe wall) was higher for higher liquid flow rates and lower for lower liquid flow rates,

compared with the one at the entrance region. The radial void fraction distribution changed very little from the entrance region to the fully developed region, except in the case of the lowest liquid flow rate (superficial velocity of 0.1 m/s). Here, the radial void faction profile changed from a wall peak to a parabolic distribution as the flow developed from the entrance region to the fully developed region.

Zun (1985) investigated the principles that govern radial phase distribution in vertical co-current air-water two-phase bubbly flow. The experiments were performed to identify the role of bubble lateral movement due to vortex feedback. The experimental facility consisted of a vertical 25.4-mm I.D. 2100-mm long tube with a transparent test section. The void fraction, bubble velocity and the bubble dispersion coefficient profiles were measured by micro-resistivity probes of a 0.011--mm tip diameter. The frequency of bubble generation was detected by laser system and determined via auto-correlation function. The results showed that the convex (parabolic), concave (saddle-type) and intermediate void profiles, or the radial locations of void peaking in a tube, at fully developed bubbly flow were determined by the bubble lateral displacement from the rectilinear path and the corresponding frequency of bubble oscillation. It was observed that the higher the frequency of bubble oscillation, the stronger was the bubble wall void peaking, while, on the other hand, the bubbles with the rectilinear motion exhibited parabolic distribution. The experimental results and the void profiles measured by Serizawa in 1974 and

by **Sekoguchi *et al.*** (1981) (reported above) were compared and they all showed a very good agreement with the proposed theoretical model. It is interesting that all the three groups of experimental results showed the saddle-type profile wall void peaking at r/R=0.8~0.9 for similar geometrical and flow conditions.

Sorour and El-Beshbeeshy (1986) experimentally investigated the void fraction profiles and the pressure fluctuations of two-phase two-component air-water bubbly flow in a vertical annulus using an electrical resistivity probe. The experimental apparatus consisted of a copper vertical annulus with 75-mm outer and 38-mm inner diameters. The effective length of the annulus was 3.25 m. The apparatus included 11 measuring stations located on the outer surface of the outer cylinder, allowing traversing of the probes in the radial direction. The authors reported that they did not assess the exact determination of the local void fraction values at the points very close to the walls, because the local void fraction measurements by the electrical resistivity probe technique at this region showed interference in the signal. It was, furthermore, assumed that the local void fraction at the wall was zero. It was observed that the concentration of the gas bubbles was closer to the inner annulus wall for low gas fluxes and that the liquid flux had a negligible effect on the average void fraction within the range of the experimental investigation. The observed radial void fraction profiles were all of the typical parabolic shape. They were compared with the (above reported) results of **Serizawa *et al.*** (1975) and those of

other researchers (Sato *et al.* in 1981 and Sadatomi *et al.* in 1982), which showed the saddle-type radial void fraction profiles in vertical cylindrical tubes for similar values of the void fraction. The difference was explained by the method of introducing air in the duct used, but it also emerges from the different geometries used: an annulus in the case of this investigation and, on the other hand, a cylinder in the case of the above-mentioned investigations. Thus, for some investigations with the similar parabolic radial void profiles as in this report, the air was introduced axially through the duct cross sectional area, while it was injected radially from the periphery of the duct in the two above-mentioned investigations.

The following experimental studies include measurements of the void fraction / radial void fraction distribution using optical fiber probes or electrical resistivity probes, although they are not strictly related to bubbly two-phase flow in vertical tubes:

Moore and Turley (1983) reported experimental work on measuring of the pressure and void fraction fluctuations in a 54-mm I.D. horizontal perspex pipe, using closely mounted pressure transducers and an **optical fiber probe**, consisted of a 55-μm single optical fiber bent into a 'U' shape. The probe was mounted to traverse horizontally across the pipe diameter, and the void fraction measurements were taken at 6 radial positions. Local void fractions obtained for each traverse position

were plotted to obtain void profiles of the flows. It was concluded that the void fraction decreased sharply at the wall location due to boundary layer effects. The plotted void fraction profiles in the horizontal pipe were all of a flat (obtuse peaked) parabolic type. The corresponding measurements of the void fraction were taken in bubbly, plug and slug flow regime. Passage of some small bubbles and droplets at velocities higher than 4 m/s could not be recorded with this optical probe.

Mann and Hackett (1985) experimentally evaluated a **miniature optical fiber** phase detection technique on a simple easily-visualized gas-liquid system, consisting of a section of double glazing partly filled with water through which nitrogen was bubbling. In the experiments, the superficial gas (nitrogen) velocity ranged from 0.01 m/s to 0.05 m/s. A **miniature optical fiber probe** with a single optical fiber sensor that was bent into a 'U' shape at the probe tip, reportedly capable of detecting bubbles down to a 0.4-mm diameter, was used to gather statistical information on bubble frequency distributions. The optical fiber had a diameter of 40 μm and provided a sensing tip of a 100-μm diameter. It was mounted in a 3-mm diameter stainless steel tube and sealed in with epoxy. The probe signal was amplified, so that the liquid phase at the probe tip produced a 5-V signal and the gas phase at the probe tip produced a signal of up to 4.4 V. The probe signal was conditioned in the static trigger level mode, which meant that when the signal rose above a certain value between 5 V and 4.4 V (the static trigger level), a step

drop appeared in the phase indicator unit (PIU) output, from 5 to 0 V. Similarly, when the probe signal fell below the static trigger level of 4.4 V, a step rise occurred in the PIU output, from 0 V to 5 V. Thus, after conditioning of the probe signal, a 5-V signal indicated gas, while a 0-V signal indicated liquid at the probe tip. A light emitting diode was connected into the static trigger level circuitry, showing the presence of the gas phase at the probe tip by flickering during experimental runs.

Annunziato and Girardi (1985) experimentally used statistical methods to identify upward air-water two-phase flow regimes by pressure drop and local void fraction fluctuations' analysis. The authors concluded from their previous work that the flow pattern maps available in literature could not be well extended to two-phase flows in large-diameter tubes, because they were produced from small-diameter tubes tests. Therefore, they tried to improve the existing flow pattern maps by the direct measurement of some two-phase flow parameters, such as "local-centerline" void fraction and "local" pressure drop, and the statistical analysis of their fluctuations related to local density fluctuations. The tests were performed in a vertical perspex tube of a 92-mm I.D. and 3700-mm long, for a wide range of gas and liquid flow rates at atmospheric pressure and room temperature, using **optical fiber probes**, pressure transducers and a γ-ray apparatus. The local void fraction measurements were made by using optical probes in the center of two different cross sections. The optical probes had 2-mm sensitive head and were used with 0.01-s integration time.

These tests were done for 20 combinations of air and water flow rates, thus covering all types of flow regimes: bubbly flow, slug flow, churn flow, pure annular flow and wispy-annular flow with some liquid wisps entering the gas core. During the tests, the flow pattern types were determined by visualisation and analyzing the signals from two optical probes located in nine different measurement points along a half diameter of the tube cross-section. These measurements were reportedly very useful in determining the flow transitions: "pure annular-wispy annular", "churn--annular", "bubbly-annular" and "bubbly-intermittent" (i.e., to slug and churn flow). The radial voidage profiles were not measured.

Barnea and Shemer (1989) studied various flow patterns and the transitions between them using a conductance (electrical resistivity) probe to detect the instantaneous void fraction at the centerline of a 10-m long 50-mm I.D. vertical Plexiglas tube in an upward air-water two-phase flow, for a wide range of gas flow rates. The purpose of the investigation was to develop a reliable and simple method for the estimation of the liquid slug length, the average holdup within the liquid slug and the voidage in the near wake of the Taylor bubble. The experiments were carried out at a constant superficial liquid velocity of 0.01 m/s and at a wide range of air flow rates, which covered void fractions from 0.1 to 0.8 and, thus, included bubbly, slug and churn flow patterns. The local instantaneous void fraction was detected by measuring the electrical conductance between a tip probe and a flat

large electrode, as a function of time. The selected length of the time "window" corresponded to a passage of a column of length equal to twice the tube diameter, 2D, at the characteristic translation velocity of Taylor bubbles. The value of 2D was assumed to be the minimum length of a Taylor bubble and therefore served as a criterion for distinguishing between dispersed and elongated bubbles.

Kocamustafaogullari and Wang (1991) experimentally investigated the internal phase distribution of co-current air-water bubbly two-phase flow in a 50.3-mm I.D. transparent horizonal pipeline, using a double-sensor electrical resistivity probe. The probe consisted of two identical stainless-steel wire sensors of a 0.25-mm diameter, whose tips were 2.5 mm apart. The smaller separation distance of 2.5 mm for horizontal bubbly flow in comparison with that of 5 mm, which has been usually used in vertical bubbly-flow experiments, was chosen because it was found that a smaller separation distance was required in horizontal bubbly flow, where maximum packing of bubbles usually occurs toward the top of the pipe. The electronic circuit used a 4.5-V D.C. power supply. The experiments were carried out under fully-developed bubbly flow conditions, by variations in the liquid and gas flow rates and the radial position of the probe. Liquid and gas volumetric superficial velocities ranged from 3.74 to 5.71 m/s and from 0.25 to 1.37 m/s, respectively, and average void fractions ranged from 4.30 to 22.5%. The experimental results showed that the void fraction, and also the interfacial area concentration and the bubble frequency

had the local maxima near the upper pipe wall and that the profiles flattened with increasing the void fraction. The observed peak local void fraction for horizontal bubbly flow could reach 0.65 or 65%. It was found that either decreasing the liquid flow rate at a constant gas flow rate, or increasing the gas flow rate at a fixed liquid flow rate would increase the local void fraction, as well as the interfacial area concentration and the bubble frequency.

Van Hout *et al.* (1992) experimentally studied the structure of vertical upward slug two-phase flow in a 10-m long 50-mm I.D. vertical Plexiglas pipe. The distribution of the phases in the Taylor bubble zone and the liquid slug zone was investigated by simultaneous measurements with **two optical fiber probes**. They were installed at the same axial position in the pipe, at about 6 m from the inlet mixing device. One of the optical fiber sensors was placed stationary at the centerline of the pipe, while the other sensor was installed such that its radial position in the pipe could be changed easily by a traversing mechanism mounted on the pipe. The center probe served as a reference, which enabled the determination of the locations of the interface between the Taylor bubbles and liquid slugs. Measurements were taken at 11 radial positions in the pipe, including the centerline, and they were carried out for 8 flow conditions, with superficial velocities of liquid and gas ranging from 0.01 to 0.75 m/s and from 0.10 to 0.75 m/s, respectively. The two optical fiber sensors used reportedly had high frequency response and good spatial resolution due to a

very small fiber tip diameter (of the order of a few μm), which did not disturb the flow. The two-dimensional spatial distribution of the void fraction within the liquid slug was investigated. At each radial location the sampled data were averaged over a relatively short time "window". The measured voidage profiles suggested that the liquid slug could be divided into three distinct regions: the wake region (long about 2 or 3 pipe diameters behind the Taylor bubble), the developed region of the liquid slug (from length of about 10 D behind the Taylor bubble), in which the voidage radial profiles attained their permanent shapes, and the region between these two, considered as an intermediate region. It was observed that the radial distributions in the developed region of the liquid slug were similar to those in the dispersed bubble flow pattern (a saddle type void profile) and that a voidage peak near the pipe wall appeared at all flow condition employed in this study, at r/R=0.79~ 0.83 or at about 4.5~5.5 mm from the wall. In this respect, the authors mentioned, among others, the previous investigations of **Serizawa *et al.*** (1975) (reported above), Zun in 1988 and Zun and Moze in 1990. It was noted that the extent of the wake region increased with increasing mixture velocity.

Hinata *et al.* (1992) reported an experimental study of void fraction and temperature profiles in nucleate pool boiling of Freon-11 around a horizontal cylindrical copper surface. The distribution of the local void fraction was measured by the miniature optical fiber sensor reported in **Hinata *et al.*** (1991), which

consisted of two optical fibers with a 45°-surface at each end. Another optical fiber sensor was attached to the sensor parallel to the axis. The probes were traversed from the heating surface along the radial direction for selected angular positions, while the distance from the heating surface was measured by a micrometer attached to the upper end of each probe. Local void fraction distributions along the radial direction at six angular positions were presented, and also constant void fraction curves around a heated wall. The error in void fraction measurement by the optical fiber probe was not estimated.

Carrica *et al.* (1992) reported a series of measurements of the local void fraction distribution in saturated water pool boiling, by means of a **sapphire optical probe** placed above a horizontal heater plate. Two sets of experiments were performed: a temporal evolution of the void fraction during a linear slow power ramp and average steady-state void fraction at fixed constant heat flux.The optical probe was located at the heater center on the horizontal plane. A locating system was used to position the probe in the vertical direction. The sensitive part of the probe was a 0.5-mm-diameter cone. A 5-V signal from the optical probe indicated presence of gas, while a 0-V signal indicated presence of liquid at the probe tip.

Andreussi *et al.* (1993) experimentally investigated air-water slug two-phase flow at atmospheric conditions in horizontal pipes of 31-mm and 53-mm I.D., using local

(optical) and cross-sectional (conductance) probes. Local measurements included the radial void fraction distribution in the liquid slugs. The local void fraction was measured by an **optical fiber probe**, which had a sensitive tip of a 0.7-mm diameter and was mounted on a micrometric head to determine the void distribution profiles in the pipe cross-section. With this probe it was reportedly possible to measure the void fraction distribution in front or at the back of a liquid slug.

Das and Pattanayak (1994) reported a method of void fraction measurement based on a technique of pulse width modulation in response to the changing electrical impedance of a gas-liquid mixture flowing through vertical small-diameter tubes. The test section was made of an acrylic tube of 11-mm I.D. and 2.9-m length. An air and water mixture was injected into the base of the test section. An electrical resistivity probe with three types of electrodes was used to measure the void fraction. The first type consisted of two electrodes made in the form of 90°-arc and glued to the inside tube wall. They were used primarily for the measurement of the average void fraction ranging from 0 to 100% and the void fraction in slug and churn flow regimes, because they reportedly had a reasonable sensitivity in all flow regimes and they minimized obstruction in the flow field and the error of measurements due to cavitation. The second pair of electrodes, "the wide-gap electrodes", was placed so that the tip of one electrode was exposed to the center of the flow passage and the other one was exposed to the inside wall. They were

the most suitable for the void fraction measurements in the bubbly flow regime. The third pair of electrodes, "the narrow-gap electrodes", had both the electrode tips exposed to the center of the flow passage, with a gap of 1.6 mm between them. They were the most suitable for the void fraction measurements in the annular flow regime. The quick-closing-valve technique was used to calibrate the resistivity probe in all flow regimes, and to compare measured values of the average void fraction with values obtained by the quick-closing-valves technique. An error of about 2% of the average void fraction value was reported. It was observed that fluid flow rates (superficial velocities) affected calibration curves in slug and churn flow regimes, while they did not affect calibration curves in bubbly and annular flow regimes. A method of flow regimes identification was proposed in terms of number and position of the peaks of the probability distribution function at the particular void fraction, depending on the type of electrodes used.

Moujaes (1990) reported a new way of constructing the tip of a **spherical dual--tipped optical fiber probe** for measurement of different two-phase flow variables, such as the local time-averaged void fraction, gas velocity and interfacial bubble passage frequency. The probe was used in co-current air-water two-phase flow in a rectangular channel and in a 4X3 rod-bundle geometry in bubbly and slug flow regimes. The spherical dual-tipped probe was made from 2 thin 76-μm optical fibers, fused to form a miniature 200-μm-diameter spherical bead. This bead was

placed inside a hypodermic tube of 330-μm O.D. and the tip was covered with epoxy. The advantages of this tip, compared with the tip of a 90°-chamfered dual tip probe, were shown experimentally. These included a superior signal-to-noise ratio with a decrease in tip size of almost 50% while using the same optical fiber thickness. Decreasing the size of the tip resulted in a faster penetration time of bubbles or slugs, which improved the probe signal and the accuracy of the void fraction measurement. Construction of the spherical tip was estimated to be easier than construction of 90° wedge tip, because no tip chamfering was needed, which was assessed as a delicate and time-consuming operation. The proposed probe tip reportedly had similar good response characteristics to the "U-shaped" single optical-fiber-probe tip at higher gas velocities, with an ample voltage discriminating threshold between gas and liquid levels. The difference in signal voltage between the tip being immersed in the gas versus liquid was experimentally found between 0.3 V and 0.5 V. The signal from the spherical tip was reportedly insensitive to changes in bubble velocity and had the same time duration as it changed from liquid to gas (and vice versa) for the same bubble velocity. The probe was calibrated by comparing the calculated gas velocity with the measured gas velocity (the bubble interface velocity) and a spreading of the gas velocity values was reported of about ±7% from the mean.

From the above review, it can be noted that the available data tend to be limited to

two-phase flow in relatively small pipe diameters, typically smaller than 10 cm. The experimental investigations of **Serizawa *et al.*** (1975), **Sekoguchi *et al.*** (1981), **Takamasa** (1988), **Liu and Bankoff** (1993) and **Leung *et al.*** (1995) gave a very good insight into the two-phase flow structure in vertical tubes. These studies also showed that a saddle-shape void profile could exist in bubbly flow in small-diameter pipes, especially at low qualities (gas flow rates) and high liquid flow rates. The reports of **Hinata *et al.*** (1991) and **Moujaes** (1990), and some other above mentioned reports, gave valuable information on optical fiber probes construction, operation, sensitivity and accuracy. It can be noted that the sensitivity, and therefore, the accuracy of an **optical fiber probe** can be increased with decreasing the size of its tip, thus approaching to the accuracy of an electrical resistivity probe.

Unfortunately, both types of local probes still provide inaccurate results when calibrated against the quick closing valves method, as the most accurate of all available techniques for the void fraction measurement. This fact, together with an obvious need for further investigations of radial void profiles in large vertical pipes, makes a strong impression that the optical fiber probe technique deserves to be further investigated and tested for the sake of improving its accuracy. This was one of the main reasons for undertaking of the present work.

CHAPTER THREE

EXPERIMENTAL TEST FACILITY

3.1. EXPERIMENTAL LOOP

The test facility used in the present investigation is schematically shown in Figure 3.1 on page 65. It was designed as a low-pressure air-water loop that can be operated either in a **natural circulation mode**, as an air lift pump, or in a **forced circulation mode** using a centrifugal water pump. The main components of the facility are the following: the riser pipe, which includes the test section, downcomer pipe, separation tank, a stand by pump, air injection line and connecting piping and valves.

The riser consisted of transparent acrylic pipes to facilitate two-phase flow visualization. A vertical pipe with 20-cm inside diameter was used for the riser during the experimental program. The height of the transparent riser section was 9.5 m. It should be mentioned that initially many tests were performed in a 10-cm-diameter 5.5-m-high riser pipe. The reasons for using 10-cm diameter pipe were: to compare the results with those of AECL's test loop, to check if slug flow exists in

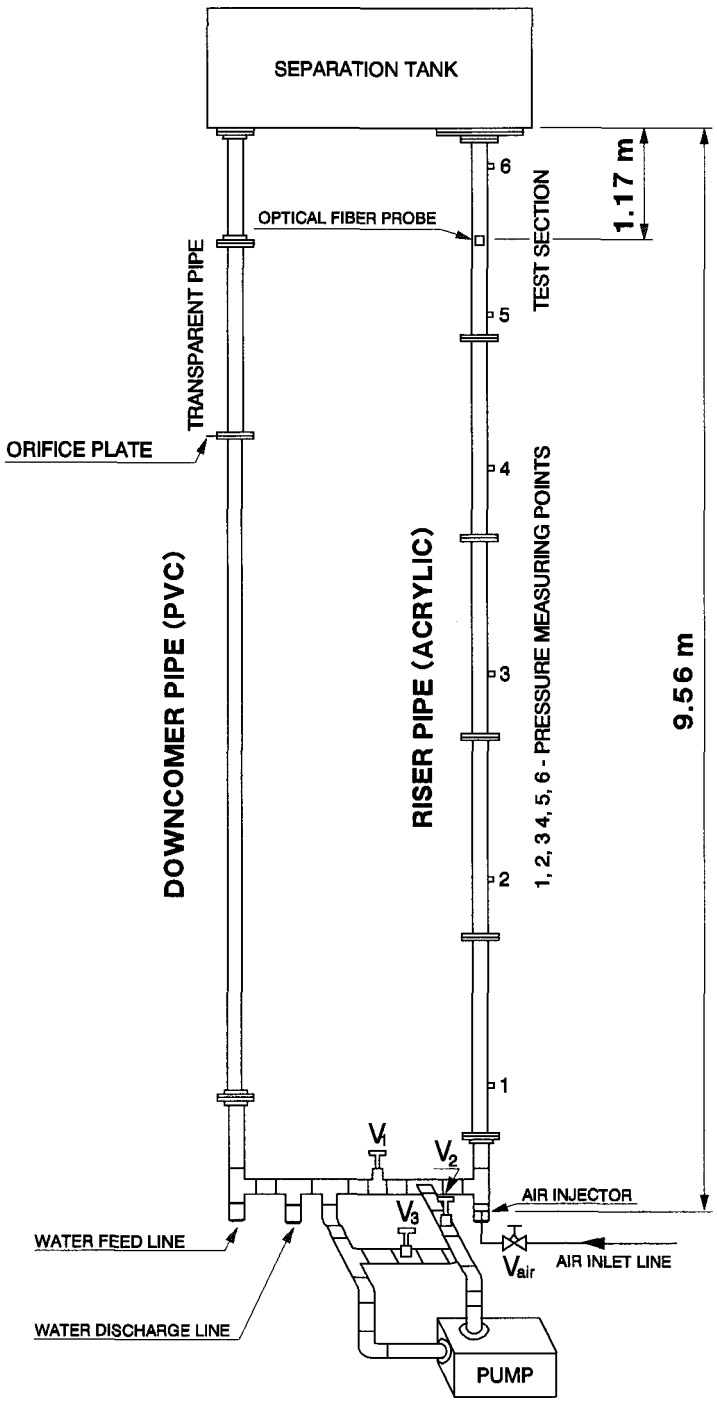

FIGURE 3.1: SCHEMATIC OF THE TEST FACILITY

a 10-cm vertical pipe and to calibrate the optical fiber probe using a gamma densitometer. The results of these tests are not presented in this thesis, but only the tests performed in the 20-cm-diameter 9.5-m-high riser pipe; readers interested in these results are referred to paper **Nada *et al.*** (1996) from the Cairo International Congress in December 1996.

The downcomer consisted of 10-cm diameter PVC pipes, including a 1.3-m long transparent acrylic section, which was installed for visual observation of the flow, to ensure that only single-phase water flow was coming down in the downcomer. The downcomer had the same height as the riser. Both the riser and the downcomer were connected at the top to an air separation tank. The riser's pipe was extended into the tank to about 50-cm height, to discharge the two-phase mixture to a level higher than the water level in the tank.

The riser and the downcomer were connected at the bottom by a 10-cm diameter PVC pipe, with a gate valve (V_1 in Figure 3.1) for controlling the water flow rate. A centrifugal stainless-steel pump, with rating of 450 US gallons/min at 10-m head, was installed in a bypass line, together with gate valves V_2 and V_3 (Figure 3.1). These valves served to start the pump and to adjust the water flow rate, respectively, when tests were to be performed in the forced circulation mode. When the facility worked in the natural circulation mode, the valve V_1 was fully open and

the valve V_2 fully closed at all times. On the other hand, the valve V_1 was fully closed while the valve V_2 was fully open always, when the facility worked in the forced circulation mode. The valve V_3 in the bypass line was fully open in both cases, but it was gradually closed to adjust the water flow rate in the riser when pump was operating.

The air separation tank was made as a 2.25-m long, 0.93-m wide and 0.79-m high rectangular stainless-steel tank. The schematic of the separation tank is shown in Figure 3.2 on page 68. The air separation from the two-phase flow mixture incoming into the tank was ensured by having long separation path and large separation interface area. As it was already mentioned, the riser pipe was extended into the tank to about 50-cm height to discharge the two-phase mixture to a level higher than the water level in the tank, which was the necessary condition for achieving successful separation of phases. In the case of low mass flux tests, the two-phase mixture was discharged at the riser exit, with liquid falling down as a free falling film. For high mass flux tests, a reflector plate, which was installed at a higher elevation in the tank than the flow exit, helped in separating of phases in the high momentum flux two-phase mixture. A baffle plate was welded in the middle of the tank, with a 2.5-cm gap between the plate and the bottom of the tank. The baffle plate reduced the flow disturbances and improved the separation by forcing any trapped bubble to flow up closer to the water surface. The separated air at the upper part of the

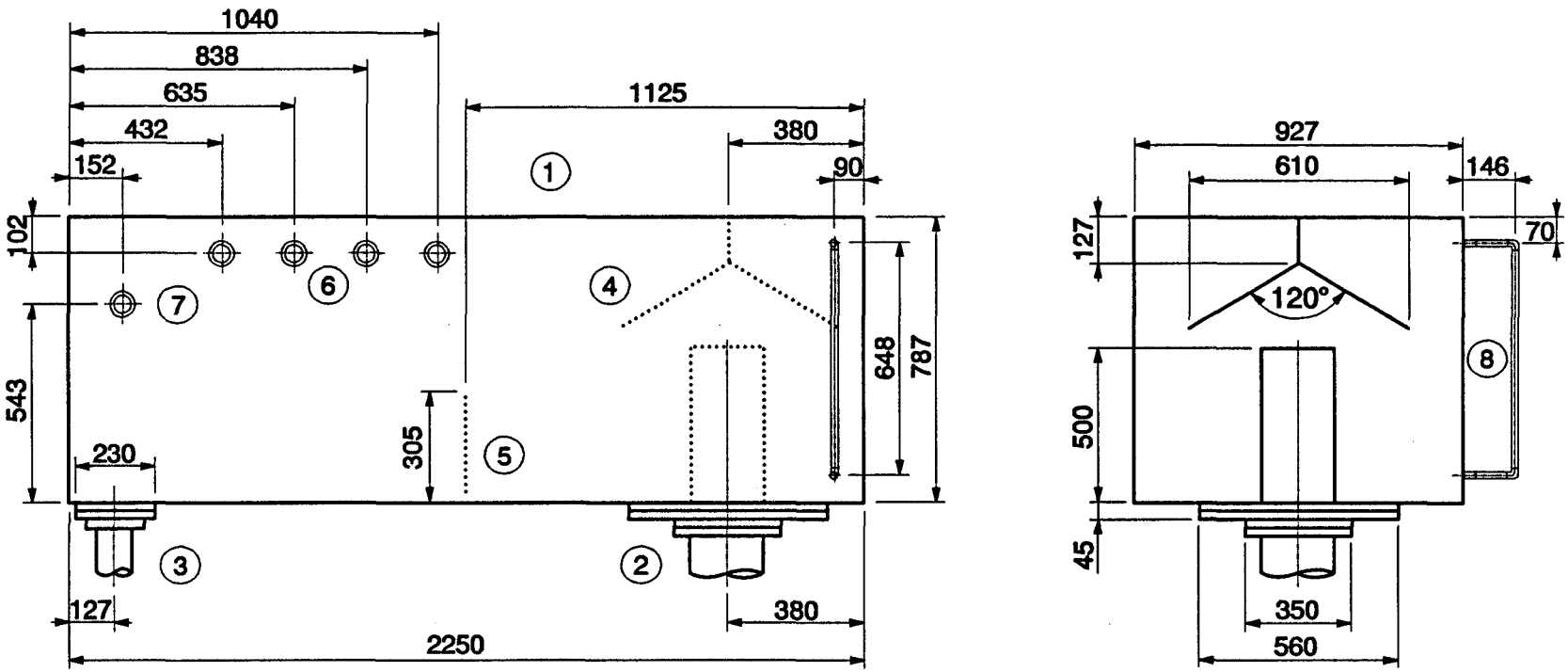

FIGURE 3.2: SCHEMATIC AND DIMENSIONS OF SEPARATION TANK

tank was finally vented out through 4 openings near the top of the tank. For natural circulation tests, an operational water level of 10 to 20 cm was sufficient to ensure perfect separation of the phases. This level needed to be raised up to about 40 cm for forced circulation tests, which was necessary to eliminate the possibility of drawing some bubbles down the downcomer by the effect of pump suction. In the case of a very high water level during the filling of the loop, the overflow was discharged through a large-diameter hose, which was attached to an appropriate opening near the top of the tank. The tank was equipped with a sight glass for water level observation.

Compressed air was supplied to the test facility by a 5.08-cm stainless-steel pipe inlet line, as shown in Figure 3.3 on page 70. The air was filtered in a filter and its pressure was manually controlled by a pressure regulator before injection into the test facility. It was then injected upstream of the riser, at an elevation lower than the horizontal PVC pipe connecting the downcomer and the riser, as shown in Figures 3.1 (page 65) and 3.10 (page 88). The air was injected upward through a circular disc made as a showerhead-like sieve, with a large number of 1-mm diameter holes and 3-mm spacings between the holes. The circular disc covered almost the entire 10-cm pipe cross-section. A honey comb flow straightener and a coarse grid mesh were installed downstream, at the inlet of the riser, to reduce swirling and to improve radial bubble distribution. The air flow rate was manually adjusted by a

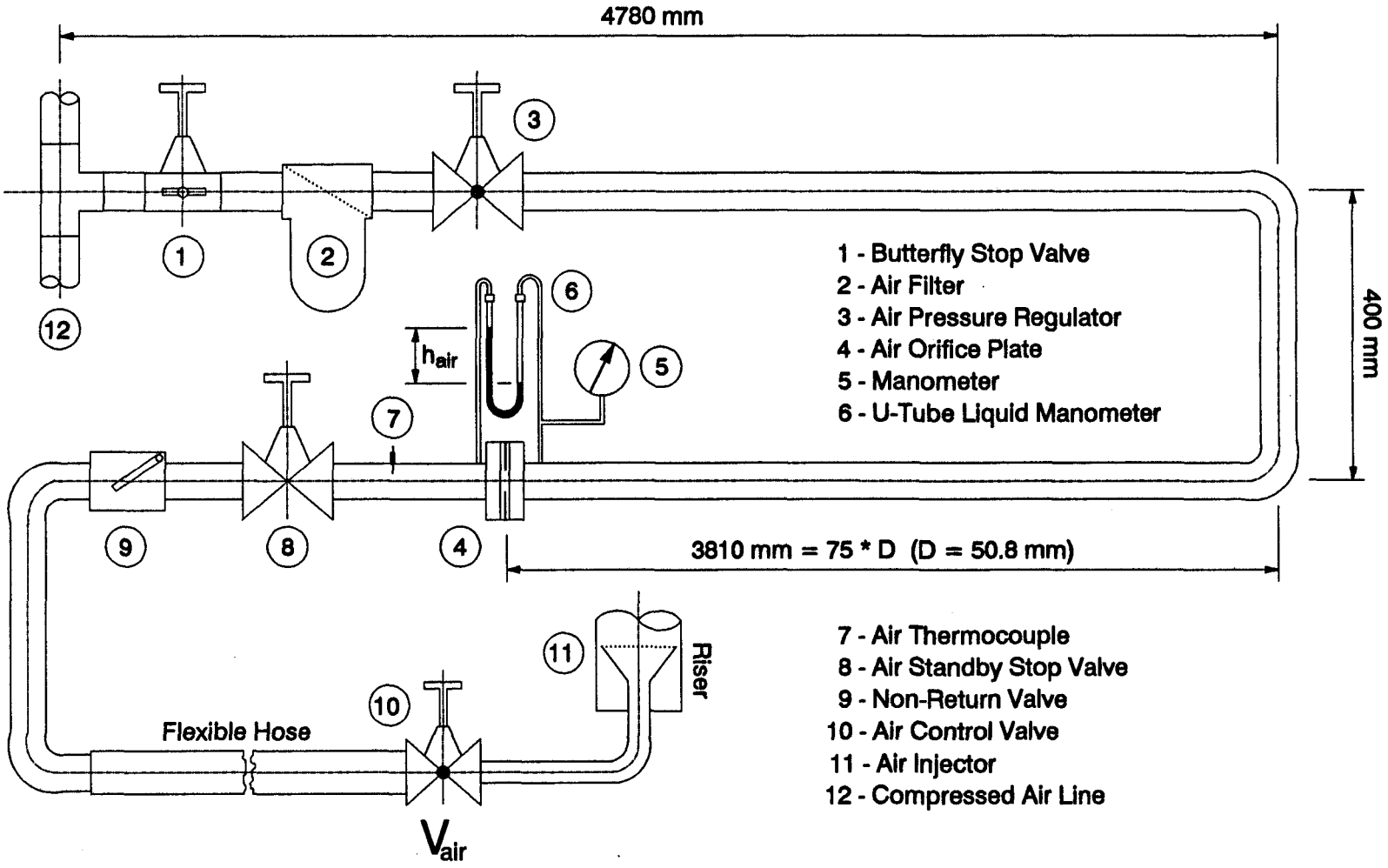

FIGURE 3.3: SCHEMATIC AND DIMENSIONS OF AIR INLET LINE

control valve (V_{air} in Figures 3.1 and 3.3). The air inlet line was also equipped with a non-return valve and a standby stop valve, to eliminate a possibility of air line flooding with water from the test loop, in case of a failure of the air control valve to close fully.

3.2. MEASUREMENTS AND INSTRUMENTATION

The measurements performed during the tests included: air and water flow rates, radial void fraction distribution, the cross-sectional averaged void fraction, pressure drop along the test section and air and water temperatures. Most of the instruments for these measurements are depicted in Figures 3.1 and 3.3.

Both air and water flow rates were measured by orifice plates (orifice meters), supplied by a manufacturer (Daniel Industries). The orifice plates corresponded to ASME Standards and, accordingly, they were not calibrated. Several orifice plates, with various orifice sizes, were used to cover the entire range of test conditions. The pressure drop across the water orifice plate was measured by a pressure transducer, while a U-tube liquid manometer was used to measure the pressure drop across the air orifice plate (Figure 3.3). For lower air flow rates the U-tube

manometer was filled with water, while for higher air flow rates the manometer liquid was mercury. Height of the liquid (h_{air} in Figure 3.3), or voltage from the pressure transducer, was then converted into a corresponding pressure drop and the volumetric flow rate of air or water was then calculated from:

$$\dot{Q}_{PH} = K * Y * \beta^2 * A * \left(\frac{2 * \Delta p_{op}}{\rho_{PH}}\right)^{1/2} \qquad (3.1)$$

where: subscript "$_{PH}$" denotes the appropriate phase, subscript "$_{op}$" means that pressure drop belongs to the appropriate orifice plate, "K" is the flow coefficient, "Y" is the compressibility (expansion) factor and "β" is a diameter ratio, that is, the ratio of the orifice plate diameter and diameter of the corresponding pipe (the air line or the downcomer pipe). The flow coefficient depends on the pipe Reynolds number and the diameter ratio. According to **ASME Report on Fluid Meters** (1959), its value is about 0.65 to 0.66 for a diameter ratio of 0.6 and a 10-cm diameter pipe (water orifice plate), or about 0.60 for a diameter ratio of 0.2 and a 5-cm diameter pipe (air orifice plate). These values of the flow coefficient were interpolated from appropriate tables of **ASME Report** (1959) for all tests, depending on the calculated air or water Reynolds numbers. The values of corresponding diameter ratios (0.6 and 0.2), used during the experiments carried out in this investigation, were provided by the manufacturer of the orifice plates (Daniel Industries). The

compressibility factor Y is, of course, equal to unity for water as an incompressible fluid, but it is somewhat smaller than one for air. It depends on the diameter ratio $ß$, the ratio of specific heats $k = c_p/c_v$ (assumed to be 1.4 for air as an ideal gas) and a pressure ratio r, defined as:

$$r = \frac{p_2}{p_1} = 1 - \frac{\triangle p_{op}}{p_{air,inl}} \tag{3.2}$$

where subscript "$_{air,inl}$" refers to the air inlet line condition. The compressibility factor was then calculated from the following equation:

$$Y = [r^{2/k} * (\frac{k}{k-1}) * (\frac{1-r^{\frac{k-1}{k}}}{1-r}) * (\frac{1-ß^4}{1-ß^4 * r^{2/k}})]^{1/2} \tag{3.3}$$

Pressure measuring points (Figure 3.1) were located at 1.5-m intervals along the riser pipe. The pressure profile along the riser can be obtained using a multi-tube mercury manometer. This was done for tests performed in the 5.5-m high riser, in which case the intervals between the pressure measuring points were 1 m long. The most important pressure measurement is the one between pressure measuring points #5 and #6, that is, in the test section, from which the pressure gradient in the test section was measured using a pressure transducer. This measurement was used to estimate the average volume void fraction in the test section. The radial

void fraction distribution was obtained from a **laser optical fiber probe** with signal processing system, supplied by AECL. The probe was located in the center of the test section, 1.17 m below the separation tank bottom (Figure 3.1). Two thermocouples of the "K" type were installed in the air inlet line and the riser pipe for temperature measuring of air and water (or two-phase mixture), respectively.

All measurements were acquired using a computer-based data acquisition system. The signals obtained during the tests included: pressure drops across the water orifice plate and the test section, temperatures of air and water (two-phase mixture), and void fraction signals from the gamma-densitometer and the optical fiber probe.

3.2.1. Void Fraction Measurements using Optical Fiber Probe

Radial distribution of the local void fraction was measured by an **optical fiber probe** (Figure 3.4 on page 75), which was traversed across the riser cross section each 10 mm, from one pipe wall to another, in case of the 10-cm diameter pipe, or each 5 mm, from the pipe center to the pipe wall, in case of the 20-cm diameter pipe. The probe was of a **dual-sensor type** with 90°-chamfered dual tip (the probe design depicted in Figure 2.6 on page 36), capable of measuring both the void

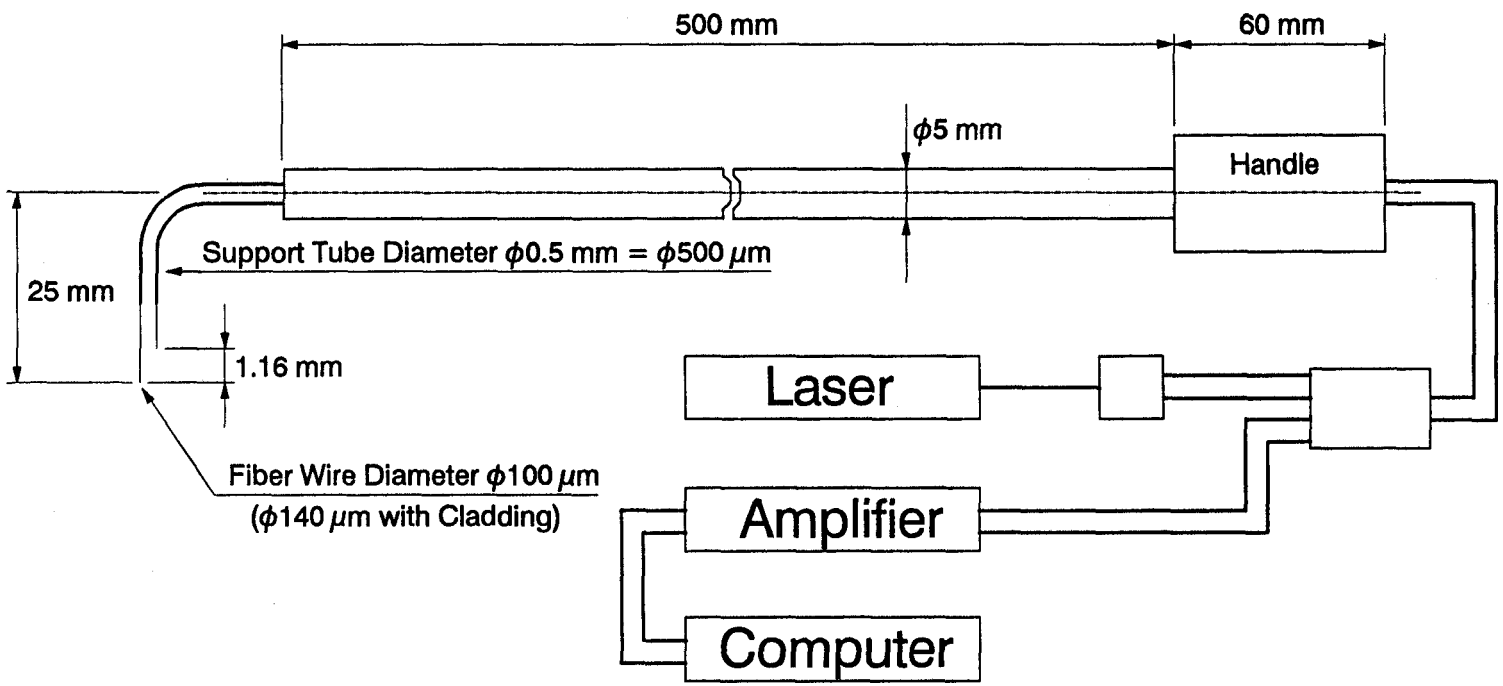

FIGURE 3.4: OPTICAL FIBER PROBE SYSTEM AND DIMENSIONS

fraction (using only the longer probe tip) and the local interface velocity (using both probe tips). The two optical fiber sensors, with a 45°-chamfered surface at each end of the tip and a wire diameter of 100 μm (140 μm with cladding), detected the difference between the liquid and gas phases based on the change of the index of refraction of the medium (phase) surrounding the sensor tip, as explained in Chapter 2, Part 2.1.2. Incident light was released from the laser source, a 15-mW Helium-Neon laser, and then transmitted through both sensors. It was then reflected at the probe tips, always when the laser beam hit a gas bubble, and returned through the same fiber sensor. In the measurements of this experimental study, only the fiber sensor with the longer tip was used at all times, since the objective was to measure only the void fraction in the two-phase mixture. The light signal returned through the optical fiber was converted into an electric current by a photodiode, whose output was subsequently amplified and recorded by a computer-based data acquisition system. Detailed dimensions of the optical fiber probe are shown in Figure 3.4 on page 75.

The time fraction during which the gas phase was surrounding the probe tip, or the probe residence time in void, was determined according to the change of intensity of the reflected light beam. The local void fraction at each radial position was calculated by the computer program LabVIEW as a ratio of the probe residence time in void and the total sampling time T, during N equal periods of sampling time,

from the following equation:

$$\alpha_T = \frac{\sum_{i=1}^{i=N} (T_{Gi})}{T} \qquad (3.4)$$

In the conducted experiments, the total sampling time of 20 s was used, divided in 100 equal periods, which means that the time length of the one period was 0.2 s. The corresponding sample rate was 100,000 scans/s and the number of data points per one "window" on the computer screen was 20,000, both of them set by the default. The same procedure was repeated twice or, sometimes, three times for each radial position, and the corresponding local void fraction was then calculated as an arithmetic mean of these 2 or 3 measurements. The selection of the sampling time and window size was made after performing experiments to ensure that the results are not sensitive to their values. This was later confirmed independently by **Sun** (1997). The total number of radial measuring points was 21 in case of the 20--cm diameter riser pipe, the probe being traversed every 5 mm from the pipe center to one wall, or from r/R = 0 to r/R = 1.

Figures 3.5, 3.6 and 3.7 on pages 79, 80 and 81, respectively, show some typical waveforms of void signals from the optical fiber probe as they appeared on the computer screen (in "windows"). A corresponding void fraction is printed below each window. The waveforms in Figure 3.5 refer to a bubbly flow regime, while those in

Figure 3.6 refer to a clear churn flow regime. Figure 3.7 shows the waveforms near the churn-to-annular flow regimes transition, with periods of continuous gas flow. From all these three figures, it can be noted that bubble size generally corresponds to the time-interval, during which the fiber sensor detects the gas phase. The largest bubble trapped in the screen is certainly one depicted in Figure 3.7 (b). The disappearance of the slug flow regime in large-diameter vertical pipes will be discussed in the following chapter.

The trigger level was set to about 10% of the signal height. It determines the border between two phases, such that all peaks above it are treated as the gas phase, while everything below this line is considered as liquid. In all the tests, the trigger level was carefully observed and kept as close as possible to the liquid level line, at the distance of about 10% of the amplitude from the liquid level line. The sensitivity of the measured void fraction to the trigger level was investigated by **Nada *et al.*** (1996), who showed that the results were insensitive to trigger level position up to about 30% of the signal height. The signal from the probe was essentially rectangular, as can be noted from all the windows in the figures. This made the void fraction rather insensitive to trigger level position.

The area-averaged void fraction can, by definition, be obtained by integration of the corresponding radial void fraction profile:

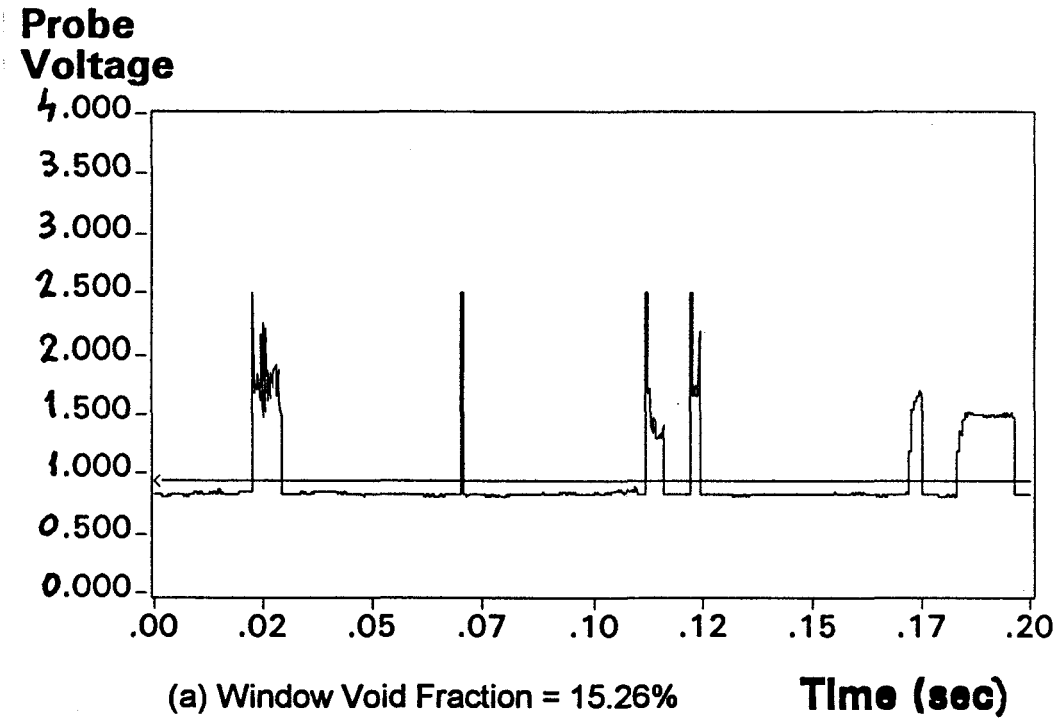

(a) Window Void Fraction = 15.26%

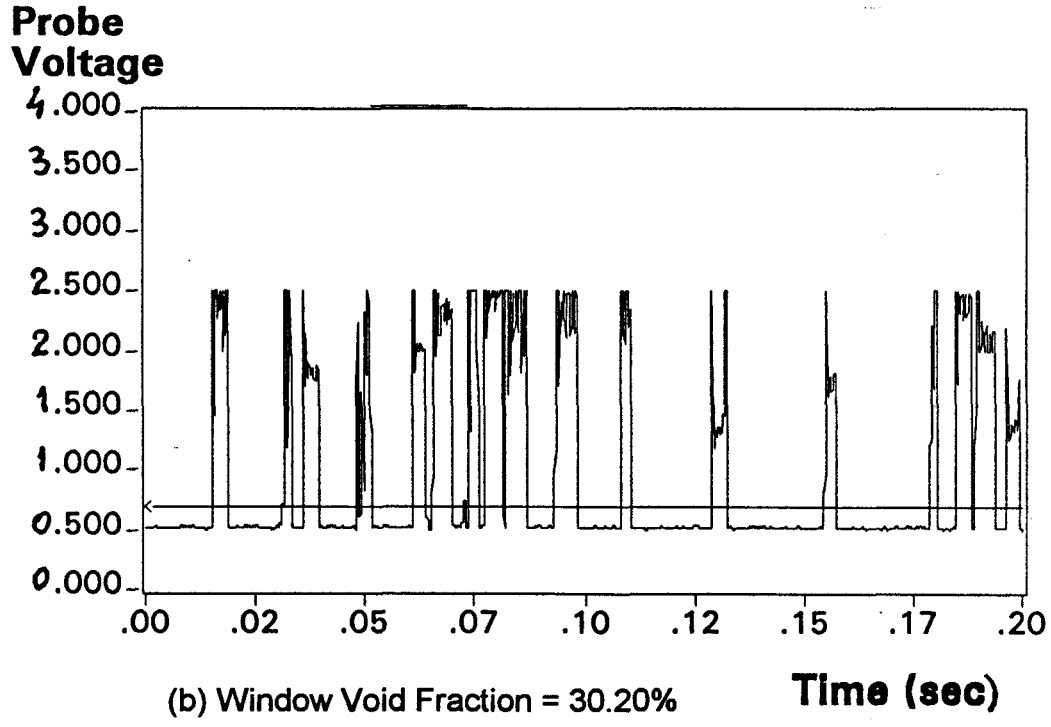

(b) Window Void Fraction = 30.20%

FIGURE 3.5: Waveforms of Void Signals Measured by the Optical Fiber Probe for Bubbly Two-Phase Flow Regime

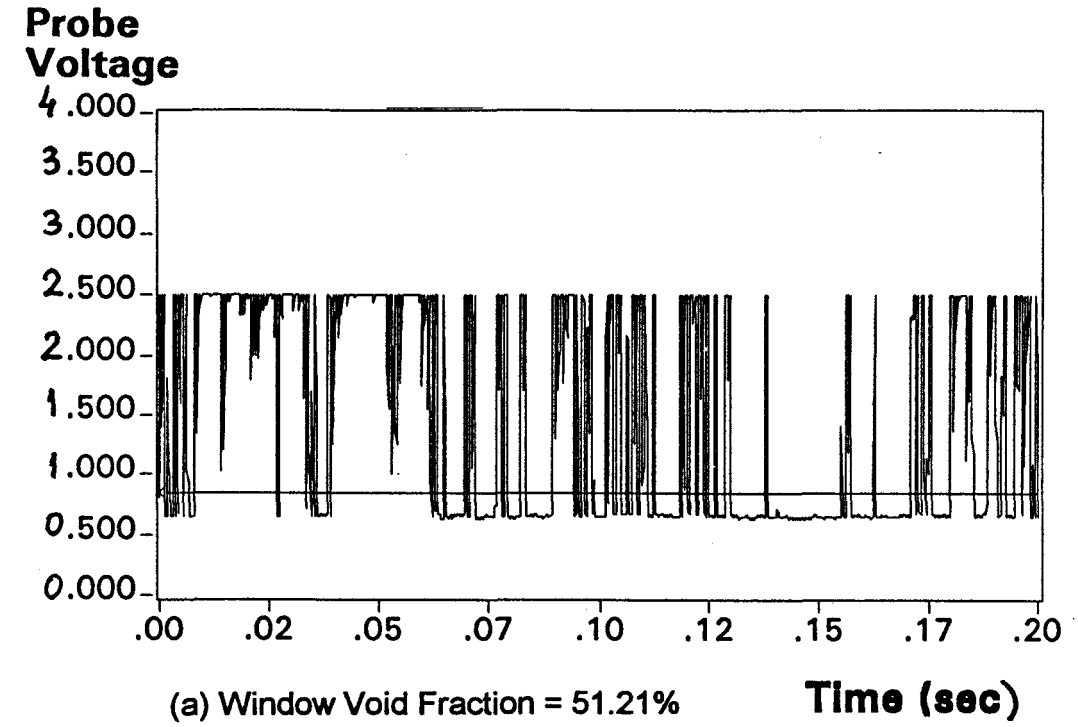

(a) Window Void Fraction = 51.21%

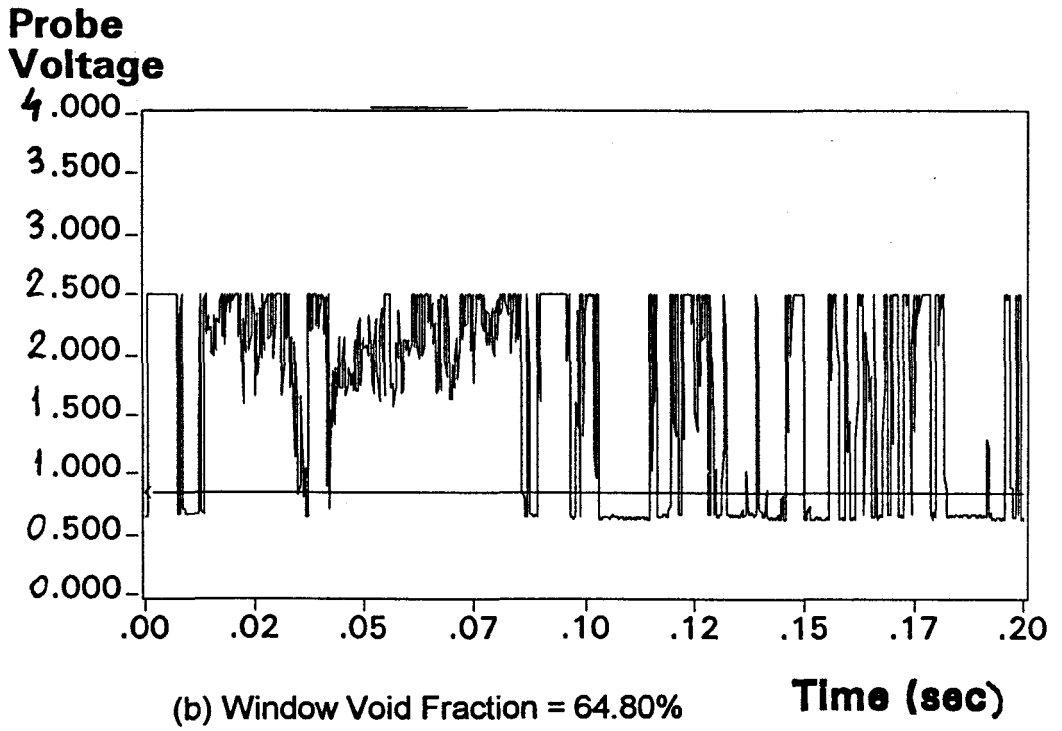

(b) Window Void Fraction = 64.80%

FIGURE 3.6: Waveforms of Void Signals Measured by the Optical Fiber Probe for Churn Two-Phase Flow Regime

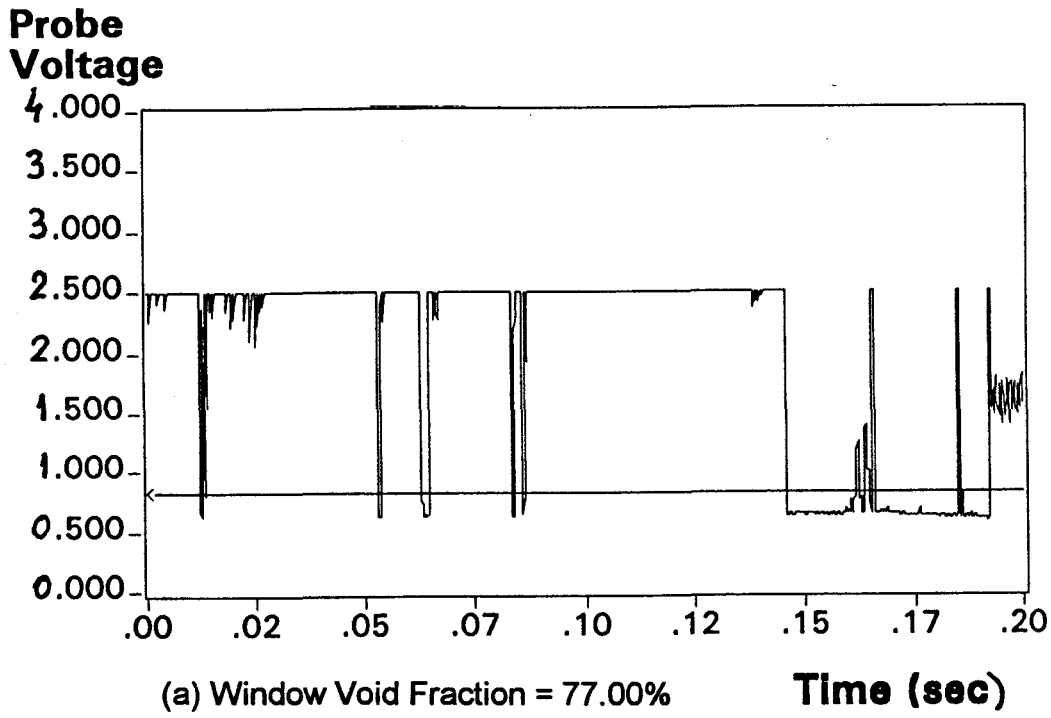

(a) Window Void Fraction = 77.00%

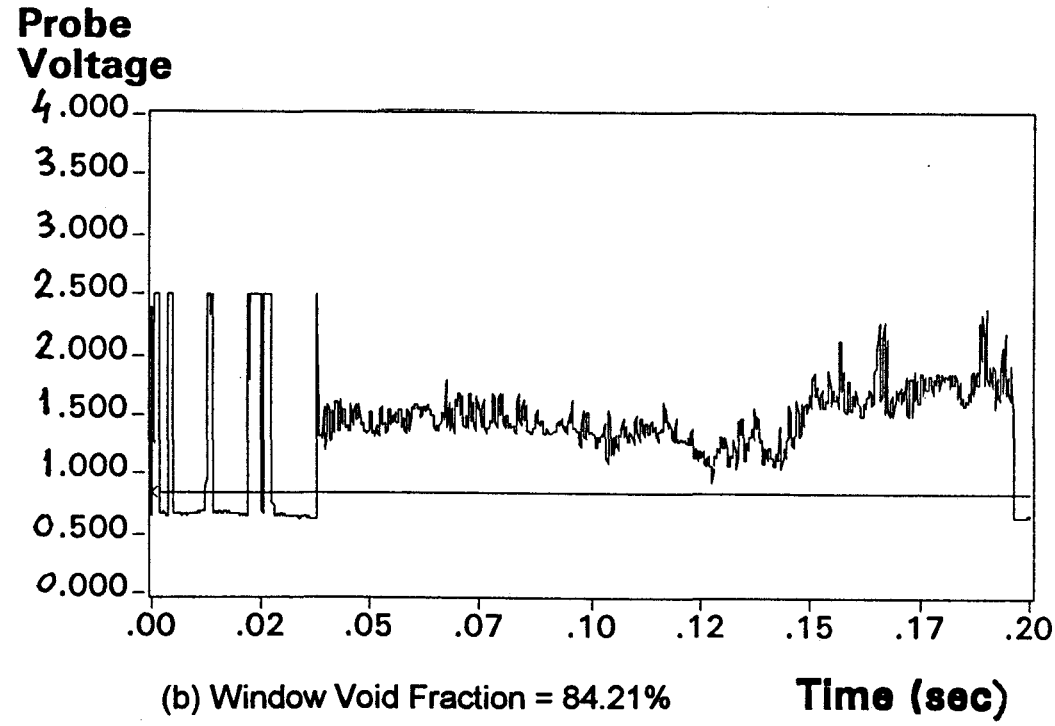

(b) Window Void Fraction = 84.21%

FIGURE 3.7: Waveforms of Void Signals Measured by the Optical Fiber Probe

Near the transition from Churn to Annular Flow Regime

$$\langle\alpha\rangle \equiv \frac{1}{A} * \int_0^R \alpha(r) * 2 * \pi * r * dr = \frac{2}{R^2} * \int_0^R \alpha(r) * r * dr \qquad (3.5)$$

In the conducted experiments, area-averaged void fractions were obtained directly from equation 3.5. The measured radial void fraction profiles were fitted with smooth continuous curves. The fitted profiles were then integrated using equation 3.5 to obtain the area-averaged void fraction.

An illustration of the approximation of measured radial void fraction is given in Figure 3.8 on page 83.

3.2.2. Void Fraction from Pressure Drop Measurements

As it was already mentioned, the pressure drop measurement between stations #5 and #6 in Figure 3.1, was used to estimate the average void fraction in the fully developed flow regime of the test section. Although this is an indirect method for estimating of the void fraction, it was used for the purposes of comparing the various measuring methods. The volume-averaged void fraction was compared with the area-averaged void fraction from the optical fiber probe.

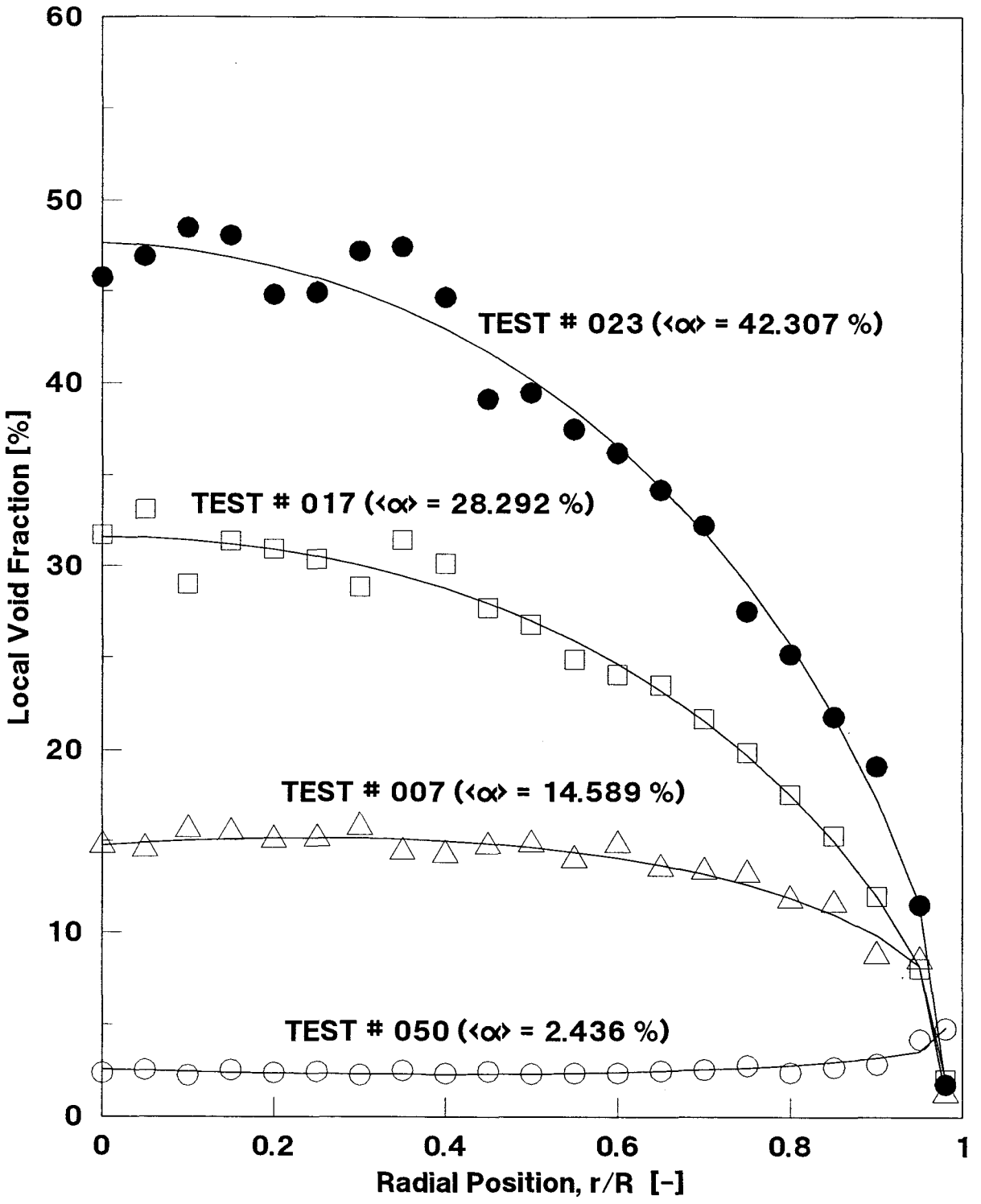

Figure 3.8: Approximation of Radial Void Fraction Profiles in the Cross Section of 20-cm I.D. Vertical Pipe

A schematic of pressure-drop measuring arrangement is shown in Figure 3.9 on page 85. The difference in water levels between the two pressure measuring points (#6 and #5) is designated as H_{ts}, and it also refers to the test section height, 1 m. The test-section pressure transducer voltage output is designated as $\triangle p_{pt}$, meaning that it is converted in a corresponding pressure drop, with a corresponding liquid (water) height H_{pt}.

In estimating of the volume-averaged void fraction in the test section, the initial equation was the following one, which defines the density of a two-phase mixture:

$$\rho_{2\phi} = \rho_G * <\alpha> + \rho_L * (1 - <\alpha>) \qquad (3.6)$$

During the two-phase flow, the measured pressure drop in the test section, $\triangle p_{pt}$, depended on the difference of the two-phase mixture density and the liquid density over the length of the test section, and on the frictional pressure drop, $\triangle p_{FR}$. This is described by the following simple equation:

$$\triangle p_{pt} = \rho_L * g * H_{pt} = g * H_{ts} * (\rho_L - \rho_{2\phi}) - \triangle p_{FR} \qquad (3.7)$$

Combining the two previous equations, the average volume void fraction in the test section can be calculated from the equation:

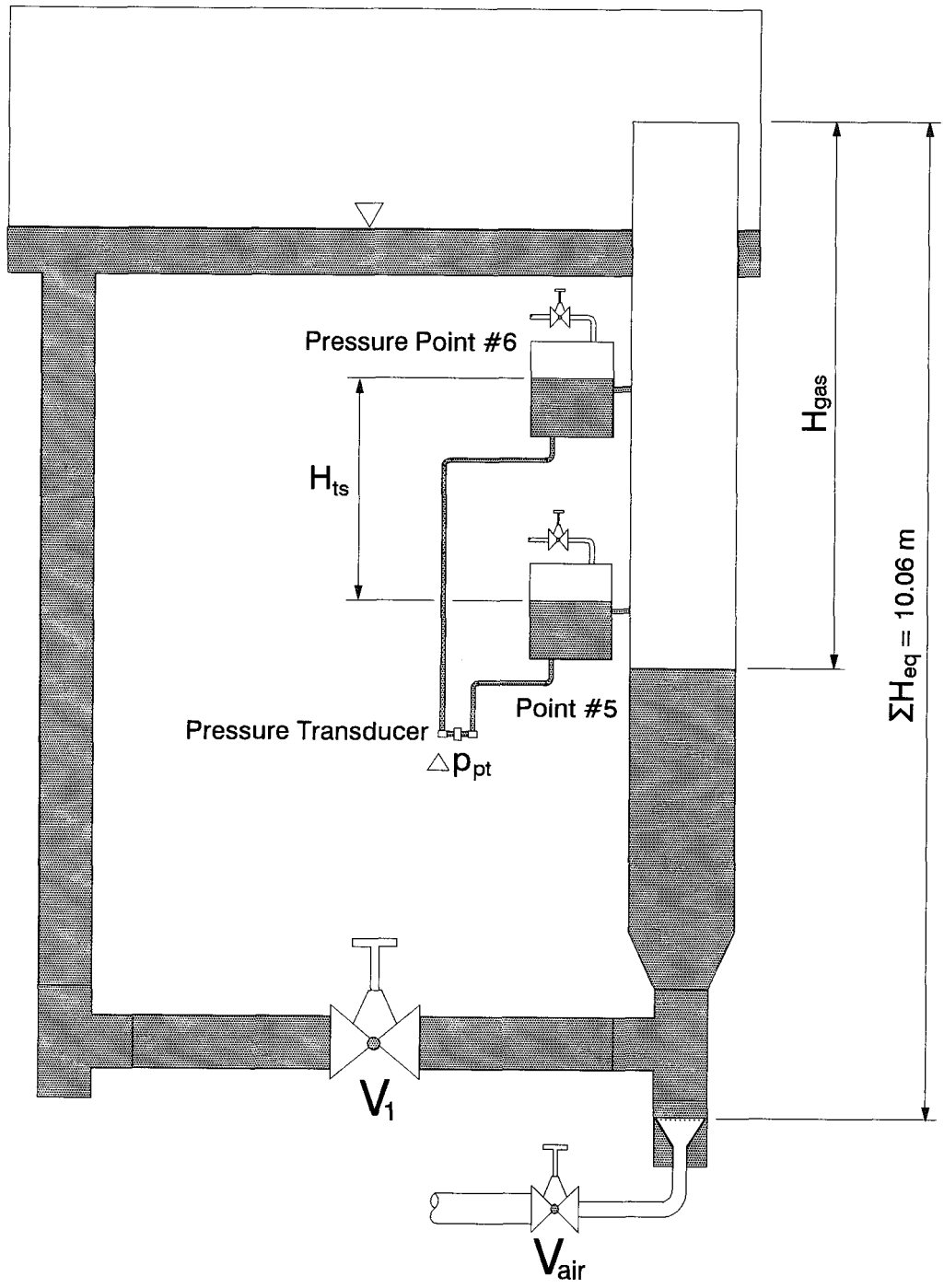

FIGURE 3.9: SCHEMATIC OF THE LOOP AND THE TEST SECTION AFTER QUICK CLOSING OF THE AIR CONTROL VALVE

$$\langle\alpha\rangle = \frac{\triangle p_{pt} + \triangle p_{FR}}{g * H_{ts} * (\rho_L - \rho_G)} = \frac{H_{pt} + \triangle p_{FR}/(g * \rho_L)}{H_{ts} * (1 - \rho_G/\rho_L)} \qquad (3.8)$$

Density of the gas phase in the test section, ρ_G, was calculated from the equation of state of ideal gases, at the appropriate temperature of the gas phase, T_G. Air pressure in the test section, p_G, was calculated from an estimate that a 1.5-m high column of the two-phase mixture lay over the center of the test section. So, the test--section gas density was calculated from the following equation:

$$\rho_G = \frac{p_G}{R * T_G} = \frac{(p_a + \rho_{2\phi} * g * 1.5)}{R * T_G} \qquad (3.9)$$

In the conducted experiments, the frictional pressure drop, $\triangle p_{FR}$, was estimated from the following equation, which uses the two-phase friction multiplier, Φ_L^2, of the single liquid-phase frictional pressure drop, $\triangle p_L$:

$$\triangle p_{FR} = \triangle p_L * \Phi_L^2 = \frac{2 * f_L * H_{ts} * \rho_L * J_L^2}{D} * \Phi_L^2 \qquad (3.10)$$

On the other hand, in case of experiments running at zero liquid flow, the frictional pressure drop was estimated from the equation that is similar to equation 3.10, which uses the two-phase friction multiplier, Φ_G^2, of the single gas-phase frictional pressure drop, $\triangle p_G$:

$$\triangle p_{FR} = \triangle p_G * \Phi_G^2 = \frac{2 * f_G * H_{ts} * \rho_G * J_G^2}{D} * \Phi_G^2 \qquad (3.10')$$

Two-phase friction multipliers for the liquid phase, Φ_L^2, and for the gas phase, Φ_G^2, are typically given as the following functions of the **Lockhart-Martinelli parameter**, X^2, defined as a ratio between single-phase frictional pressure drops $\triangle p_L$ and $\triangle p_G$:

$$\Phi_L^2 = 1 + \frac{20}{X} + \frac{1}{X^2} = 1 + 20 * \left(\frac{\triangle p_G}{\triangle p_L}\right)^{1/2} + \left(\frac{\triangle p_G}{\triangle p_L}\right) \qquad (3.11)$$

$$\Phi_G^2 = 1 + 20 * X + X^2 = 1 + 20 * \left(\frac{\triangle p_L}{\triangle p_G}\right)^{1/2} + \left(\frac{\triangle p_L}{\triangle p_G}\right) \qquad (3.11')$$

Finally, it is important to mention that corresponding friction factors f_L and f_G of single-phase frictional pressure drops $\triangle p_L$ and $\triangle p_G$, respectively, were estimated from the following equations, depending on Reynolds numbers of liquid and gas:

$$f_L = \frac{0.079}{Re_L^{1/4}} \qquad (3.12) \qquad f_G = \frac{0.079}{Re_G^{1/4}} \qquad (3.12')$$

3.3. REGULAR EXPERIMENTAL TEST PROCEDURE

A regular experimental test procedure included the following steps:

1 - Switch on all the instruments.

2 - Fill the loop with water (if it is empty) to a required operational water level in the separation tank.

3 - Check all the instruments' readings and adjust zeroes if necessary.

4 - Inject air into the loop and adjust the air and water flow rates to required values.

5 - Set the data acquisition system and adjust the threshold value of the optical fiber signal.

6 - Obtain 50% of the local void fraction measurements at different radial positions by traversing of the optical fiber probe across the pipe diameter, continuously checking and adjusting the threshold value.

7 - Get the data using the data acquisition system at a rate of 10 Hz for a 60 seconds period.

8 - Obtain other 50% of the local void fraction measurements at different radial positions by traversing of the optical fiber probe across the pipe diameter, continuously checking and adjusting the threshold value.

9 - Take the mercury (or water) manometer reading of a pressure drop at the air orifice plate and, eventually, the multi-tube mercury manometer readings for all pressure measuring points along the riser.

10 - After completion of all the measurements, shut off the air supply and, eventually, turn off the pump.

11 - Check all the instruments' readings for the no flow condition, adjusting zeroes if necessary.

CHAPTER FOUR

EXPERIMENTAL RESULTS AND DATA ANALYSIS

The analysis of experimental results, obtained in experiments with the 20-cm riser pipe, includes several parts: (1) the first part deals with flow patterns and flow regime maps; (2) the second part compares various void fraction measuring techniques; (3) the third part shows characteristics of the local void fraction profile, including eventual comparisons with experimental results of other investigators, and (4) the fourth part gives correlations of the data using the drift-flux model for predicting of the void fraction in vertical upward two-phase flow.

The main objectives of the experiments presented here were to investigate two--phase flow patterns and radial void fraction profiles in a 20-cm diameter vertical pipe, and to determine the accuracy of void fraction measurements in large--diameter pipes using an optical fiber probe, by comparing it with the accuracies of other void fraction measuring techniques. A total of 70 tests was done. Several tables of the results are enclosed in the convenient form in the **Appendix**. The test conditions were in the following ranges:

Mass flux of water, G_L	0 - 780 kg/m^2*s
Mass flux of air, G_G	0.03 - 1.0434 kg/m^2*s
Two-phase density in the test section, $\rho_{2\phi}$	446.517 - 975.672 kg/m^3
Average void fraction, $<\alpha>$	2.436 - 55.419 %
Flow quality (mass flow rate fraction of gas), x	0.006 - 5.417 %
Average superficial liquid velocity, $<J_L>$	0 - 0.755 m/s
Average superficial gas velocity, $<J_G>$	0.021 - 0.788 m/s
Pipe length to pipe diameter ratio, L/D	42

4.1. Flow Patterns and Flow Regime Maps in a 20-cm Diameter Vertical Pipe

Since one of the main objectives of the experiments performed in the 20-cm diameter riser pipe was to explore existing two-phase flow patterns, a wide range of superficial gas and liquid velocities was investigated. The flow patterns were identified by visual observation, and only bubbly and churn flow regimes were observed. After covering of a wide range (particularly low values) of superficial gas

and liquid velocities, it was concluded that slug flow did not exist in the 20-cm diameter, 10-m high vertical riser pipe. Accordingly, a bubble coalescence and/or breakup is believed to be a strong function of the pipe diameter. It appears that in large-diameter vertical pipes, the coalescence mechanism of bubbles, which governs the transition from bubbly to slug flow, is affected so that the slug flow regime may not exist at all. Although Figure 3.7 on page 81 shows some interesting waveforms of optical probe void signals, captured on the computer screen, it is not considered as an evidence of the existence of slug flow in 20-cm diameter vertical pipe. It was observed that, although some periodicity existed between consecutive liquid slugs, they were much more disordered and chaotic, which leads to a definition of churn flow. Because very large air bubbles flowed within the central portion of the pipe cross section, followed by these disordered liquid slugs, this variant of churn flow is believed to be near the transition to annular flow.

The flow patterns observed in these tests were compared with the predictions of flow regime maps of: **Taitel *et al.*** (1980), **Mishima and Ishii** (1984), and **Weisman and Kang** (1981) in Figures 4.1 (on page 93), 4.2 (on page 94) and 4.3 (on page 95), respectively. Flow regime maps in Figures 4.1 and 4.2 are plotted in terms of superficial gas velocity, J_G, versus superficial liquid velocity, J_L , while the flow regime map of **Weisman and Kang** in Figure 4.3, in addition, includes the appropriate correction functions ϕ_1 and ϕ_2.

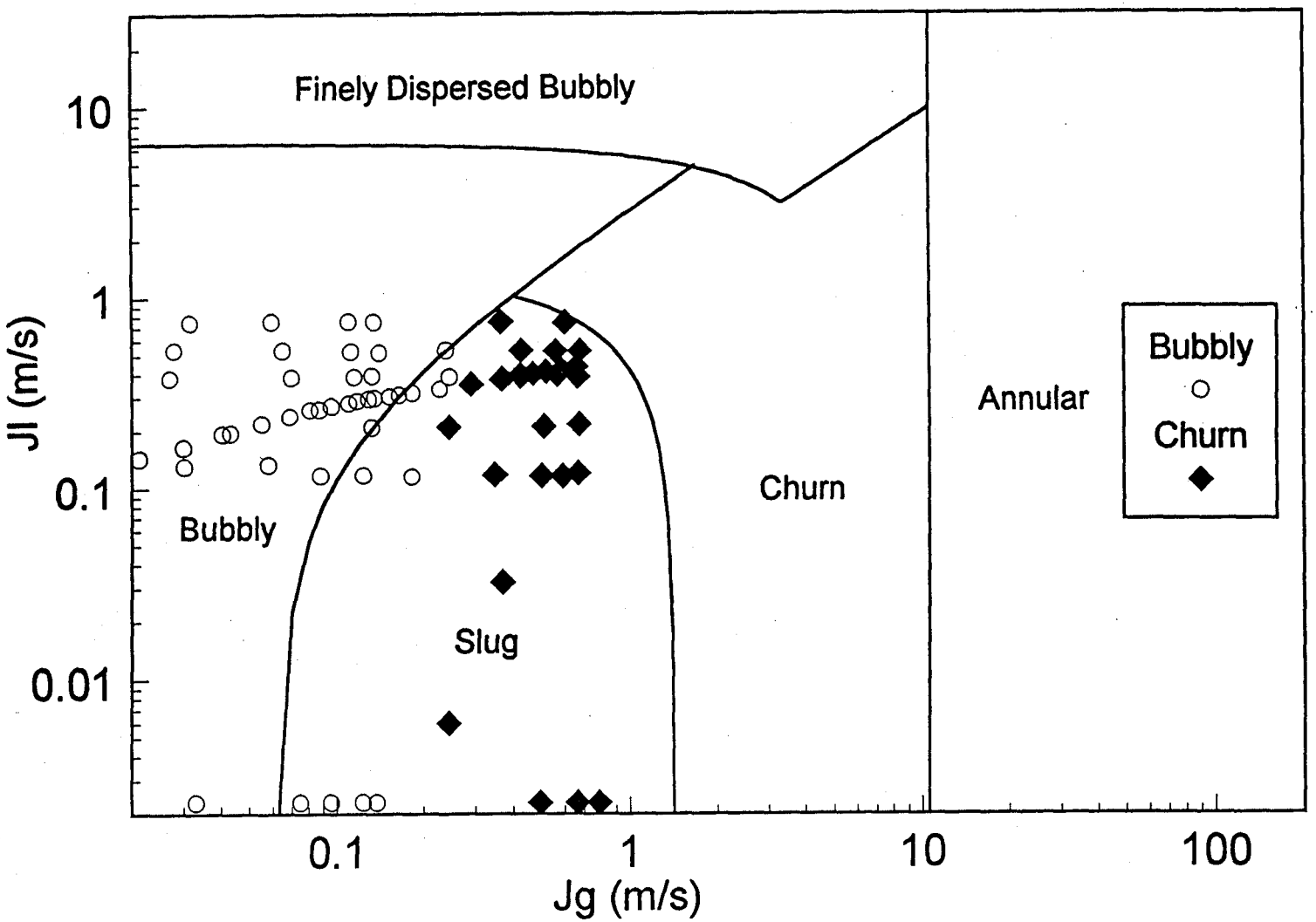

Figure 4.1 : Two-Phase Flow Regime Map of ***Taitel et al.*** (1980) in a Vertical Pipe of I.D. = 20 cm and L = 10 m, at air density of 1.38 kg/m3 (20°C)

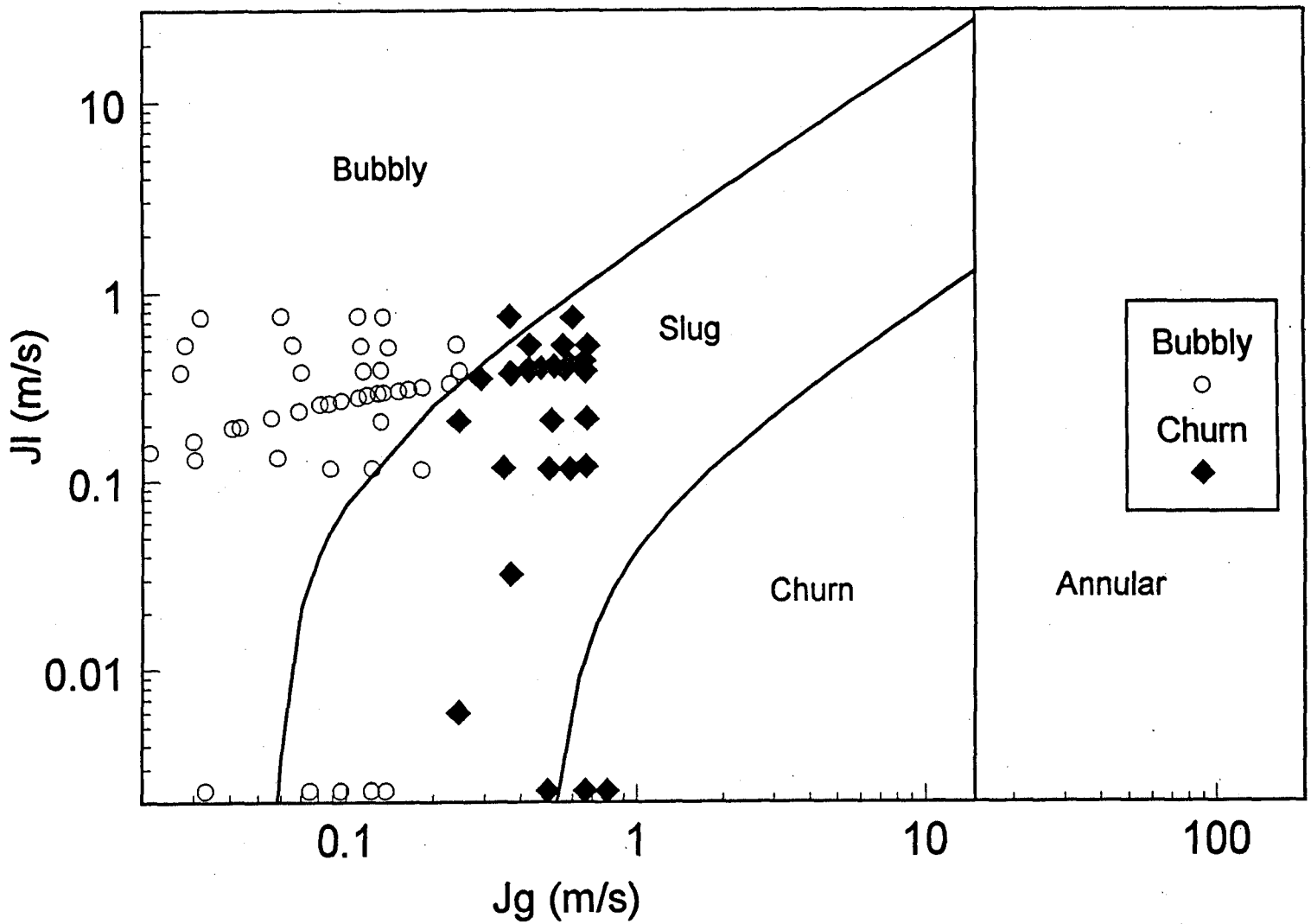

Figure 4. 2 : Two-Phase Flow Regime Map of ***Mishima and Ishii*** (1984) in a Vertical Pipe of I.D. = 20 cm and L = 10 m, at air density of 1.38 kg/m3 (20°C)

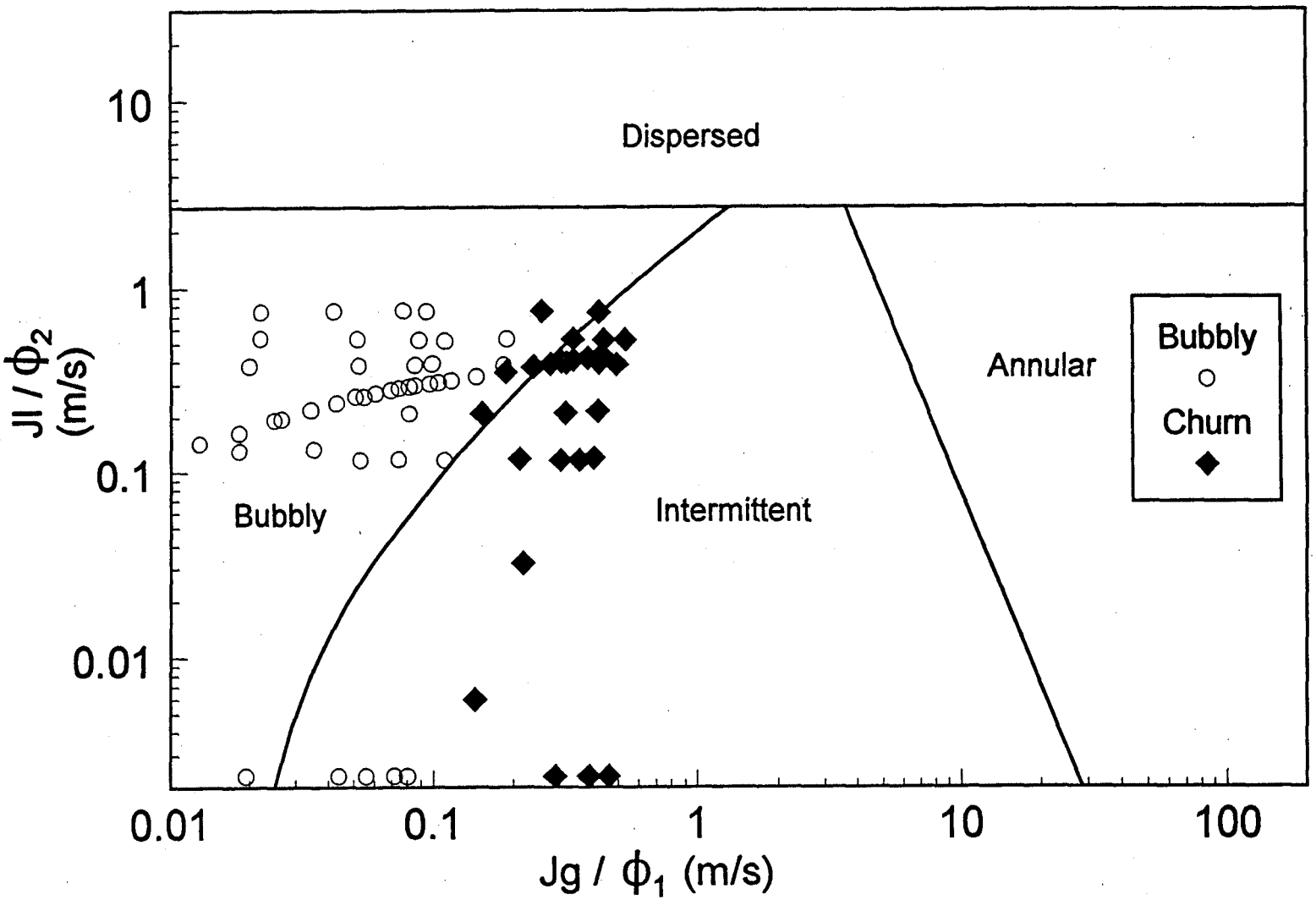

Figure 4..3 : Two-Phase Flow Regime Map of ***Weisman and Kang*** (1981) in a Vertical Pipe of I.D. = 20 cm and L = 10 m, at air density of 1.38 kg/m3 (20°C)

It can be noted that performed tests can determine the transition boundary from bubbly to intermittent (churn, in this case) flow, for a 20-cm diameter vertical pipe. The most interesting fact, which can be deduced from all the flow regime maps enclosed, is that these results suggest that the bubbly-to-intermitent flow transition boundary (in large-diameter vertical pipes) should be corrected so that it can be represented with a **slightly inclined line** in such a flow regime map. In formulating this conclusion, of particular importance were the results obtained with zero liquid flow rate, that is, in stagnant liquid, with the results from the forced circulation tests (in which the pump was used). In other words, the results obtained in the 20-cm diameter riser pipe suggest that the bubbly-to-intermittent flow transition boundary is a rather weak function of the superficial liquid velocity, and that it occurs in a narrow range of superficial gas velocities **between 0.15 and 0.30 m/s** (for 20-cm diameter pipes only). Also, by comparing these results with "A"-curve on the flow regime map of **Taitel *et al.*** (Figure 2.2 on page 14), it appears that both the position and shape of the bubbly-to-intermittent flow transition depend on the pipe diameter. It is, however, certain that this conclusion should be verified in many similar future experiments in large-diameter vertical pipes.

During these tests in the 20-cm diameter riser pipe, it was observed that transition from bubbly to intermittent flow occurred at void fractions of about 25%, based on the void fraction measurements from the optical fiber probe, which is in very good

agreement with **Taitel *et al.*'s** approach used in generation of their flow regime map. Also, experimental results from investigations of some other researchers suggest that, in large-diameter pipes, the void fraction at the transition from bubbly to intermittent flow decreases with an increase of the pipe diameter.

Transition from intermittent to annular flow and transition to dispersed bubbly flow boundaries could not be verified in these experiments, since high liquid or two-phase mixture flow rates caused undesirable vibrations of both the downcomer and riser pipe. The problem with downcomer can be overcome by replacing of the existing downcomer pipe with a larger one (a 20-cm diameter pipe, for instance).

The flow regime results obtained in the 20-cm diameter pipe were similar to those presented by **Nada *et al.*** (1996) for air-water flow in a 10-cm diameter pipe, using the same experimental facility. **Nada *et al.*** (1996) did not observe slug flow and showed that the transition from bubbly flow was well predicted by the flow regime map proposed by **Mishima and Ishii** (1984).

4.2. COMPARISON BETWEEN DIFFERENT VOID FRACTION MEASURING TECHNIQUES

The area-averaged void fraction obtained by the optical fiber probe and volume--averaged void fraction calculated from the pressure drop measurements are compared in Figure 4.4 on page 99. This comparison was undertaken to verify the validity of optical fiber probe measurements.

Figure 4.4 on page 99 shows a slight disagreement between the void fraction measurements of the optical probe and the pressure transducer in the test section. The difference in these two techniques results in a 10-15% overestimation of the results obtained by the optical probe compared with the pressure transducer results. Although the frictional pressure drop was taken into account in calculations of the void fraction, it is possible that the chosen method of calculation of the frictional pressure drop underestimates it. This implies that pressure-drop technique slightly underestimated the void fraction, meaning that the optical fiber probe could be closer (that is, less overestimating) to accurate results of the void fraction.

The present optical fiber probe was also used by **Nada *et al.*** (1996) to measure the void fraction in a 10-cm diameter pipe. The results were also compared with gamma densitometer measurements. The measurements obtained by both techniques were similar within ±10%.

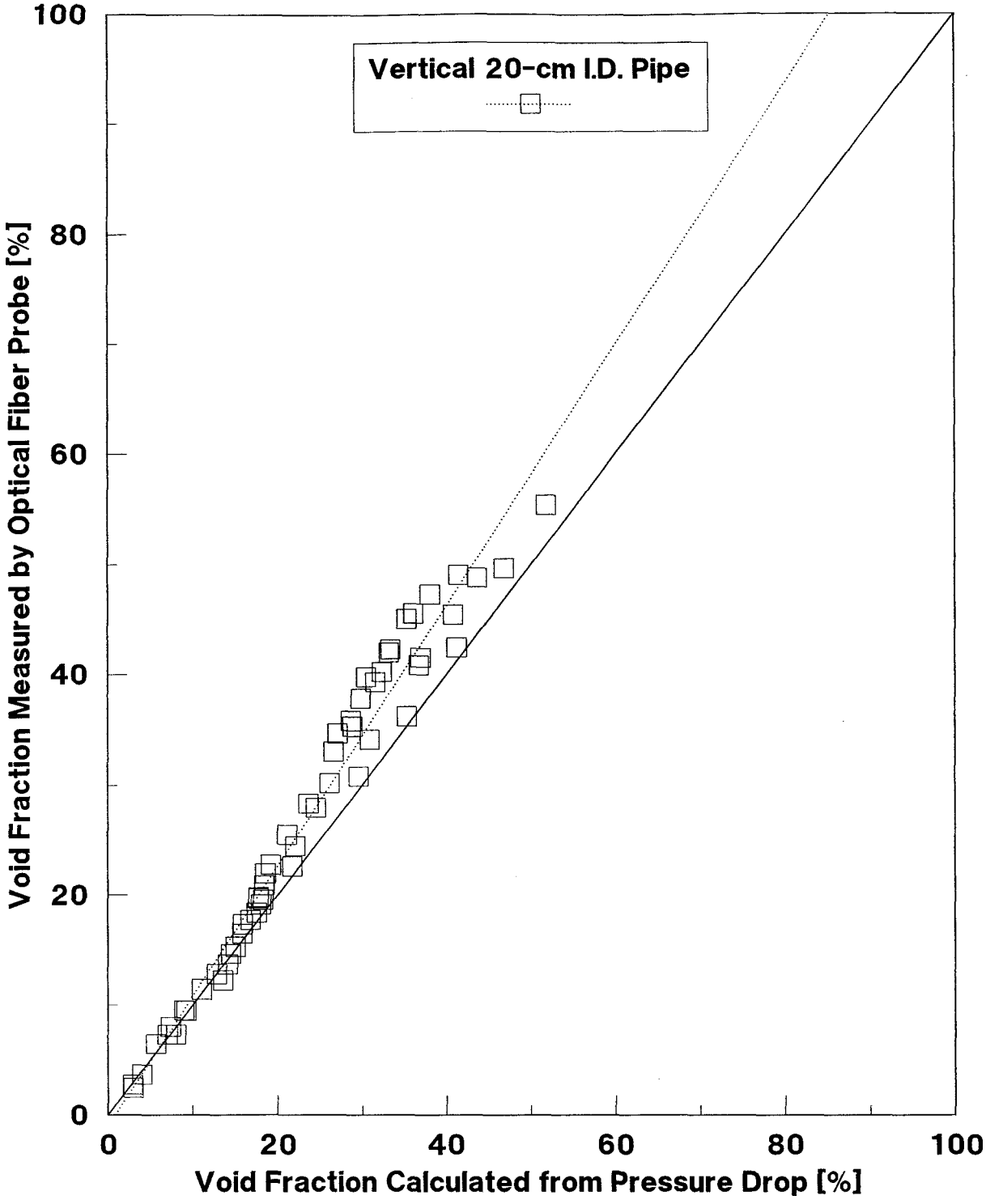

Figure 4.4: Comparison Between Void Fraction Measurements of Optical Fiber Probe and Pressure Transducer

The above suggests that the void fraction measurements by the optical fiber probe in the 20-cm diameter pipe are fairly accurate. We estimate the uncertainties of the measurements to be better than ±10%.

4.3. RADIAL VOID FRACTION PROFILES:

4.3.1. Measured Radial Void Fraction Profiles in a 20-cm Diameter Pipe

Radial void fraction profiles from these tests, measured by the optical fiber probe in the 20-cm diameter riser pipe, are shown in Figures 4.5 to 4.21. It has to be emphasized that, besides the fact that the optical probe was very accurate in void fraction measurements in the 20-cm diameter vertical pipe, it gave a valuable insight into the radial distribution of void fraction for bubbly and churn flow regimes.

Figures 4.5 and 4.6 on pages 101 and 102, respectively, show radial distribution of the void fraction in **bubbly flow** for various liquid flow rates at constant superficial gas velocities of about 0.03 m/s and 0.134 m/s, respectively.

Figures 4.7 to 4.11 on pages 103 to 107, show radial distribution of the void fraction

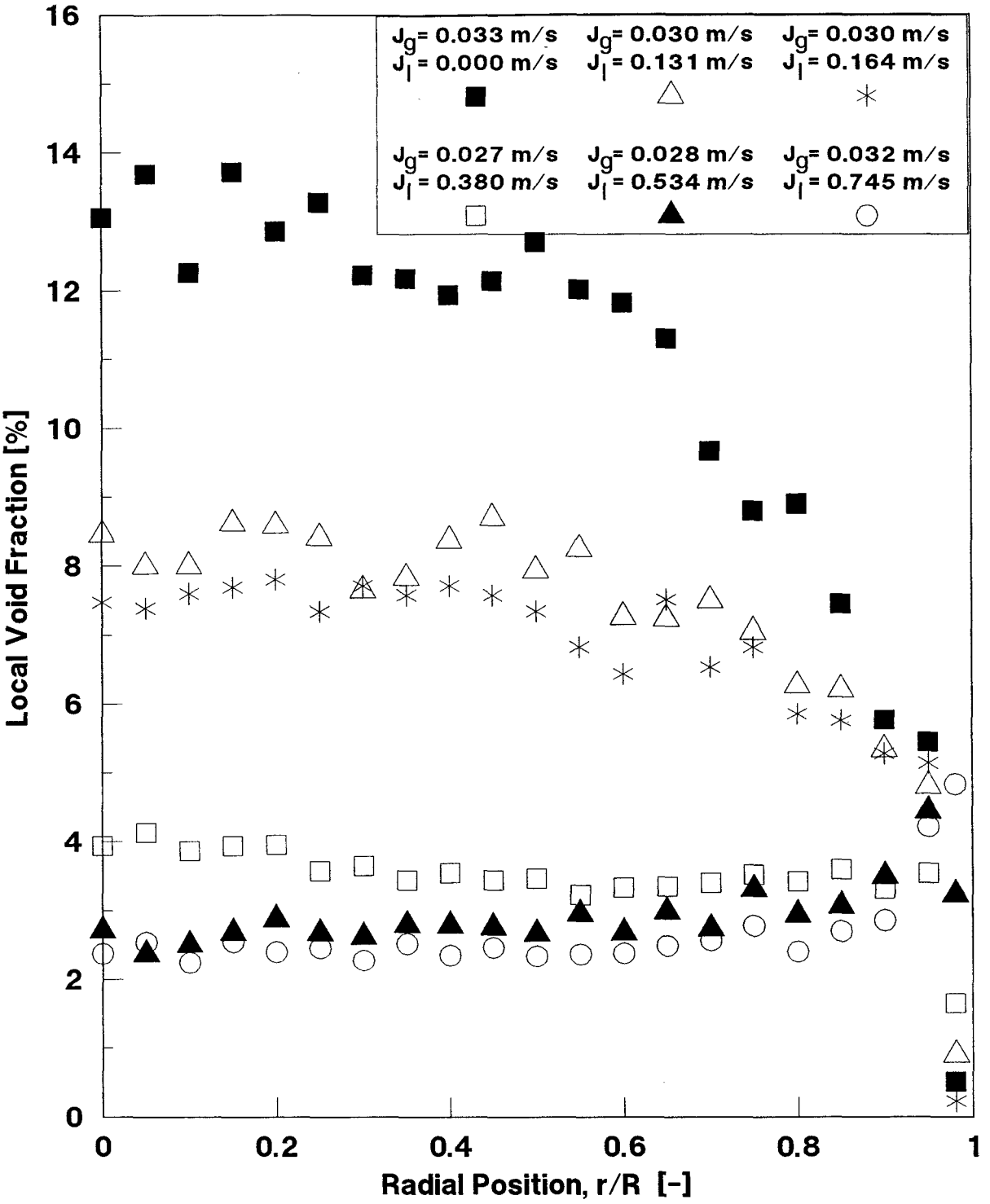

Figure 4.5: Radial Distribution of the Void Fraction in a 20-cm I.D. Vertical Pipe for Bubbly Flow Regime at $J_G \approx 0.03$ m/s

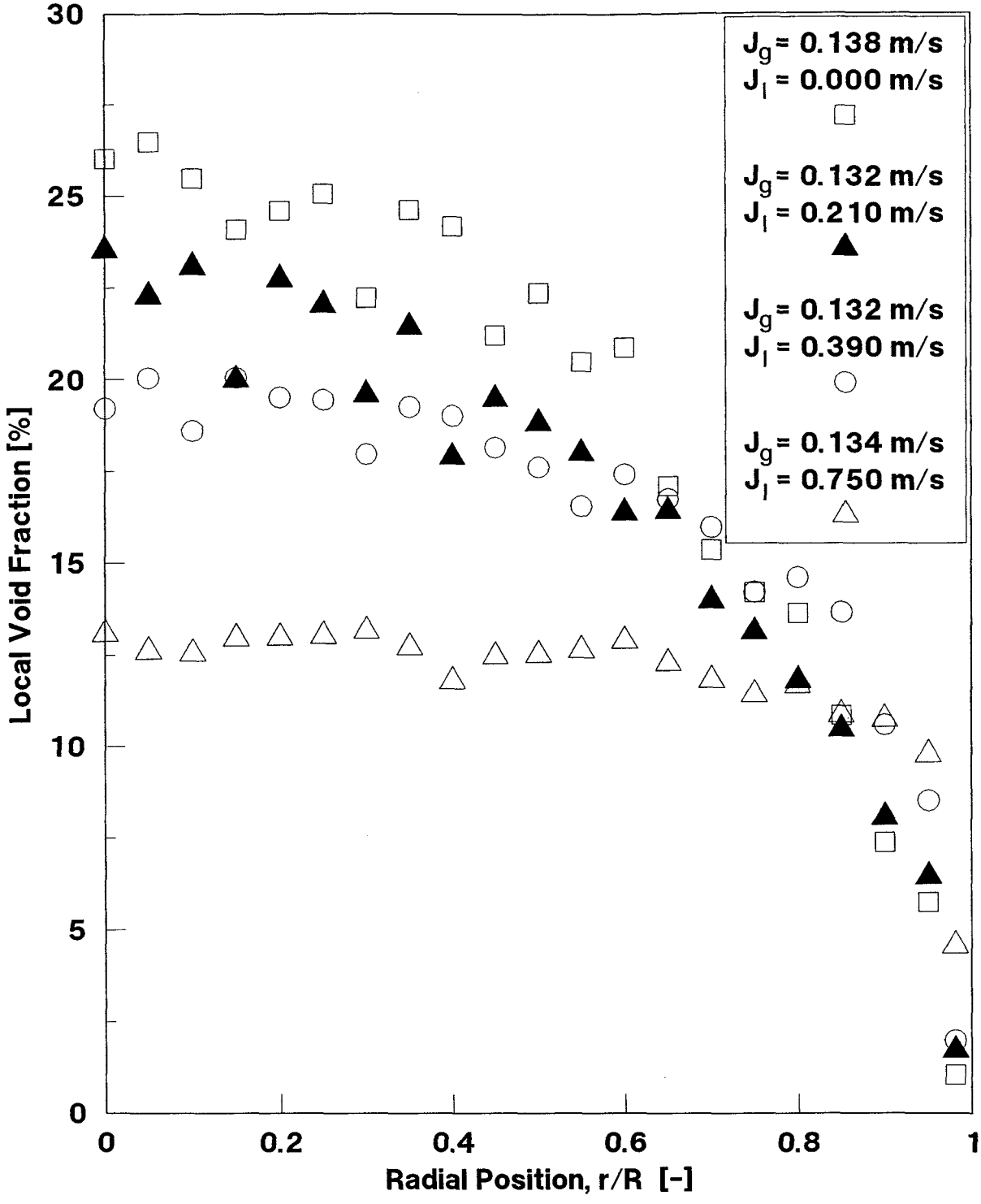

Figure 4.6: Radial Distribution of the Void Fraction in a 20-cm I.D. Vertical Pipe for Bubbly Flow Regime at $J_G \approx$ 0.134 m/s

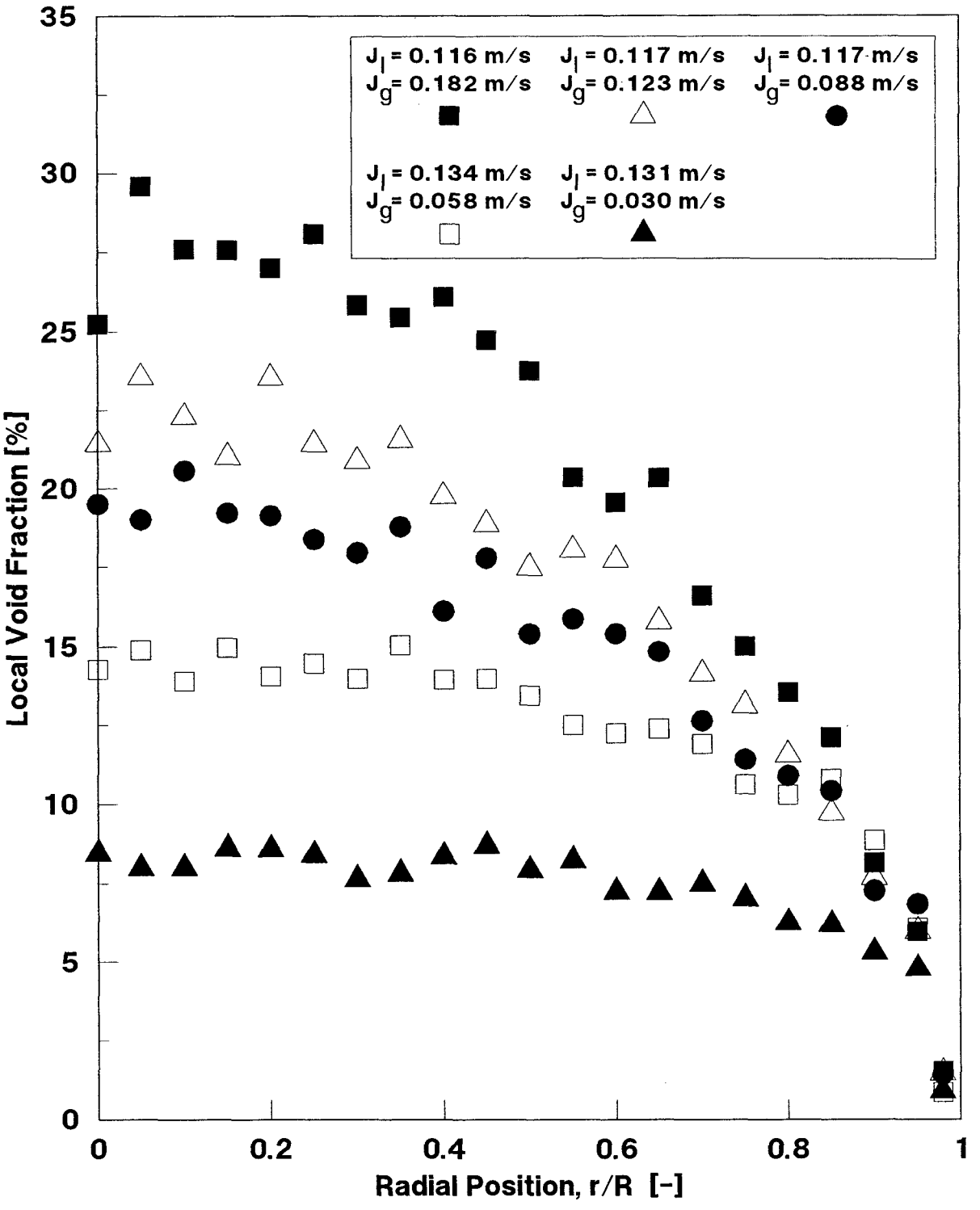

Figure 4.7: Radial Distribution of the Void Fraction in a 20-cm I.D. Vertical Pipe for Bubbly Flow Regime at $J_L \approx 0.12$ m/s

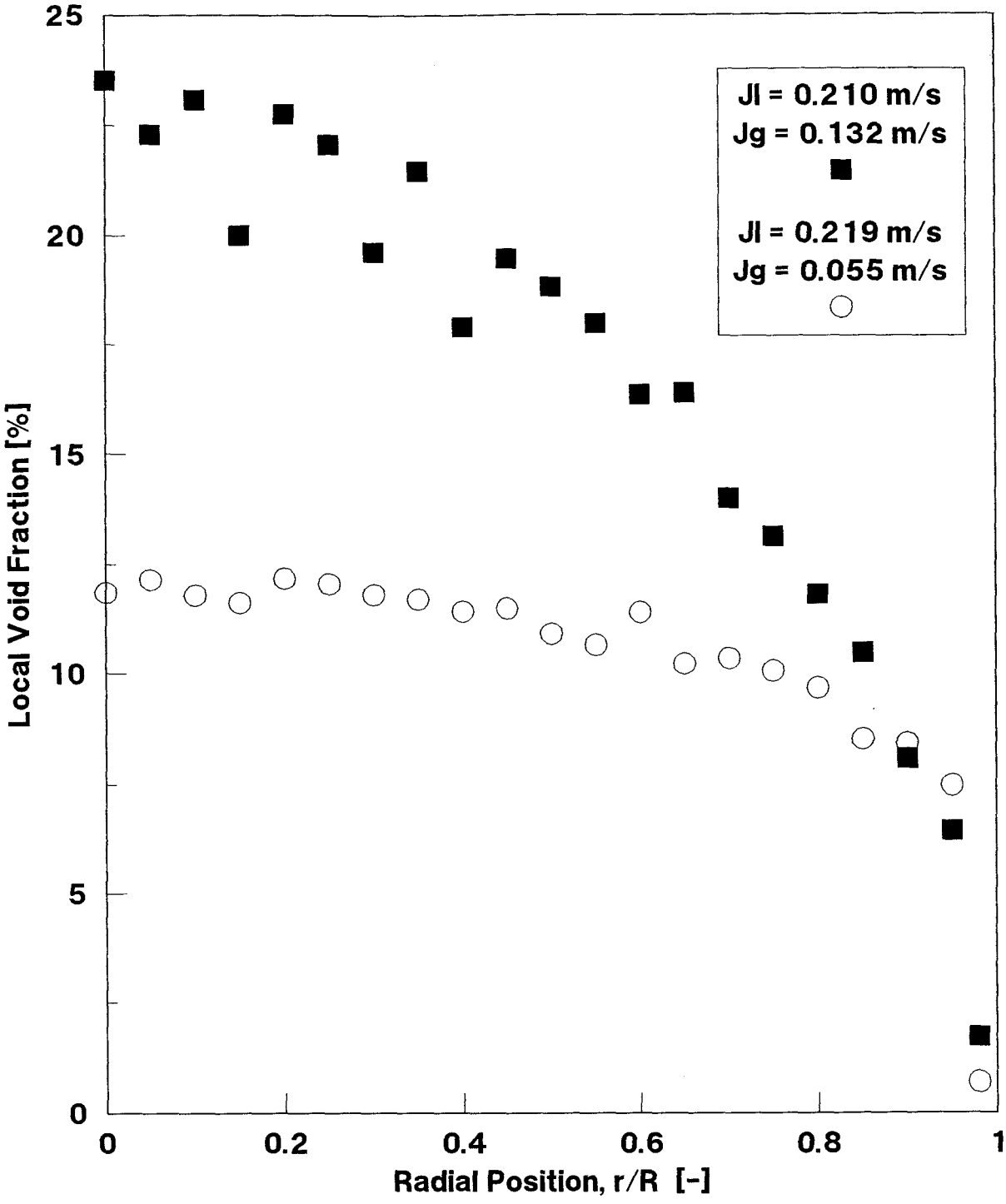

Figure 4.8: Radial Distribution of the Void Fraction in a 20-cm I.D. Vertical Pipe for Bubbly Flow Regime at $J_L \approx 0.21$ m/s

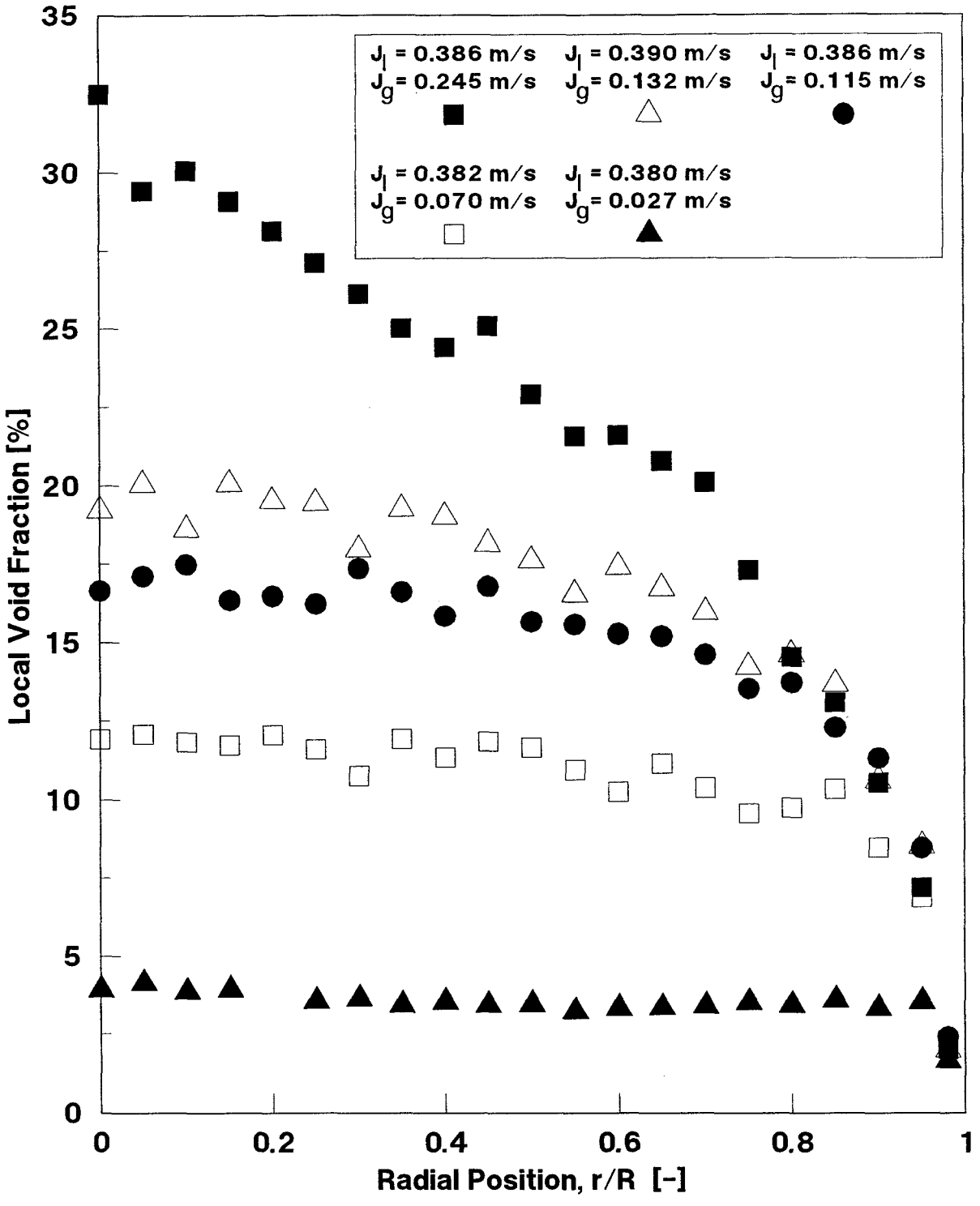

Figure 4.9: Radial Distribution of the Void Fraction in a 20-cm I.D. Vertical Pipe for Bubbly Flow Regime at $J_L \approx 0.38$ m/s

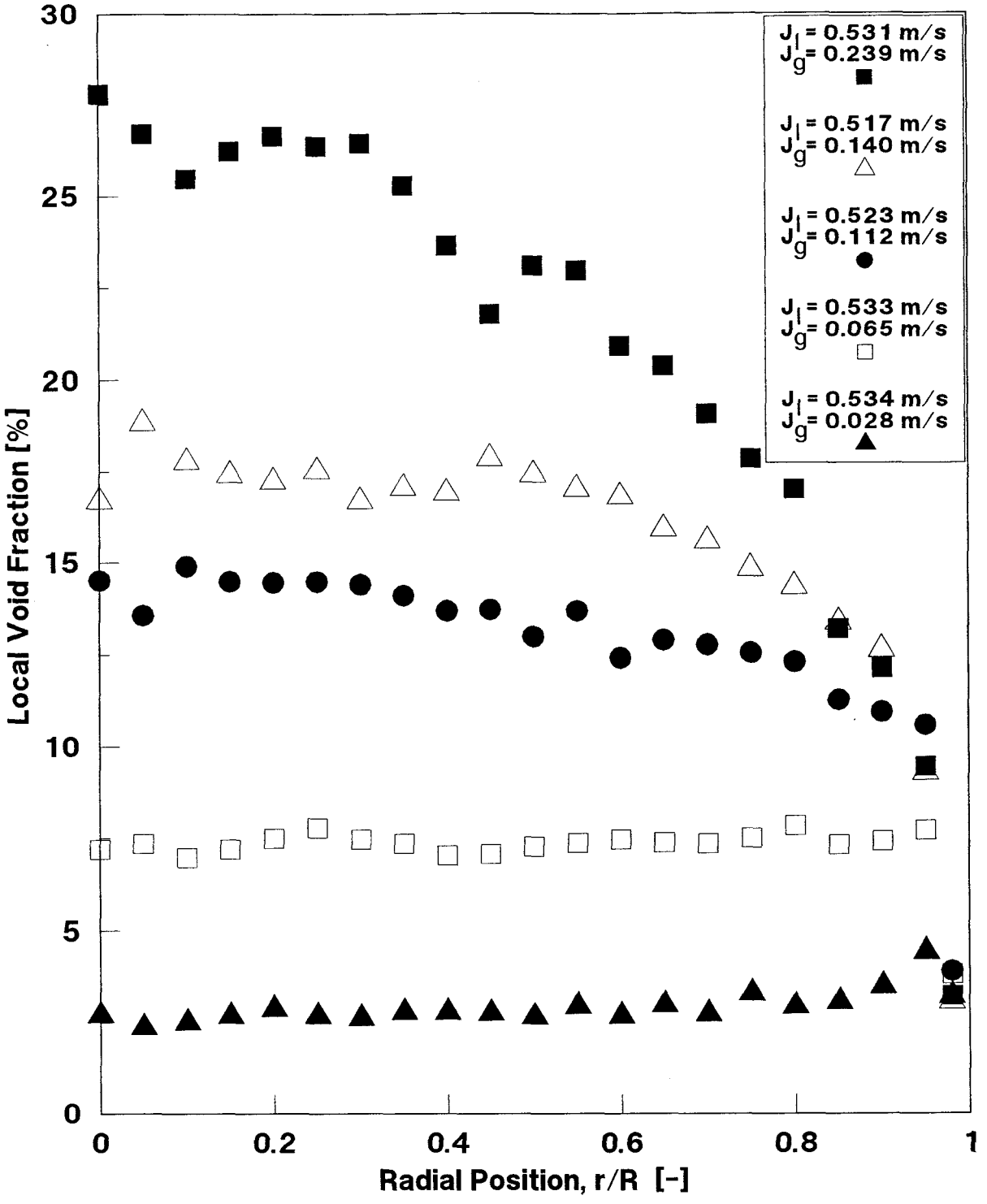

Figure 4.10: Radial Distribution of the Void Fraction in a 20-cm I.D. Vertical Pipe for Bubbly Flow Regime at $J_L \approx 0.53$ m/s

in **bubbly flow**, for various supreficial gas velocities at constant superficial liquid velocities of about 0.12, 0.21, 0.38, 0.53 and 0.75 m/s, respectively.

As shown in these Figures, a common characteristic of two-phase flow can be noted, that the average void fraction increases with decreasing of the liquid flow rate, at a constant value of the superficial gas velocity, or with increasing of the gas flow rate at constant superficial liquid velocity. However, the local radial void fraction distribution is clearly a function of the combination of gas and liquid flow rates.

The main features of the observed radial void fraction distributions for **bubbly flow** can be summarized as follows:

(I) A saddle-type void fraction distribution (sharp peak in the void fraction distribution near the wall, with low and near uniform void fraction distribution in the center region of the pipe cross section) can be encountered at low average void fractions ($<\alpha> < 5\%$). The saddle-type radial profile was observed in the present experiments at low superficial gas velocity (typically less than 0.05 m/s) combined with high superficial liquid velocity (typically higher than 0.4 m/s).

(ii) The radial void fraction profile changes from flat uniform profile to a more

parabolic-type profile with increasing the average void fraction, i.e. increasing the superficial gas velocity at constant liquid flow rate or decreasing the superficial liquid velocity at constant gas flow rate.

The measured void fraction distributions in **churn flow** are shown in Figures 4.12 to 4.17 on pages 110 to 115. Figure 4.12 shows the radial void fraction distribution at constant superficial gas velocity of about 0.24 m/s for various liquid flow rates. Figures 4.13 to 4.17 show the radial void fraction distribution for various superficial gas velocities at constant superficial liquid velocities of about 0.12, 0.21, 0.39, 0.53 and 0.75 m/s, respectively. As shown in these Figures, in **churn flow**, the radial void fraction profile is generally parabolic in shape. The peak of the parabolic distribution, however, increases with increasing the average void fraction; obtained by increasing gas flow rate at a constant liquid flow rate, or decreasing liquid flow rate at a constant gas flow rate.

Two-phase flow regimes at zero liquid flow rate (stagnant water) are shown in Figures 4.18 and 4.19 on pages 117 and 118, respectively. Figures 4.18 and 4.19 show radial distribution of the void fraction for various increasing superficial gas velocities at constant zero superficial liquid velocity, for bubbly and churn flow regimes, respectively. These Figures once again confirm the developing trend of flat-type radial profiles to profiles with obtuse center peaks in large-diameter vertical

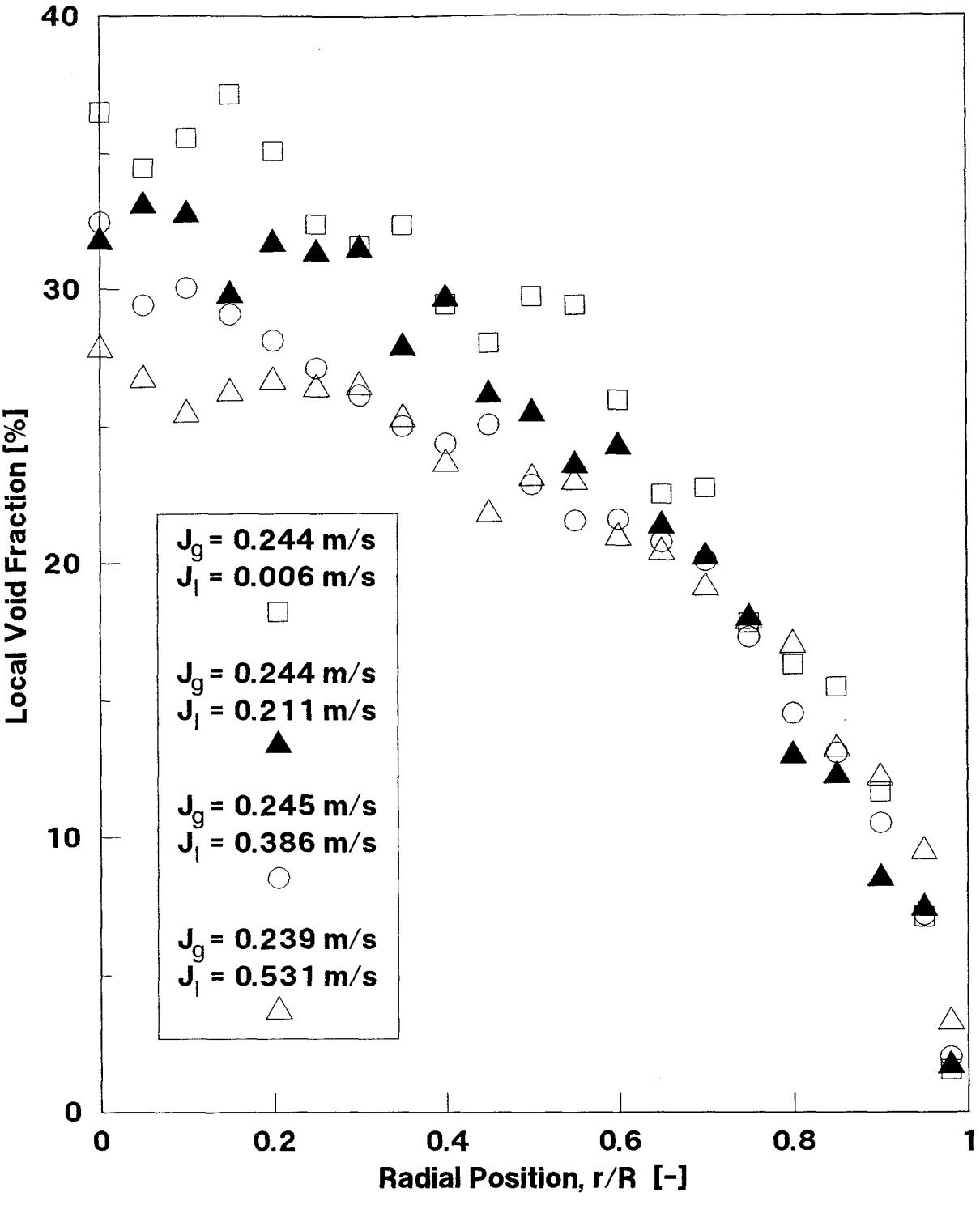

Figure 4.12: Radial Distribution of the Void Fraction in a 20-cm I.D. Vertical Pipe for Churn Flow Regime at $J_G \approx 0.24$ m/s

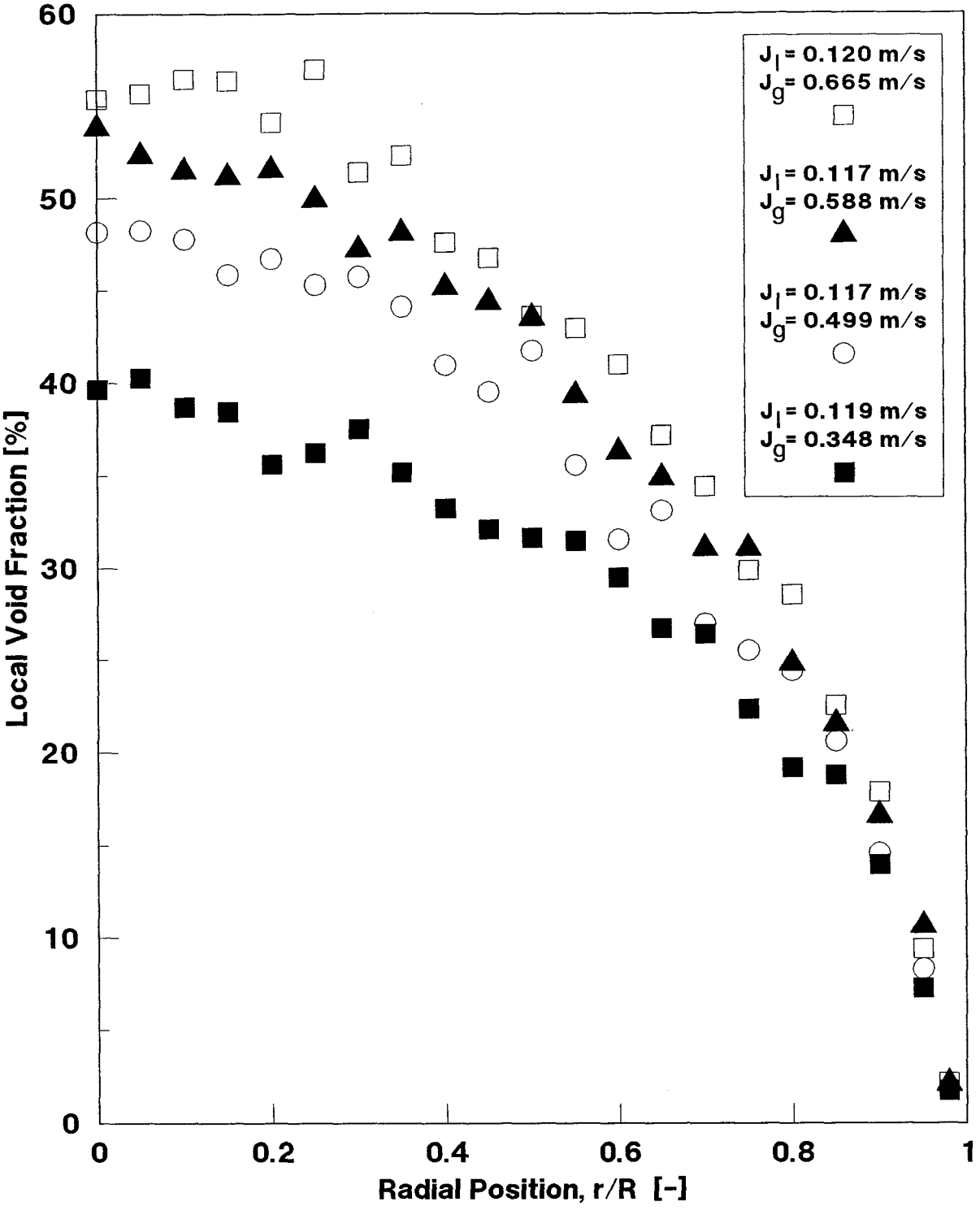

Figure 4.13: Radial Distribution of the Void Fraction in a 20-cm I.D. Vertical Pipe for Churn Flow Regime at $J_L \approx 0.12$ m/s

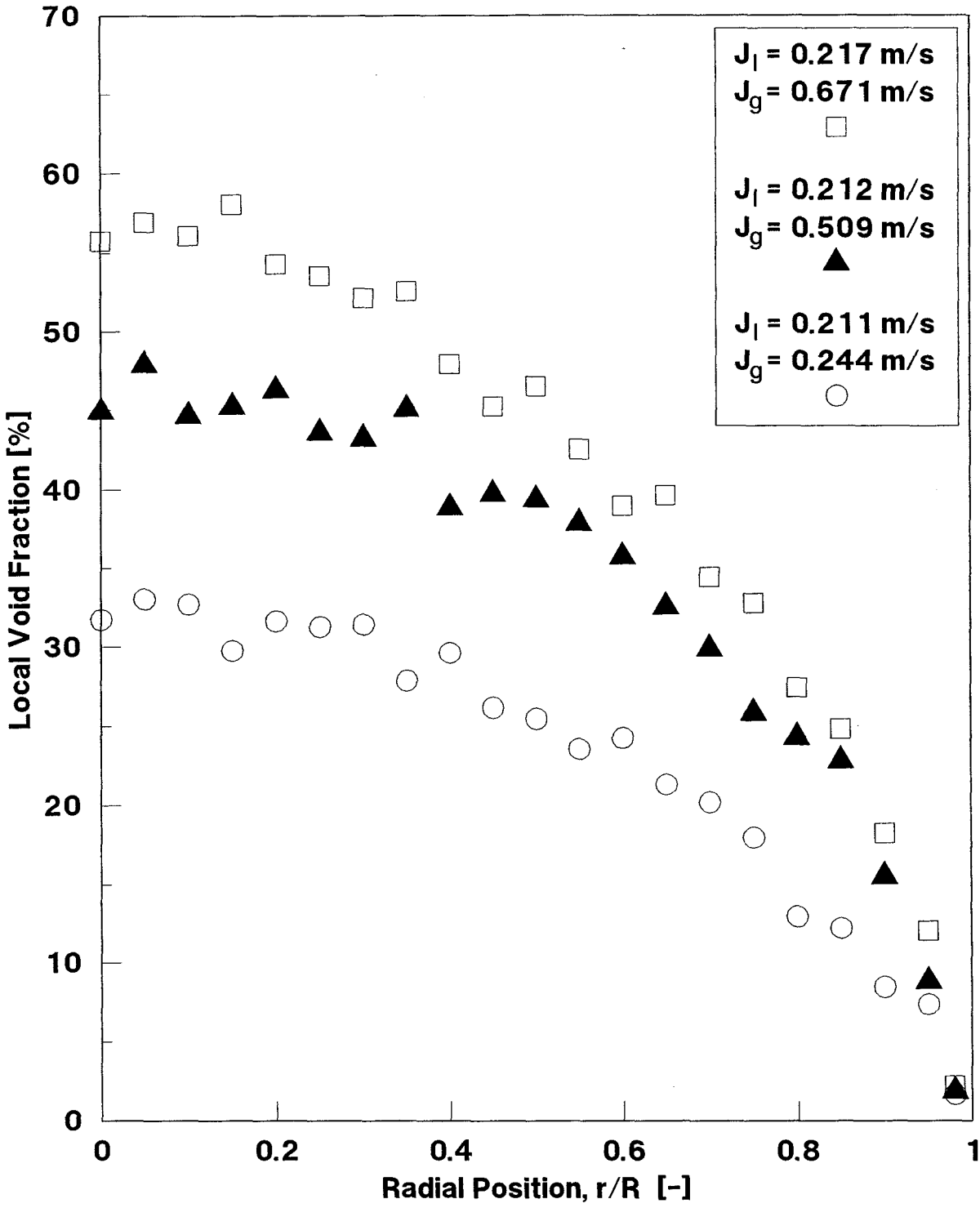

Figure 4.14: Radial Distribution of the Void Fraction in a 20-cm I.D. Vertical Pipe for Churn Flow Regime at $J_L \approx 0.21$ m/s

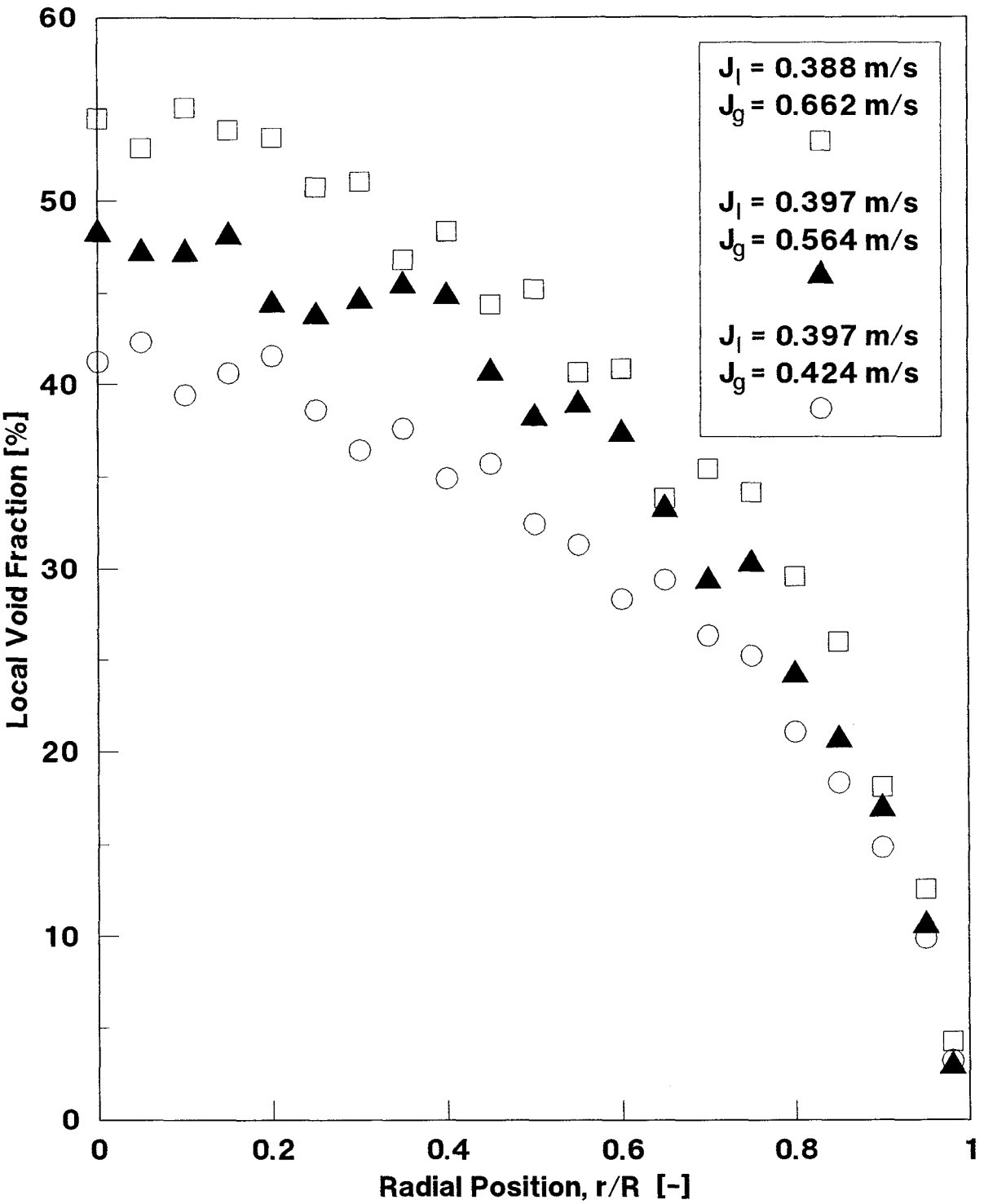

Figure 4.15: Radial Distribution of the Void Fraction in a 20-cm I.D. Vertical Pipe for Churn Flow Regime at $J_L \approx 0.39$ m/s

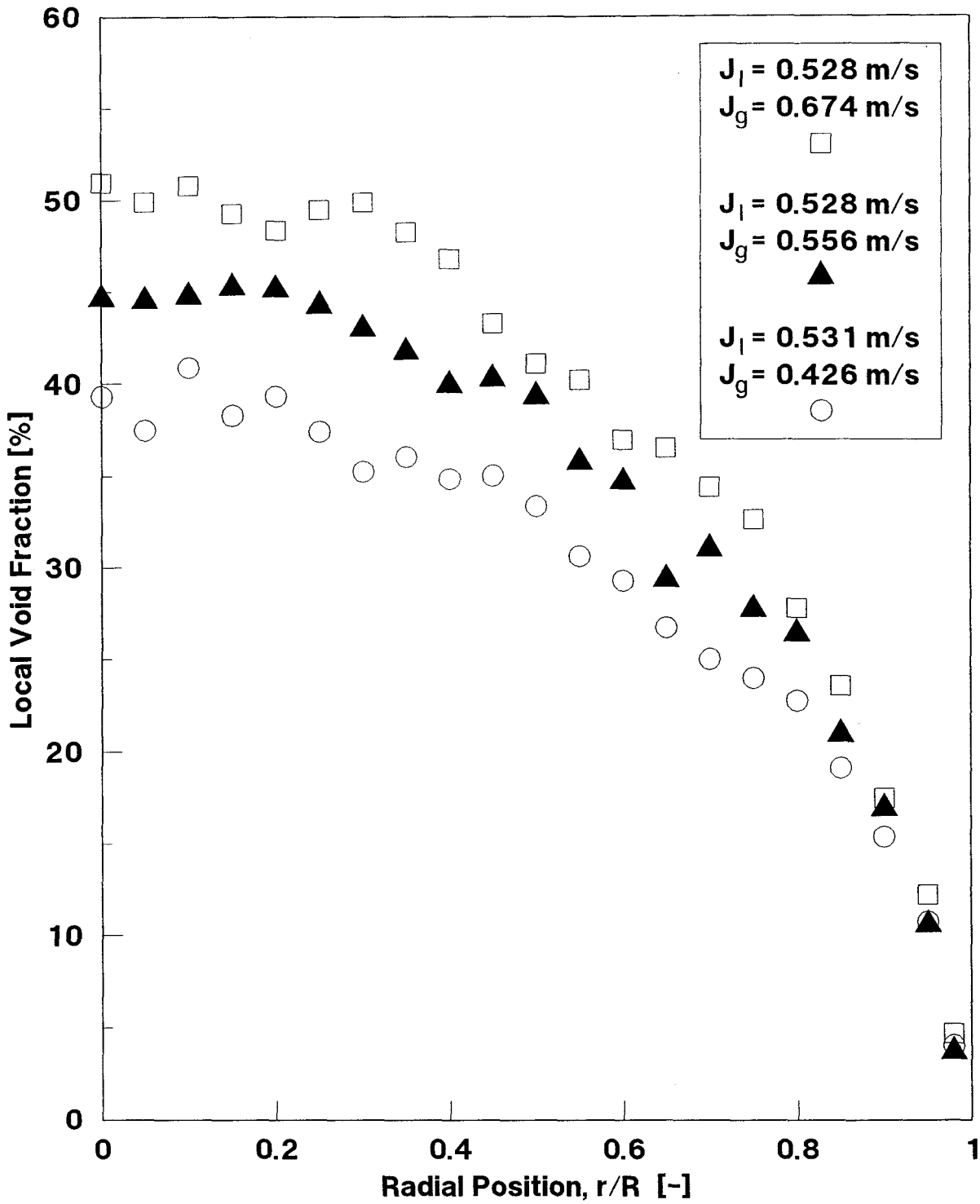

Figure 4.16: Radial Distribution of the Void Fraction in a 20-cm I.D. Vertical Pipe for Churn Flow Regime at $J_L \approx 0.53$ m/s

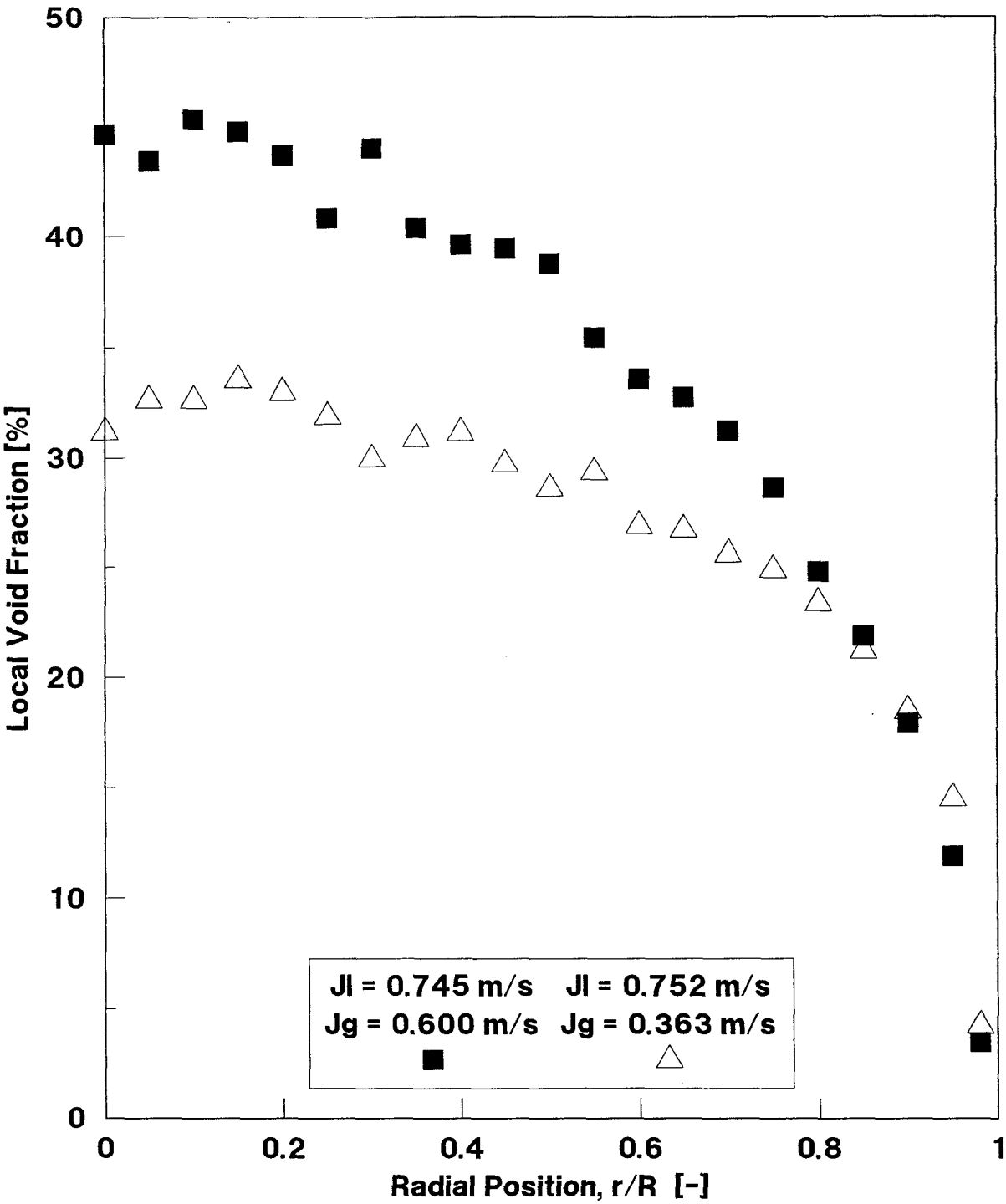

Figure 4.17: Radial Distribution of the Void Fraction in a 20-cm I.D. Vertical Pipe for Churn Flow Regime at $J_L \approx 0.75$ m/s

pipes, with increasing of the gas flow rate.

Void profiles obtained by operating the loop in the natural-circulation mode are shown in Figures 4.20 and 4.21. Figures 4.20 and 4.21 on pages 119 and 120, respectively, show radial distribution of the void fraction for various increasing superficial gas velocities and corresponding liquid flow rates, at fully open water control valve, for bubbly and churn flow regimes, respectively.

4.3.2. Comparison with Measured Void Profiles in Small Diameter Pipes

Of particular importance are radial profiles of forced-circulation two-phase flow regimes at low void fractions. To emphasize similarities and differences between small- and large-diameter pipes regarding existing of the saddle-type radial profile, results of this work were compared with results of other investigations. To examine the effect of a pipe diameter, comparisons were made between results obtained at almost the same superficial velocities and L/D ratio.

Figure 4.22 on page 122 shows a comparison between the results of **Liu and Bankoff** (1993) and the appropriate results of this work, for superficial liquid

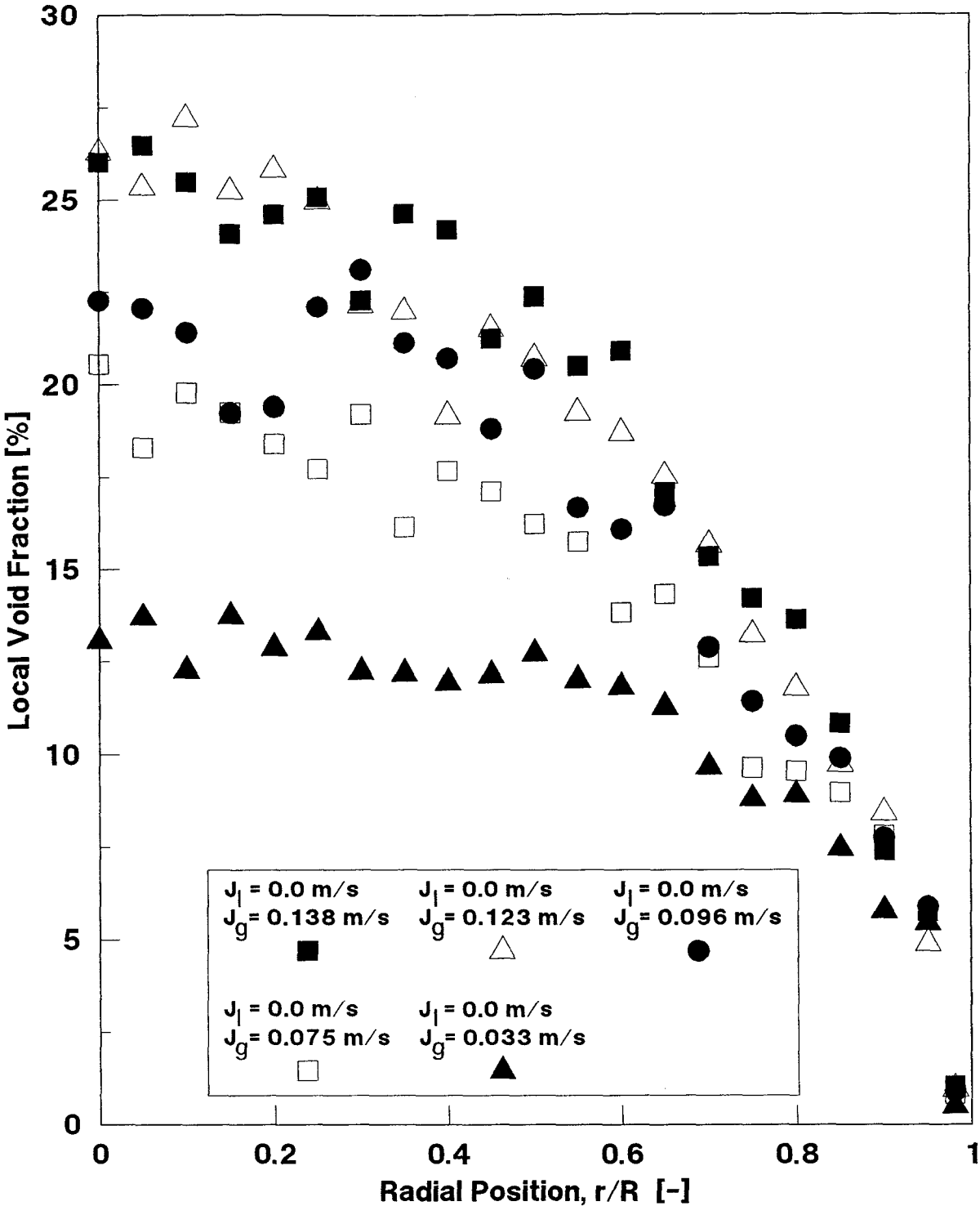

Figure 4.18: Radial Distribution of the Void Fraction in a 20-cm I.D. Vertical Pipe for Bubbly Flow Regime at Zero Liquid Flow Rate

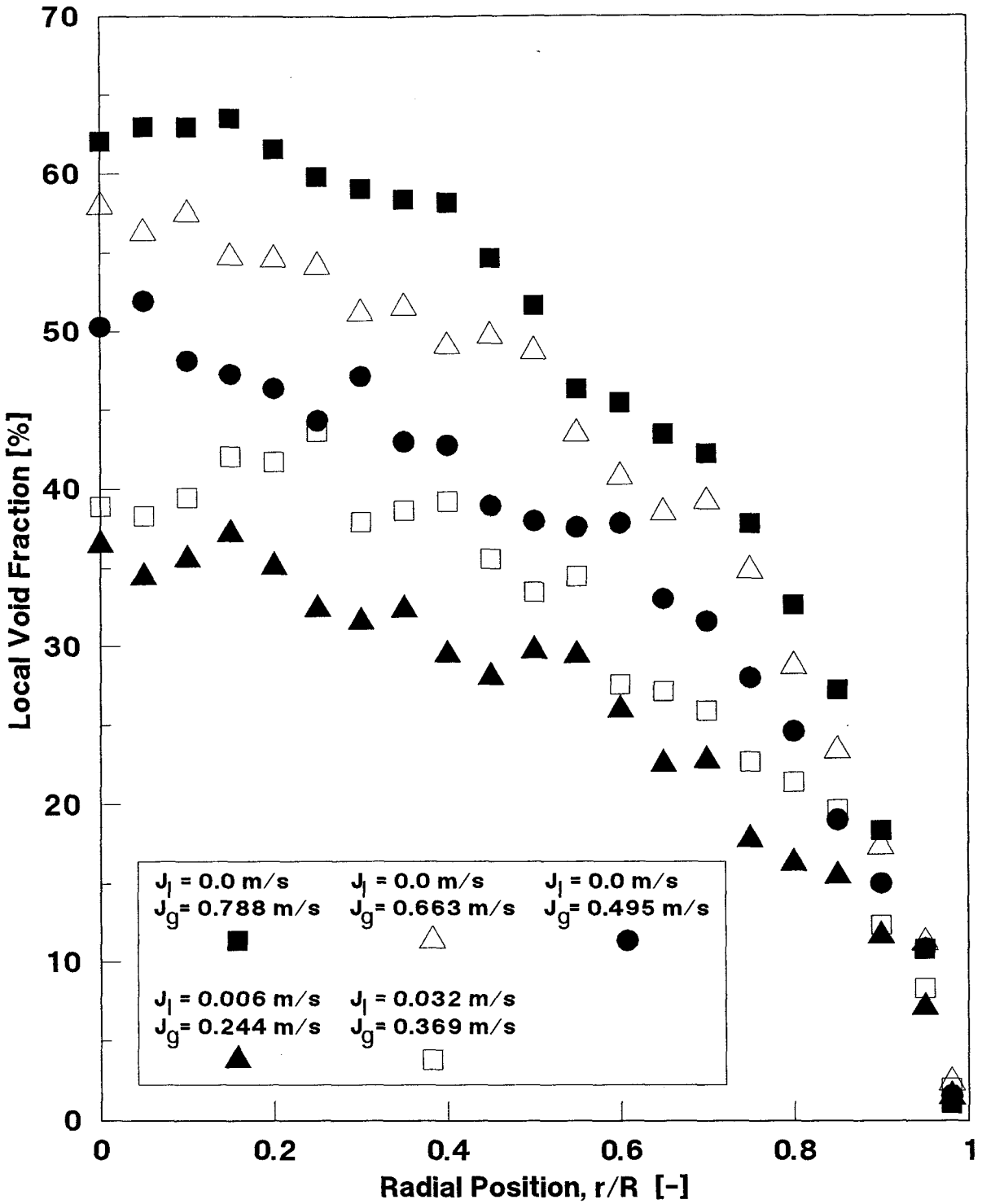

Figure 4.19: Radial Distribution of the Void Fraction in a 20-cm I.D. Vertical Pipe for Churn Flow Regime at Zero Liquid Flow Rate

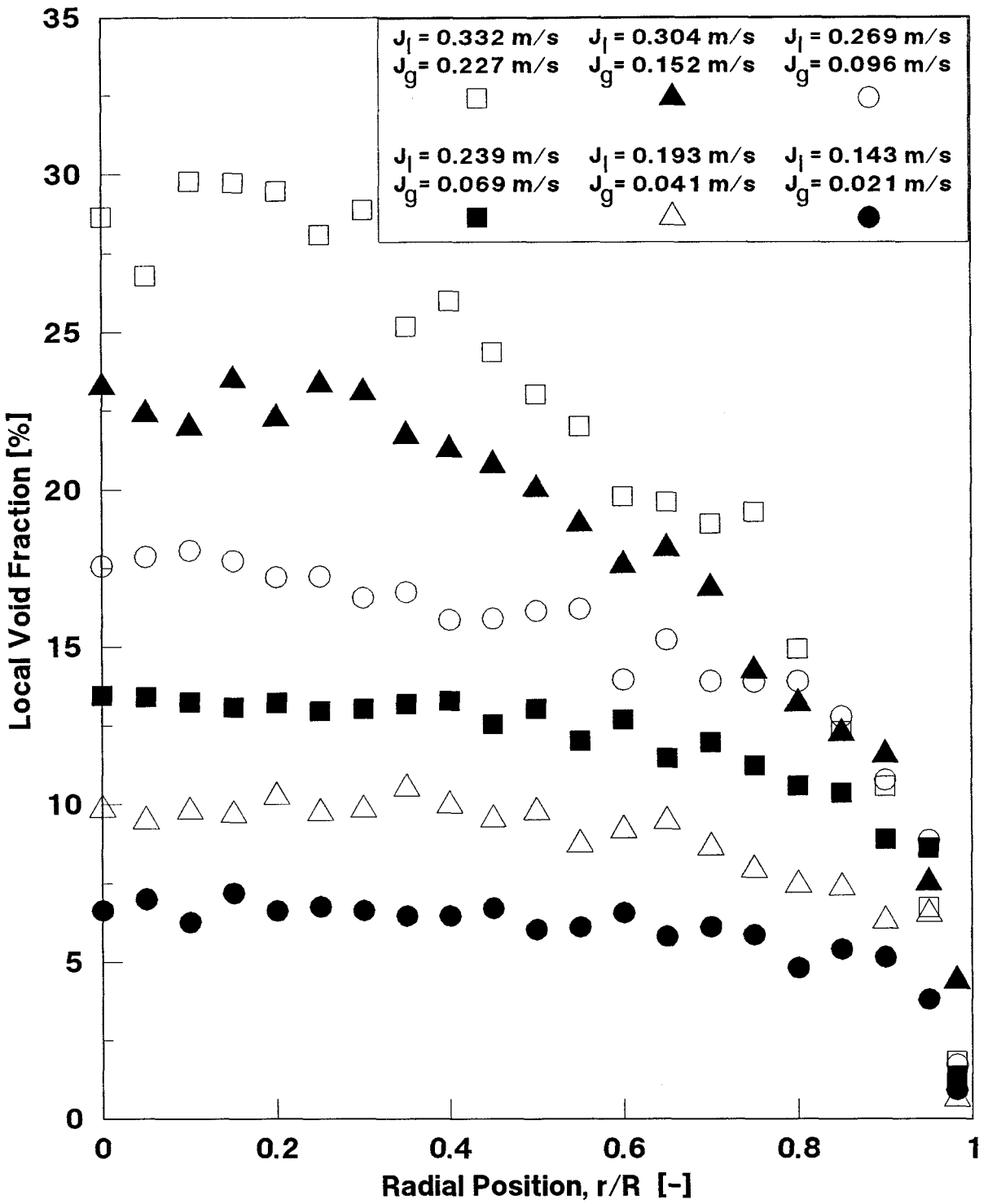

Figure 4.20: Radial Distribution of the Void Fraction in a 20-cm I.D. Vertical Pipe for Bubbly Two-Phase Flow Regime

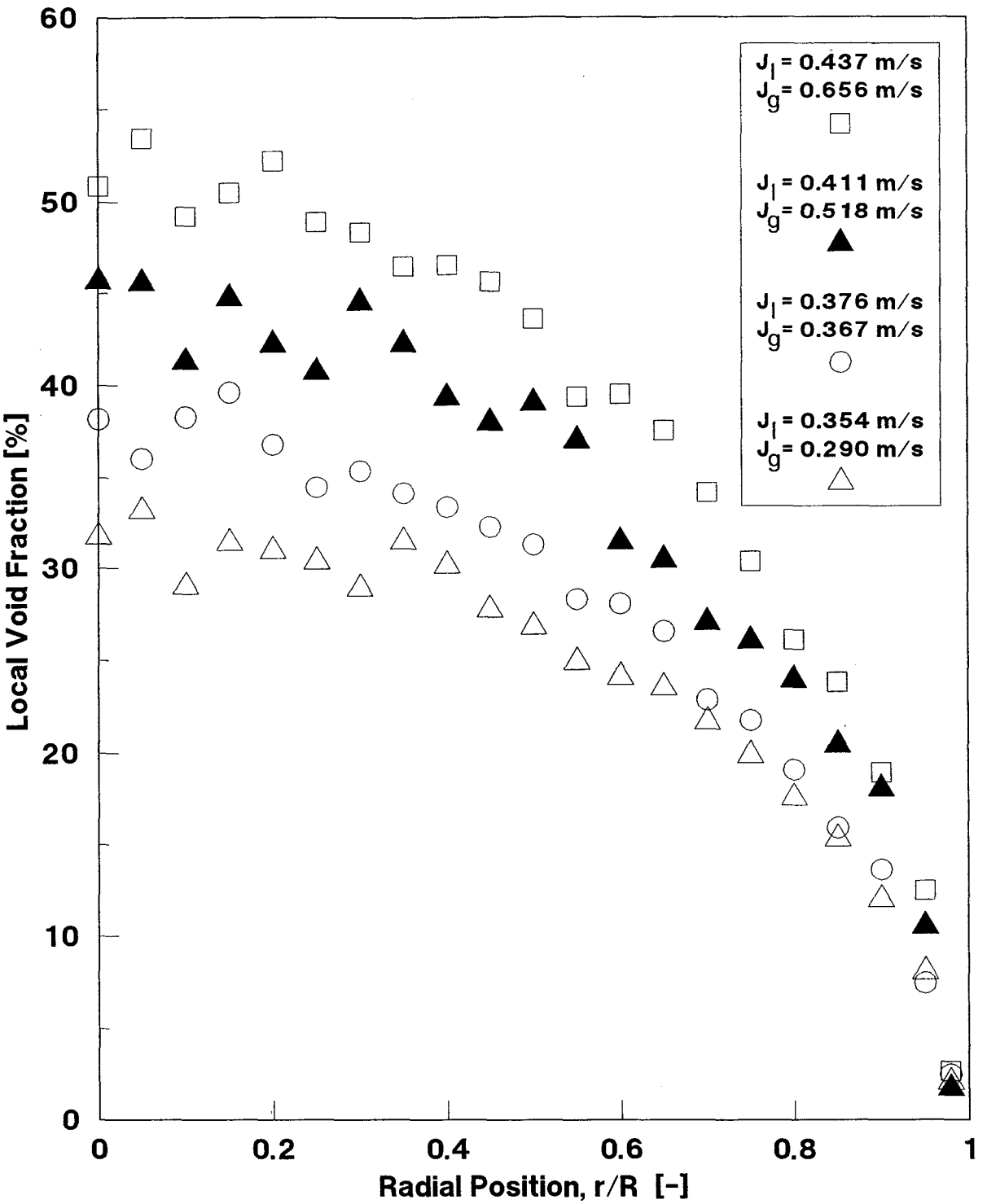

Figure 4.21: Radial Distribution of the Void Fraction in a 20-cm I.D. Vertical Pipe for Churn Two-Phase Flow Regime

velocity of about 0.75 m/s and superficial gas velocity of about 0.03 m/s. It can be noted that some similarity exists between the two profiles, according to these results. While a saddle-type radial void profile appears to exist in both cases, the peak value is much lower and closer to the wall in the large pipe. Also, in the large pipe, the void profile is almost flat in most of the pipe cross section.

Figure 4.23 on page 123 shows a comparison between the results of **Liu and Bankoff** (1993), **Serizawa *et al.*** (1975) and the appropriate results of this work, for superficial liquid velocity of about 0.75 m/s and comparable superficial gas velocities. It can be noted that a considerable difference in the type of radial void profile exists between small- and large-diameter vertical pipes, according to these results. While a typical saddle-type radial void profile characterizes two-phase flow in small-diameter vertical pipes, according to **Liu and Bankoff's** and **Serizawa *et al.*'s** results, flat-type radial void profiles dominate in two-phase flow in large-diameter vertical pipes, according to the results of this work.

Figure 4.24 on page 124 shows a comparison between the results of **Liu and Bankoff** (1993) and appropriate results of this work, for superficial liquid velocity of about 0.75 m/s and superficial gas velocity of about 0.3 m/s. It can be noted that, while the void distribution in large-diameter vertical pipe (present data) showed a flat parabolic profile, saddle-type profiles were obtained pipe by **Liu** and **Bankoff**

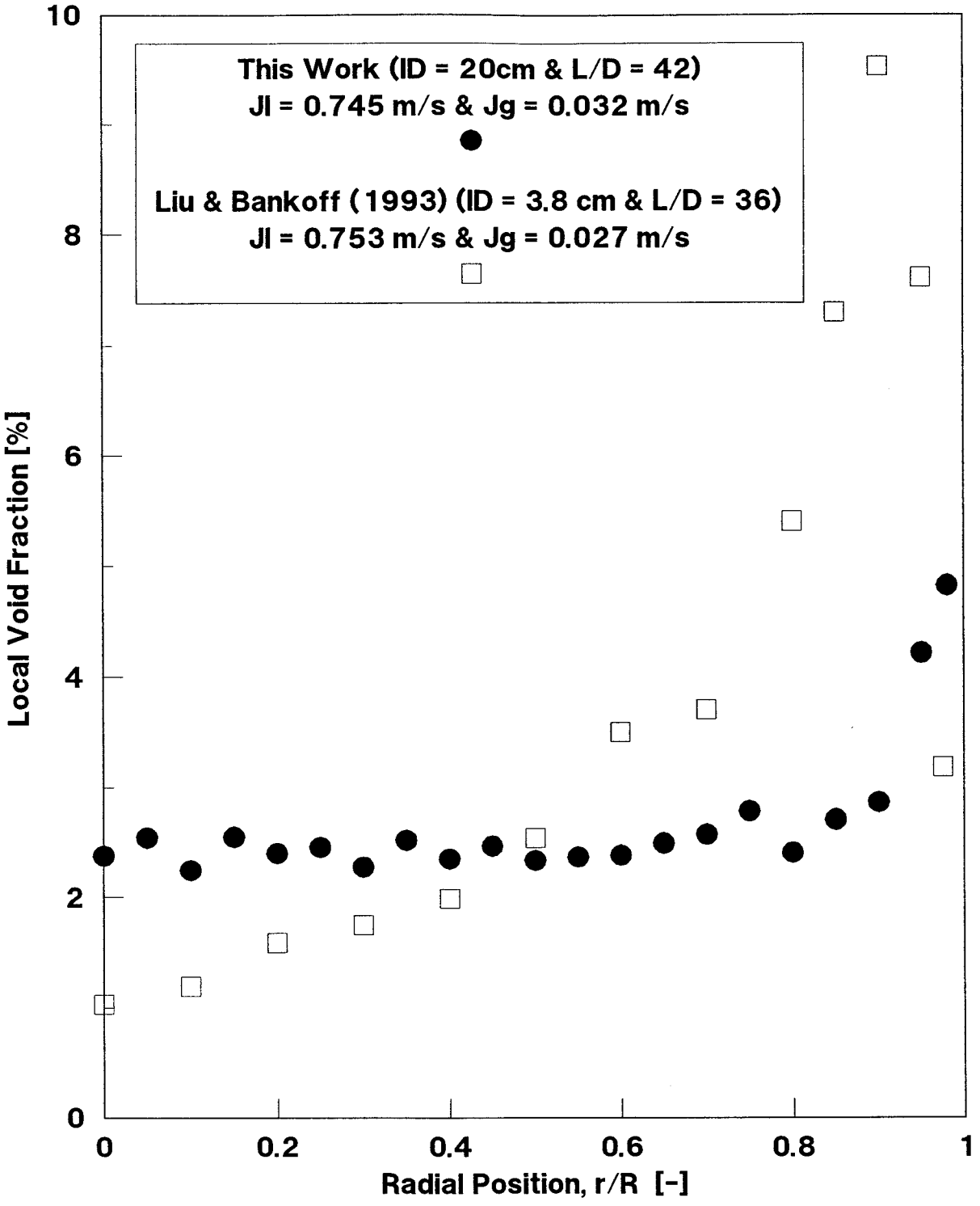

Figure 4.22: Comparison of Void Fraction Data of This Work with Data of Other Authors for $J_L \approx 0.75$ m/s and $J_G \approx 0.03$ m/s

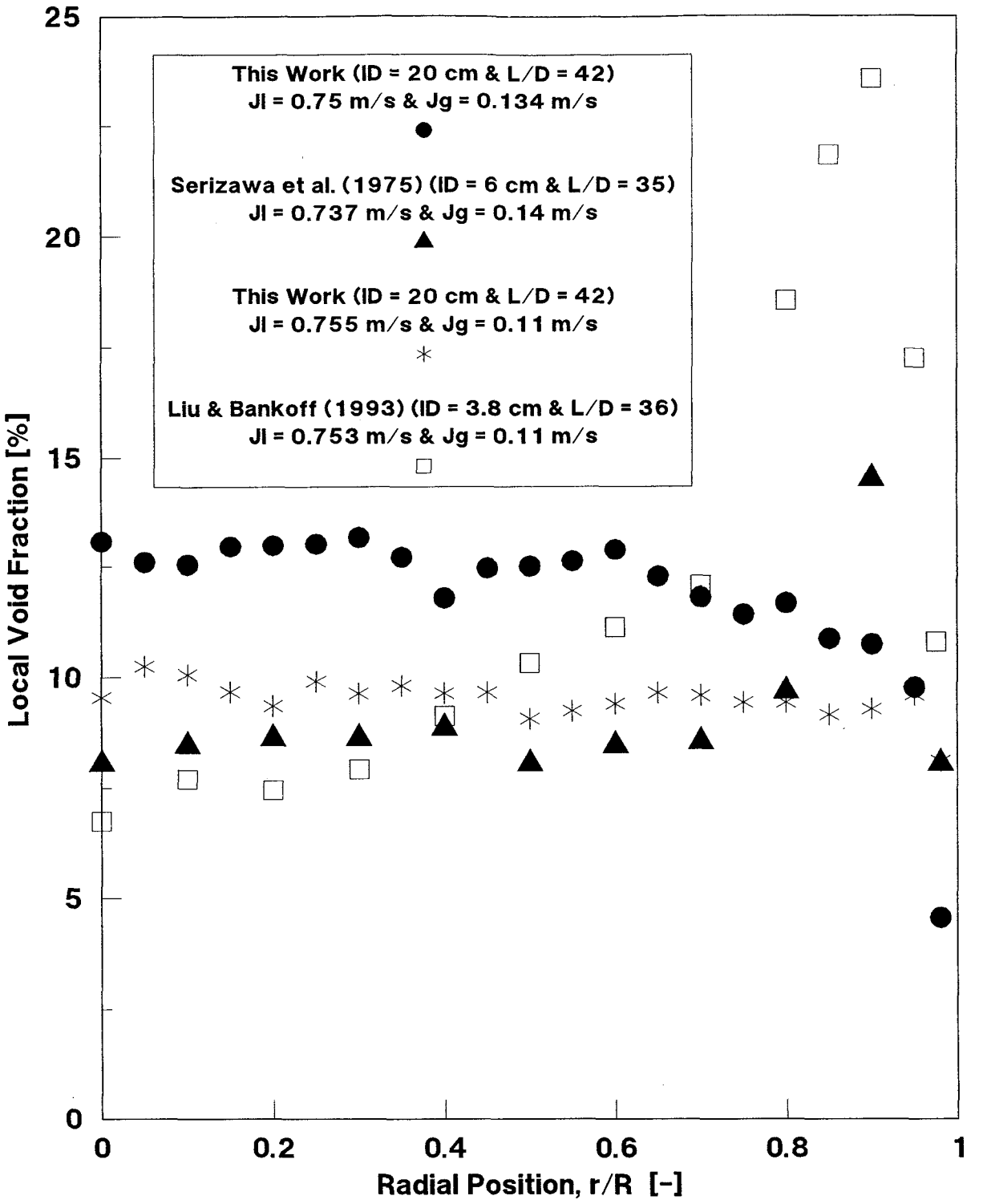

Figure 4.23: Comparison of Void Fraction Data of This Work with Data of Other Authors for $J_L \approx 0.75$ m/s and $J_G \approx 0.125$ m/s

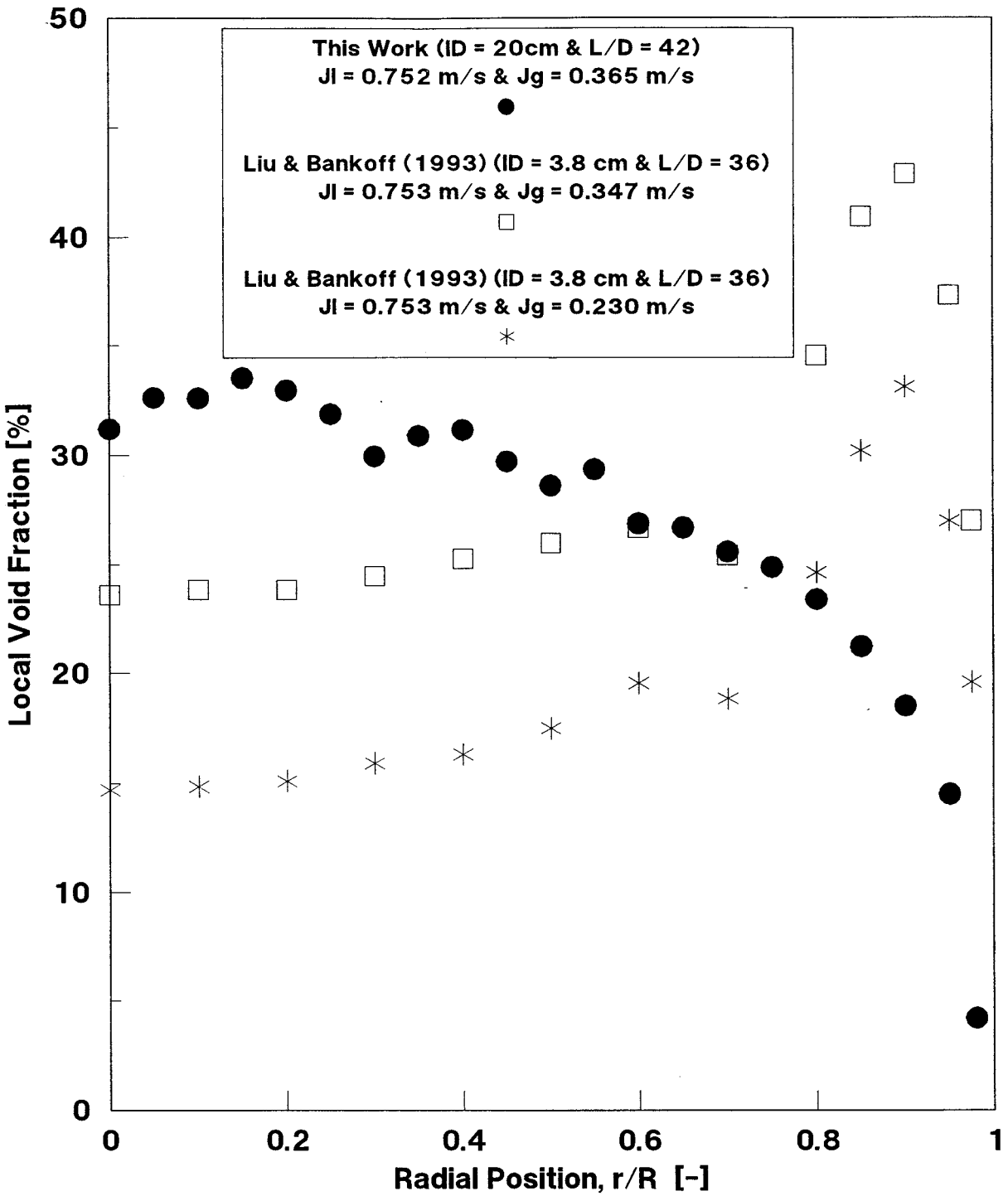

Figure 4.24: Comparison of Void Fraction Data of This Work with Data of Other Authors for $J_L \approx 0.75$ m/s and $J_G \approx 0.3$ m/s

in small-diameter vertical pipe.

The above results suggest that for low-void-fraction bubbly flow in large-diameter vertical pipes, the saddle-type void profile is typically encountered at lower superficial gas velocities, for a given liquid flow rate, as compared with small-diameter vertical pipes.

4.4. DRIFT-FLUX CORRELATIONS FOR A 20-cm DIAMETER VERTICAL PIPE

The data obtained in the 20-cm riser pipe were used to determine the two main parameters of the drift-flux model: the distribution parameter C_0 and the average local drift velocity U_{Gj}. As it was already explained in Chapter 2.2.2., the distribution parameter represents the effect of radial non-uniform velocity and concentration profiles, while the average local drift velocity represents the local velocity difference between the phases. It was shown that $C_0 < 1$ when the void fraction near the wall is higher than the void fraction in the center of a pipe (a saddle-type radial void profile) and, similarly, $C_0 > 1$ for a parabolic void fraction profile. When $C_0 > 1$ it was

analytically shown that the value of the distribution parameter varies between 1 for flat void profiles, up to 1.5 for parabolic void profiles. The drift velocity U_{Gj} can be estimated from **Harmathy's** correlation (1960) (equation 2.17) as the bubble terminal velocity and it results in a value of 0.24 m/s for air-water two-phase flow near atmospheric conditions.

The analysis was carried out by grouping of the flow regimes into the two main patterns observed during the tests, i.e., bubbly and churn flow patterns. For each flow regime (bubbly or churn) the data were plotted in terms of $\langle J_G \rangle / \langle \alpha \rangle$ versus $\langle J \rangle$ and fitted with a straight line. The slope of the line equals the distribution parameter, while the drift velocity was obtained by extrapolation of the line to $\langle J \rangle = 0$. The drift-flux correlations were only determined from the void fraction data obtained using measurements of the test-section pressure drop, because of less scatter of the results, especially for churn flow, in comparison with similar correlations from the optical-probe void fraction data.

Figure 4.25 on page 127 depicts drift-flux correlation, in terms of the two main drift--flux model parameters C_0 and U_{Gj}, for bubbly flow regime in the 20-cm diameter vertical pipe using void fraction results calculated from pressure drop measurements. The near-to-unity distribution parameter of 0.946, obtained for

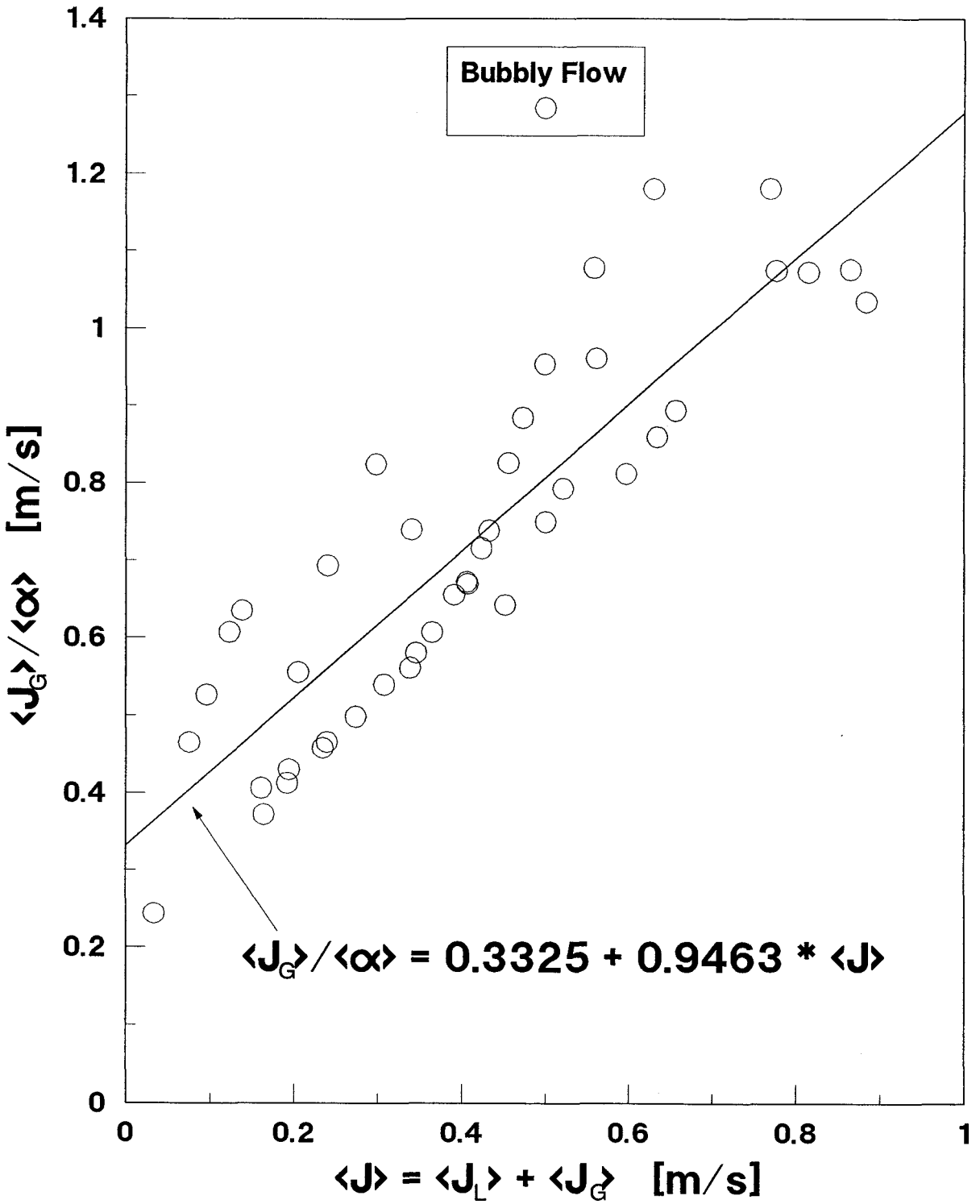

Figure 4.25: Drift-Flux Correlation for Bubbly Flow in a 20-cm I.D. Vertical Pipe from Pressure Drop Void Calculations

bubbly flow, reflects an essentially flat radial distribution of either the void fraction or the mean superficial velocity in bubbly two-phase flow through large-diameter vertical pipes. This value is different from estimations of **Hasan** (1988), who recommended a value of 1.2 for turbulent bubbly flow and a value of 2.0 for laminar bubbly flow, based on the assumption that gas bubbles occupy mostly the central portion of a vertical pipe (that is, for a parabolic void fraction profile). Since the radial void fraction distribution was found to be more uniform in large-diameter vertical pipes, according to these results, such difference appears to be a normal consequence of this fact. On the other hand, the drift velocity obtained for bubbly flow (0.33 m/s) is reasonably close to, and thus in good agreement with the typical value of 0.24 m/s recommended by many researchers.

Figure 4.26 on page 129 depicts drift-flux correlation, in terms of the two main drift--flux model parameters C_0 and U_{Gj}, for churn flow regime in the 20-cm diameter vertical pipe, using void fraction results calculated from pressure drop measurements. The distribution parameter very close to unity (0.998) obtained for churn flow is again slightly different from recommendations of **Hasan** (1988) (1.15 for churn flow) through a vertical pipe. Although this difference might be attributed to scattering of results due to inaccurate estimating of the average void fraction, on the other hand it confirms again that more uniform radial void distribution occurs in large-diameter vertical pipes, also for churn flow. According to these results, it

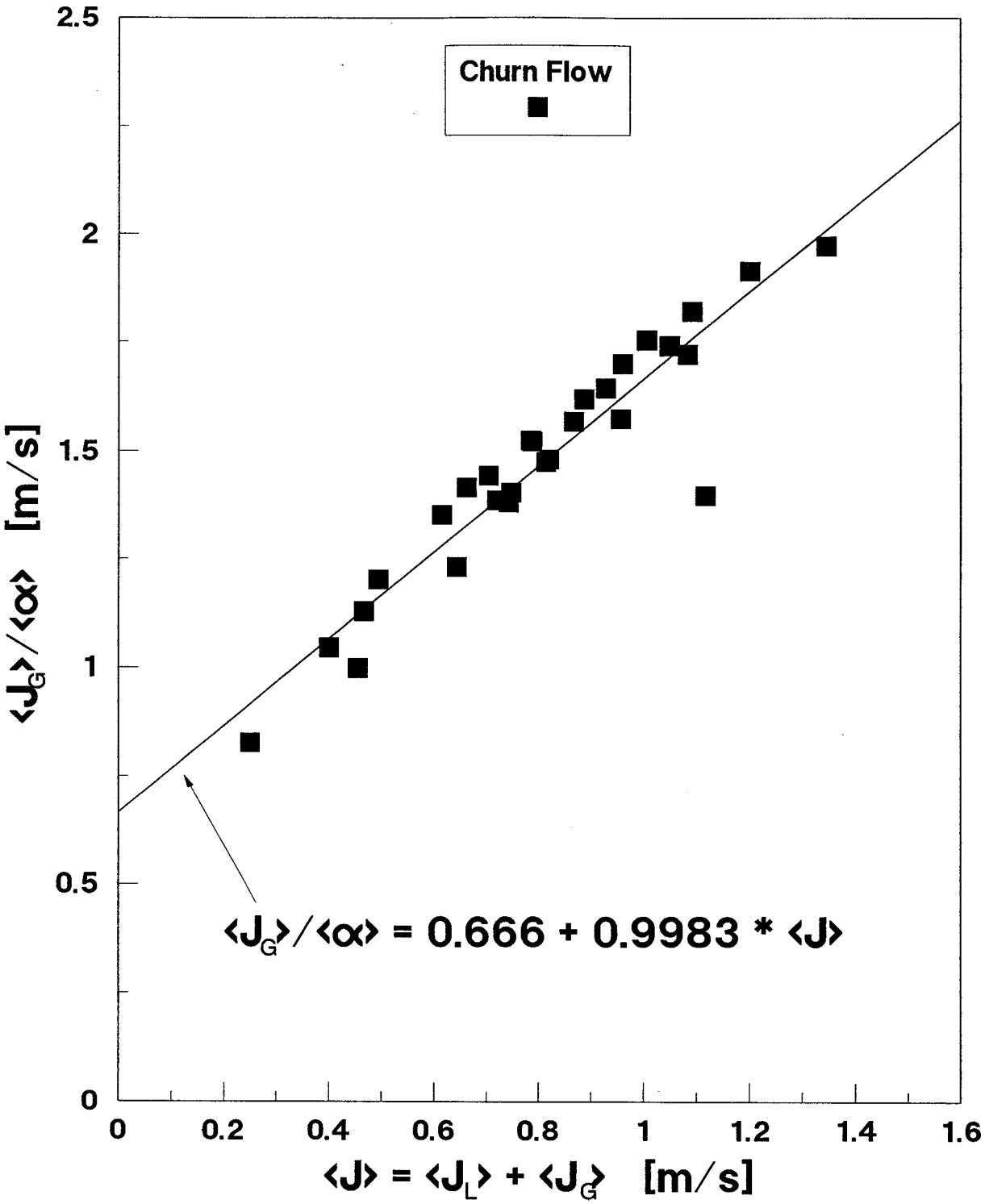

Figure 4.26: Drift-Flux Correlation for Churn Flow in a 20-cm I.D. Vertical Pipe from Pressure Drop Void Calculations

follows that radial distribution of phases in bubbly and churn flow depends on the pipe diameter. The close-to-unity distribution parameter reflects an essentially flat radial distribution of either the void fraction or the mean superficial velocity in two--phase flow through large-diameter vertical pipes. The drift velocity (0.666 m/s) obtained for churn flow, differs significantly from the typical recommended value of 0.24 m/s. So, according to these results, it appears that the drift velocity for churn flow increases with increasing of the pipe diameter, which agrees well with experimental results of some researchers (**Kataoka and Ishii** in 1987).

CHAPTER FIVE

CONCLUSIONS

The present investigation was driven by the need to obtain experimental data on flow regimes and the void fraction in large-diameter vertical pipes, in support of the design of a new passive moderator cooling system in CANDU reactors. The two--phase flow patterns depend on the local void fraction distribution in the cross section of a pipe. Also, the local void fraction is one of the most fundamental two--phase flow structure parameters because it has a significant effect on the pressure drop and the local heat transfer coefficient. It is, therefore, important to find a reliable method for measuring of the local void fraction with reasonable accuracy. In the present work, an **optical fiber probe** was used for local void fraction measuring and its accuracy was compared with accuracies of other measuring techniques.

A literature review was carried out for experimental work on local void fraction measurements in gas-liquid two-phase flow in vertical and horizontal pipes, using electrical resistivity probes and optical fiber probes. Also, a review of most important one-dimensional flow regime maps was given, with explanation of their

mathematical formulations. A common characteristic of the available data is a tendency to be limited to two-phase flow in small-diameter pipes, with a few exceptions.

An experimental test facility was designed and constructed for experiments on air--water co-current two-phase flow through vertical pipes of different diameters. The facility was designed to operate in either a natural circulation mode, as an air lift pump, or a forced circulation mode, using a centrifugal pump. Two different vertical pipe diameters were tested: 10 cm and 20 cm, but only the 20-cm diameter pipe results were presented in this thesis. The 10-cm diameter pipe results can be found in **Nada *et al.*** (1996). Measurements performed during the tests included: air and water flow rates, radial void fraction distribution, average cross-sectional void fraction, average volume void fraction, pressure drop across the test section, and air and water (two-phase mixture) temperatures. The radial distribution of the local void fraction was measured using an optical fiber probe, and the average volume void fraction in the test section was calculated from pressure drop measurements. A comparison between these two methods was presented.

The data were analysed in four parts. The first part dealt with flow patterns and flow regime maps, the second part compared various void fraction measuring techniques , the third part showed characteristics of local void fraction profiles and included

comparisons with experimental results of other investigators, and the fourth part involved correlating of the data using the drift-flux model. The following conclusions can be derived from this analysis:

1 - Based on visual observations, slug flow did not appear in the 20-cm diameter pipe during all tests.

2 - The data for 20-cm diameter pipe suggested that the bubbly-to-intermittent flow transition boundary should be corrected in the flow regime maps of **Taitel *et al.*** (1980), **Mishima and Ishii** (1984) and **Weisman and Kang** (1981). The present data suggest that the transition to intermittent flow is a weak function of the superficial liquid velocity and occurs in a narrow range of superficial gas velocity (between 0.15 m/s at very low superficial liquid velocity and 0.30 m/s at $J_L \approx 1$ m/s).

3 - A comparison of the data for the 20-cm diameter pipe and transition boundary curves from the flow regime maps, showed that both the position and shape of the bubbly-to-intermittent flow transition boundary depend on the pipe diameter. The transition from bubbly to intermittent flow in the 20-cm diameter pipe occurred at the void fraction of about 25%, which is in very good agreement with **Taitel *et al.*'s** assumption used in generation of their flow regime map.

4 - According to comparisons between different void fraction measuring techniques, the optical fiber probe showed very good accuracy in the 20-cm diameter pipe. This conclusion was deduced from comparison of void fraction measurements using the optical fiber probe and the test-section pressure drop from the pressure transducer. The optical fiber probe slightly overestimated the void fraction in comparison with the pressure transducer in the 20-cm diameter pipe, which was probably caused by underestimating of the calculated frictional pressure drop at high superficial liquid velocities.

5 - For low-void-fraction bubbly flow at high superficial liquid velocities (J_L > 0.5 m/s) a typical saddle-type void distribution at higher liquid flow rates and low void fractions was observed. A near wall void peak, typical for the saddle-type radial profile, was gradually reduced and changed to the parabolic shaped profile, with increasing of the gas flow rate. This agrees well with the findings of previous investigators for small-diameter pipes.

6 - Radial void profiles in the 20-cm diameter pipe for bubbly flow at low liquid flow rates typically changed from a flat-type shape to a parabolic shape with obtuse center peak, with increasing the gas flow rate. Radial profiles for churn flow at low liquid flow showed essentially parabolic shapes. The data showed absence of a parabolic profile with sharp center peak, which was attributed to a uniform radial

void distribution in the 20-cm diameter pipe.

7 - In the range of high liquid flow rates and very low void fractions, a similarity with saddle-type radial void profiles in small-diameter pipes was observed. According to comparison of these data to corresponding data of **Liu and Bankoff** (1993), it was deduced that in large-diameter pipes the saddle-type profile is more flat, with lower peak near the pipe wall than in small-diameter pipes. With increasing the gas flow rate, radial void profiles in large-diameter pipes rapidly changed from saddle--type to flat-type shape, or even to parabolic shape. In the same situation, radial void profiles in small-diameter pipes remained with saddle-type shape, according to results of **Serizawa *et al.*** (1975) and **Liu and Bankoff** (1993).

8 - The data were correlated using the drift-flux model. A near unity distribution parameter was obtained for data in the 20-cm diameter pipe. This showed that a nearly flat radial distribution of the void fraction or the mean superficial velocity in two-phase flow through large-diameter vertical pipes. The data showed an increase of the drift velocity with the increase of the pipe diameter. This effect was much more dominant in churn flow than in bubbly flow. The results confirmed the dependence of the radial distribution of phases on the pipe diameter both in bubbly and churn flow.

REFERENCES

ASME Research Committee Report on Fluid Meters, 1959, "Fluid Meters, Their Theory and Application", American Society of Mechanical Engineers, New York.

Andreussi, P., Bendiksen, K.H. and Nydal, O.J., 1993, "Void distribution in slug flow", International Journal of Multiphase Flow, Vol. 19, No. 5, pp. 817-828.

Annunziato, M. and Girardi, G., 1985, "Statistical methods to identify two-phase regimes: experimental results for vertical large diameter tubes", Proceedings of the 2nd International Conference on Multi-Phase Flow, London, England, June 1985, Paper G5, pp. 361-380.

Barnea, D. and Shemer, L., 1989, "Void fraction measurements in vertical slug flow: Applications to slug characteristics and transition", International Journal of Multiphase Flow, Vol. 15, No. 4, pp. 495-504.

Carrica, P.M., Moraga, F., and Clausse, A., 1992, "Measurements of void fraction spatial distribution in pool boiling", International Communications in Heat and Mass Transfer, Vol. 19, No. 4, pp. 499-505.

Clark, N. and Flemmer, R., 1986, "The effect of varying gas voidage distributions on average holdup in vertical bubble flow", International Journal of Multiphase Flow, Vol. 12, No. 2, pp. 299-302.

Das, R. and Pattanayak, S., 1994, "Measurement of void fraction in different flow regimes of a vertical gas-liquid flow through narrow tubes", Measurement Science & Technology, Vol. 5, No. 12, pp. 1538-1545.

Delhaye J.M., 1981, "Instrumentation", Chapter 15 of "Two-Phase Flow and Heat Transfer in the Power and Process Industries", Hemisphere Publishing Corporation, pp. 455-483.

Harmathy, T.Z., 1960, "Velocity of large drops and bubbles in media of infinite or restricted extent", AICHE Journal, Vol. 6, pp. 281.

Hasan, A.R., 1988, "Void fraction in bubbly, slug and churn flow in vertical two--phase up-flow", Chemical Engineering Communications, Vol. 66, pp. 101-111.

Hasan, A.R. and Kabir, C.S., 1992, "Two-phase flow in vertical and inclined annuli", International Journal of Multiphase Flow, Vol. 18, No. 2, pp. 279-293.

Hewitt, G.F. and Roberts D.N., 1969, "Studies of two-phase flow patterns by simultaneous X-ray and flash photography", AERE-M2.

Hinata, S., Sakurai, M., Nakazawa, M., Venart, J.E.S., Sousa, A.C.M. and Zhou, B., 1991, "Miniature optical fiber sensor used to measure local void fractions", Heat Transfer - Japanese Research, Vol. 20, No. 5, pp. 429-440.

Hinata, S., Sakurai, M., Kuga, O., Nakazawa, M., Venart, J.E.S., Sousa, A.C. M. and Ahn, K.J., 1992, "Void fraction and temperature measurements for pool boiling around a horizontal cylindrical surface", Heat Transfer - Japanese Research, Vol. 21, No. 4, pp. 404-411.

van Hout, R., Shemer, L. and Barnea, D., 1992, "Spatial distribution of void fraction within a liquid slug and some other related slug parameters", International Journal of Multiphase Flow, Vol. 18, No. 6, pp. 831-845.

Ishii, M., 1977, "One-dimensional drift-flux model and constitutive equations for relative motion between phases in various flow regimes", Argonne National Laboratory Report ANL-77-47.

Jones, O.C., Abuaf, N., Zimmer, G.A. and Feierabend, T., 1981, "Void fluctuation dynamics and measurement techniques", Proceedings of 1979' Japan-US Seminar on Two-Phase Flow Dynamics, Hemisphere Publishing Corporation, pp. 145-163.

Kataoka, I. and Ishii, M., 1987, "Drift-flux model for large diameter pipe and new correlation for pool void fraction", International Journal of Heat and Mass Transfer, Vol. 30, No. 9, pp. 1927-1939.

Keska, J.K. and Fernando, R.D., 1994, "Average physical parameters in an air--water two-phase flow in a small, square-sectioned channel", Journal of Fluids Engineering, Transactions of ASME, Vol. 116, No. 2, pp. 247-256.

Khartabil, H.F. and Spinks, N.J., 1995, "An experimental study of a flashing-driven CANDU moderator cooling system", Proceedings of the 1995 16th Annual Conference of the Canadian Nuclear Society, AECL Report.

Kocamustafaogullari, G. and Wang, Z., 1991, "An experimental study on local interfacial parameters in a horizontal bubbly two-phase flow", International Journal of Multiphase Flow, Vol. 17, No. 5, pp. 553-572.

Leung, W.H., Revankar, S.T., Ishii, Y. and Ishii, M., 1995, "Axial development of interfacial area and void concentration profiles measured by double-sensor probe

method", International Journal of Heat and Mass Transfer, Vol. 38, No. 3, pp. 445--453.

Liu, T.J. and Bankoff, S.G., 1993, "Structure of air-water bubbly flow in a vertical pipe - II. Void fraction, bubble velocity and bubble size distribution", International Journal of Heat and Mass Transfer, Vol. 36, No. 4, pp. 1061-1072.

Mann, R. and Hackett, L.A., 1985, "Interpretation of bubble cloud statistics gathered by fibre optic phase detection", Proceedings of the 2nd International Conference on Multi-Phase Flow, London, England, June 1985, Paper G4, pp. 345--354.

Michiyoshi, I., Serizawa, A. and Yamaoka, N., 1986, "Turbulence in two-phase bubbly flow", Nuclear Engineering and Design, Vol. 95, Japan-US Seminar on Two--Phase Flow Dynamics, Lake Placid, NY, August 1984, pp. 253-267.

Mishima, M. and Ishii, M., 1984, "Flow regimes transition criteria for upward two--phase flow in vertical tubes", International Journal of Heat and Mass Transfer, Vol. 27, No. 5, pp. 723-736.

Moore, A.E. and Turley D.N., 1983, "Two-phase flow information from simple, rapid response time instruments", Proceedings of the International Conference on the Modelling and Multi-Phase Flow, Coventry, England, April 1983, Paper H2, pp. 353--376.

Moujaes, S.F., 1990, "Testing of a spherical dual-tipped optical fiber probe for local measurements of void fraction and gas velocity in two-phase flows", Canadian Journal of Chemical Engineering, Vol. 68, No. 3, pp. 504-510.

Nada, S.M., Abdul-Razzak, A., Stankovic, B. and Shoukri, M., 1996, "Flow regimes and drift-flux correlations for gas-liquid flow in large diameter vertical pipes", International Congress of Fluid Dynamics and Propulsion, Cairo, Egypt, December 27-30, 1996.

Ohashi, H., Matsumoto, Y., Ichikawa, Y. and Tsukiyama, T., 1990, "Air / water two-phase flow test tunnel for airfoil studies", Experiments in Fluids, Vol. 8, No. 5, pp. 249-256.

Ohnuki, A., Akimoto, H. and Sudo, Y., 1995, "Flow pattern and its transition in gas-liquid two-phase flow along a large vertical pipe", Proceedings of the 2nd International Conference on Multiphase Flow '95, Kyoto, Japan.

Qazi, M.K., Lavalle, G. Guido and Clausse, A., 1993, "Axial development of void fraction profiles in vertical two-phase flow", International Journal of Multiphase Flow, Vol. 19, No. 2, pp. 385-389.

Sekoguchi, K., Fukui, H. and Sato, Y., 1981, "Flow characteristics and heat transfer in vertical bubble flow", Proceedings of 1979' Japan-US Seminar on Two--Phase Flow Dynamics, Hemisphere Publishing Corporation, pp. 59-74.

Serizawa, A, Kataoka, I. and Michiyoshi, I., 1975, "Turbulence structure of air--water bubbly flow - II. Local properties", International Journal of Multiphase Flow, Vol. 2, pp. 235-246.

Serizawa, A., Tsuda, K. and Michiyoshi, I., 1983, "Real-time measurement of two--phase flow turbulence using a dual-sensor anemometry", Proceedings of Symposium on the Measuring Techniques in Gas-Liquid Two-Phase Flows, Nancy, France, July 1983, pp. 495-523.

Sorour, M.M. and El-Beshbeeshy, M.S., 1986, "Void fraction and pressure fluctuations of bubbly flow in a vertical annular channel", Experiments in Fluids, Vol. 4, No. 3, pp. 163-170.

Sun, G., 1997, "Private communication".

Takamasa, T., 1988, "Effects of wall roughness and entry length on void profile in vertical bubbly flow", Journal of Nuclear Science and Technology, Vol. 25, No. 2, pp. 180-189.

Taitel, Y., Barnea, D. and Dukler, A.E., 1980, "Modelling flow pattern transitions for steady upward gas-liquid flow in vertical tubes", AIChE Journal, Vol. 26, No. 3, pp. 345-354.

Tawfik, H., 1979, "Experimental and theoretical investigation of void measurement accuracy using resistivity probes", Doctoral Thesis, University of Waterloo, Waterloo, Ontario.

Todreas, N.E. and Kazimi, M.S., 1990, "Nuclear Systems I: Thermal Hydraulic Fundamentals", Hemisphere Publishing Corporation, pp. 463-473.

Tokuhiro, A.T. and Lykoudis, P.S., 1994, "Natural convection heat transfer from a vertical plate - I. Enhancement with gas injection; - II. With gas injection and transverse magnetic field", International Journal of Heat and Mass Transfer, Vol. 37, No. 6, pp. 997-1003 (Part I), pp. 1005-1012 (Part II).

Weisman, J., 1981, "Flow pattern identification in concurrent vapor-liquid flow", Proceedings of 1979' Japan-US Seminar on Two-Phase Flow Dynamics, Hemisphere Publishing Corporation, pp. 95-117.

Weisman, J. and Kang, S.Y., 1981, "Flow pattern transitions in vertical and upwardly inclined lines", International Journal of Multiphase Flow, Vol. 7, pp. 271--291.

Zuber, N. and Hench, J., 1962, "Steady-state and transient void fraction of bubbling systems and their operating limits", General electric Company Report, No. 62 GL 100, Schenectady, NY.

Zuber, N. and Findlay, J.A., 1965, "Average volumetric concentration in two-phase flow systems", Journal of Heat Transfer, pp. 453-468.

Zun, I., 1985, "The role of void peaking in vertical two-phase bubbly flow", Proceedings of the 2nd International Conference on Multi-Phase Flow, London, England, June 1985, Paper C3, pp. 127-139.

APPENDIX

TABLES OF EXPERIMENTAL RESULTS FOR 20-cm DIAMETER PIPE

TABLE 1 - LOCAL MEASUREMENT LOCATIONS

LOCATION (AREA NO.)	r/R -
1	0.980
2	0.950
3	0.900
4	0.850
5	0.800
6	0.750
7	0.700
8	0.650
9	0.600
10	0.550
11	0.500
12	0.450
13	0.400
14	0.350
15	0.300
16	0.250
17	0.200
18	0.150
19	0.100
20	0.050
21	0.000

TABLE 2 - LOCAL VOID FRACTIONS IN 20-cm DIAMETER PIPE

TEST	SUPERFICIAL	SUPERFICIAL	LOCAL	VOID	FRACTION	AT	RELATIVE	LOCATION	r/R		
NUMBER	GAS VELOCITY	LIQUID VELOCITY	0.000	0.050	0.100	0.150	0.200	0.250	0.300	0.350	0.400
-	[m/s]	[m/s]	[%]	[%]	[%]	[%]	[%]	[%]	[%]	[%]	[%]
TEST #001	0.021	0.143	6.66	7.015	6.275	7.195	6.64	6.77	6.645	6.48	6.475
TEST #002	0.030	0.164	7.47	7.385	7.595	7.69	7.8	7.335	7.705	7.57	7.705
TEST #003	0.041	0.193	9.85	9.475	9.78	9.66	10.235	9.73	9.83	10.51	9.955
TEST #004	0.043	0.196	9.805	9.955	9.535	9.74	10.38	10.19	9.915	9.595	9.96
TEST #005	0.055	0.219	11.845	12.145	11.785	11.61	12.17	12.045	11.79	11.68	11.4
TEST #006	0.069	0.239	13.47	13.415	13.255	13.09	13.23	12.97	13.035	13.18	13.285
TEST #007	0.081	0.258	14.76	14.57	15.63	15.47	15.07	15.135	15.775	14.42	14.265
TEST #008	0.096	0.269	17.57	17.865	18.06	17.73	17.215	17.24	16.56	16.74	15.855
TEST #009	0.087	0.259	16.215	15.61	15.82	15.565	15.39	16.28	15.695	16.635	15.255
TEST #010	0.110	0.281	19.59	18.67	18.77	19.115	19.015	18.7	18.325	19.17	18.26
TEST #011	0.118	0.288	20.3	19.25	18.405	19.67	18.79	20.825	19.2	19.52	18.305
TEST #012	0.129	0.295	21.355	20.63	20.54	20.645	21.185	19.605	19.89	19.68	18.67
TEST #013	0.135	0.298	20.965	21.45	21.44	21.715	19.91	20.315	22.115	20.085	19.585
TEST #014	0.152	0.304	23.26	22.39	21.975	23.475	22.24	23.34	23.07	21.685	21.255
TEST #015	0.164	0.309	26.19	24.435	24.045	25.915	23.93	23.49	22.805	21.815	22.905
TEST #016	0.183	0.317	25.795	26.115	25.875	25.035	24.435	23.535	25.235	22.385	23.825
TEST #017	0.290	0.354	31.74	33.15	29	31.365	30.94	30.35	28.885	31.43	30.13
TEST #018	0.367	0.376	38.175	36.03	38.27	39.59	36.785	34.45	35.33	34.09	33.345
TEST #018A	0.370	0.378	36.775	38.725	37.715	35.725	36.56	36.385	32.345	34.285	33.3
TEST #019	0.425	0.390	38.745	40.83	43.11	38.275	40.45	37.63	38.075	38.125	34.13
TEST #020	0.227	0.332	28.66	26.795	29.775	29.74	29.47	28.085	28.87	25.17	25.98
TEST #021	0.467	0.401	41.965	41.135	41.74	42.815	41.55	39.835	40.98	39.88	39.31
TEST #022	0.518	0.411	45.655	45.555	41.265	44.73	42.21	40.7	44.48	42.21	39.3
TEST #023	0.585	0.422	45.775	46.92	48.51	48.095	44.84	44.945	47.195	47.44	44.665
TEST #024	0.656	0.437	50.865	53.43	49.2	50.48	52.205	48.88	48.315	46.42	46.52
TEST #025	0.665	0.120	55.36	55.67	56.445	56.38	54.11	56.995	51.425	52.31	47.595
TEST #026	0.588	0.117	53.815	52.31	51.48	51.165	51.56	49.945	47.22	48.13	45.18
TEST #027	0.499	0.117	48.175	48.26	47.775	45.865	46.72	45.325	45.765	44.15	40.97
TEST #028	0.348	0.119	39.655	40.265	38.715	38.455	35.635	36.235	37.52	35.17	33.21
TEST #029	0.182	0.116	25.24	29.58	27.585	27.565	27	28.07	25.825	25.455	26.085
TEST #030	0.123	0.117	21.425	23.56	22.285	21.005	23.545	21.415	20.875	21.545	19.74
TEST #031	0.088	0.117	19.505	19.005	20.565	19.215	19.135	18.375	17.945	18.775	16.13
TEST #032	0.058	0.134	14.275	14.89	13.905	14.975	14.065	14.475	13.98	15.055	13.95
TEST #033	0.030	0.131	8.455	7.995	7.995	8.61	8.585	8.405	7.645	7.825	8.36
TEST #034	0.028	0.534	2.715	2.375	2.505	2.685	2.88	2.675	2.625	2.79	2.785
TEST #035	0.065	0.533	7.21	7.355	6.97	7.195	7.5	7.78	7.47	7.36	7.03
TEST #036	0.112	0.523	14.52	13.575	14.9	14.485	14.46	14.48	14.4	14.11	13.695
TEST #037	0.140	0.517	16.685	18.84	17.77	17.405	17.22	17.505	16.675	17.035	16.905
TEST #038	0.239	0.531	27.805	26.715	25.47	26.235	26.645	26.365	26.45	25.285	23.635
TEST #039	0.426	0.531	39.31	37.5	40.875	38.305	39.325	37.415	35.23	36.025	34.815
TEST #040	0.556	0.528	44.635	44.53	44.76	45.235	45.135	44.24	42.98	41.71	39.91
TEST #041	0.674	0.528	50.98	49.905	50.795	49.26	48.315	49.43	49.865	48.22	46.73
TEST #042	0.662	0.388	54.45	52.86	55.035	53.81	53.405	50.72	51.025	46.795	48.305
TEST #043	0.564	0.397	48.23	47.19	47.14	48.045	44.34	43.7	44.54	45.385	44.795
TEST #044	0.424	0.397	41.24	42.295	39.415	40.6	41.545	38.585	36.395	37.57	34.865
TEST #045	0.245	0.386	32.455	29.42	30.055	29.08	28.13	27.12	26.13	25.015	24.39
TEST #046	0.132	0.390	19.22	20.045	18.605	20.055	19.52	19.45	17.965	19.255	19.005
TEST #047	0.115	0.386	16.655	17.11	17.485	16.345	16.485	16.235	17.36	16.61	15.84
TEST #048	0.070	0.382	11.92	12.06	11.82	11.73	12.055	11.59	10.76	11.915	11.325
TEST #049	0.027	0.380	3.935	4.135	3.86	3.935	3.955	3.57	3.645	3.435	3.54
TEST #050	0.032	0.745	2.38	2.545	2.245	2.55	2.4	2.455	2.275	2.52	2.35
TEST #051	0.060	0.755	5.27	5.45	5.435	5.325	5.07	5.3	5.215	4.88	5.22
TEST #052	0.110	0.755	9.545	10.245	10.05	9.67	9.355	9.905	9.635	9.805	9.64
TEST #053	0.134	0.750	13.08	12.605	12.545	12.96	12.98	13.02	13.165	12.71	11.785
TEST #054	0.365	0.752	31.185	32.63	32.595	33.515	32.95	31.86	29.915	30.845	31.12
TEST #055	0.600	0.745	44.645	43.43	45.345	44.75	43.7	40.84	44.02	40.38	39.615
TEST #056	0.671	0.217	55.77	56.95	56.11	58.1	54.305	53.55	52.14	52.56	47.93
TEST #057	0.509	0.212	44.92	47.87	44.63	45.215	46.26	43.57	43.19	45.065	38.875
TEST #058	0.244	0.211	31.745	33.055	32.72	29.77	31.655	31.29	31.435	27.865	29.635
TEST #059	0.369	0.032	38.875	38.29	39.43	42.05	41.72	43.615	37.87	38.59	39.16
TEST #060	0.244	0.006	36.485	34.445	35.55	37.14	35.09	32.37	31.565	32.35	29.44
TEST #061	0.131	0.210	23.515	22.285	23.065	20	22.74	22.045	19.595	21.445	17.88
TEST #062	0.138	0.000	26.025	26.48	25.48	24.07	24.6	25.06	22.245	24.615	24.155
TEST #063	0.123	0.000	26.3	25.34	27.195	25.225	25.815	24.955	22.12	21.95	19.145
TEST #064	0.096	0.000	22.265	22.055	21.395	19.24	19.405	22.08	23.085	21.1	20.68
TEST #065	0.075	0.000	20.54	18.315	19.78	19.26	18.41	17.725	19.2	16.135	17.67
TEST #066	0.033	0.000	13.055	13.69	12.26	13.72	12.865	13.275	12.225	12.17	11.93
TEST #067	0.495	0.000	50.3	51.95	48.12	47.243	46.335	44.285	47.077	42.94	42.725
TEST #068	0.663	0.000	57.97	56.275	57.455	54.705	54.56	54.09	51.13	51.47	49.01
TEST #069	0.788	0.000	62.075	62.975	62.960	63.505	61.580	59.800	59.050	58.360	58.160

TABLE 2 - LOCAL VOID FRACTIONS IN 20-cm DIAMETER PIPE

	LOCAL	VOID	FRACTION	AT	RELATIVE	LOCATION	r/R					
TEST	0.450	0.500	0.550	0.600	0.650	0.700	0.750	0.800	0.850	0.900	0.950	0.980
-	[%]	[%]	[%]	[%]	[%]	[%]	[%]	[%]	[%]	[%]	[%]	[%]
TEST #001	6.715	6.04	6.115	6.575	5.815	6.12	5.87	4.815	5.41	5.155	3.825	0.92
TEST #002	7.57	7.335	6.825	6.435	7.505	6.535	6.82	5.85	5.755	5.265	5.13	0.225
TEST #003	9.52	9.755	8.72	9.18	9.455	8.625	7.925	7.445	7.365	6.31	6.525	0.63
TEST #004	9.44	9.18	9.2	8.965	8.925	8.1	7.555	7.65	7.01	7.265	5.67	0.97
TEST #005	11.475	10.9	10.645	11.39	10.215	10.34	10.055	9.67	8.505	8.41	7.47	0.695
TEST #006	12.54	13.035	12.015	12.7	11.48	11.97	11.235	10.595	10.355	8.9	8.615	1.375
TEST #007	14.715	14.825	13.985	14.81	13.52	13.36	13.195	11.8	11.55	8.75	8.48	1.23
TEST #008	15.895	16.14	16.205	13.955	15.225	13.905	13.88	13.9	12.785	10.765	8.85	1.725
TEST #009	15.325	15.4	15.445	14.365	14.585	13.51	12.965	12.135	10.845	10.69	7.955	1.355
TEST #010	17.82	15.52	15.96	16.56	15.45	16.36	14.08	13.555	12.205	11.01	8.25	2.18
TEST #011	17.7	17.27	16.725	17.415	16.465	17.09	15.445	14.085	12.685	12.01	9.31	1.975
TEST #012	19.355	18.42	17.785	18.475	16.08	15.4	13.695	14.77	12.9	10.935	7.87	3.01
TEST #013	19.53	18.365	18.395	17.855	16.135	16.085	15.815	13.93	12.96	10.97	9.46	3.085
TEST #014	20.775	20.005	18.89	17.575	18.1	16.845	14.23	13.185	12.245	11.565	7.52	4.415
TEST #015	19.575	20.865	19.655	19.35	18.085	15.93	15.315	13.23	12.015	10.55	7.885	4.225
TEST #016	23.42	19.97	21.33	17.56	20.025	17.49	14.35	14.485	12.45	10.24	7.28	2.98
TEST #017	27.73	26.805	24.905	24.1	23.535	21.7	19.88	17.55	15.305	11.97	8.06	2.04
TEST #018	32.245	31.275	28.31	28.07	26.575	22.885	21.79	19.085	15.91	13.615	7.465	2.47
TEST #018A	30.95	30.67	28.63	25.51	25.72	24.285	20.975	16.91	16.51	12.875	9.705	2.175
TEST #019	32.695	31.715	31.625	27.655	29.445	26.23	21.88	21.905	18.645	15.22	8.73	3.33
TEST #020	24.36	23.005	21.98	19.775	19.61	18.9	19.27	14.93	12.31	10.575	6.735	1.835
TEST #021	37.795	36.81	35.945	31.565	29.125	27.87	25.05	24.99	19.41	17.335	9.845	2.02
TEST #022	37.955	39.01	36.99	31.43	30.455	27.03	26.045	23.935	20.445	18.05	10.515	1.7
TEST #023	39.12	39.465	37.485	36.225	34.215	32.245	27.54	25.2	21.825	19.115	11.52	1.76
TEST #024	45.605	43.595	39.35	39.485	37.56	34.165	30.375	26.1	23.82	18.945	12.485	2.645
TEST #025	46.745	43.615	42.99	40.99	37.2	34.43	29.9	28.58	22.525	17.88	9.405	2.17
TEST #026	44.375	43.54	39.325	36.28	34.885	31.055	31.055	24.79	21.525	16.585	10.64	2.095
TEST #027	39.51	41.755	35.585	31.545	33.115	26.99	25.52	24.42	20.615	14.585	8.31	1.84
TEST #028	32.07	31.625	31.46	29.515	26.72	26.425	22.345	19.19	18.795	13.99	7.28	1.75
TEST #029	24.735	23.765	20.355	19.555	20.34	16.62	15.02	13.555	12.12	8.155	5.99	1.535
TEST #030	18.855	17.485	18.04	17.725	15.795	14.14	13.135	11.565	9.72	7.7	6	1.475
TEST #031	17.78	15.41	15.885	15.415	14.845	12.65	11.425	10.91	10.43	7.29	6.87	1.44
TEST #032	13.975	13.45	12.515	12.25	12.405	11.91	10.63	10.29	10.8	8.87	6.115	0.855
TEST #033	8.69	7.925	8.235	7.255	7.23	7.495	7.045	6.27	6.21	5.325	4.8	0.9
TEST #034	2.76	2.665	2.95	2.68	2.985	2.74	3.305	2.94	3.065	3.495	4.44	3.23
TEST #035	7.075	7.275	7.375	7.47	7.385	7.36	7.515	7.855	7.33	7.435	7.725	3.84
TEST #036	13.73	12.995	13.685	12.42	12.905	12.78	12.56	12.315	11.295	10.965	10.6	3.92
TEST #037	17.865	17.405	17.005	16.795	15.91	15.59	14.845	14.345	13.37	12.64	9.295	3.07
TEST #038	21.79	23.105	22.96	20.92	20.385	19.095	17.865	17.015	13.21	12.145	9.455	3.245
TEST #039	35	33.335	30.62	29.285	26.735	25.02	23.995	22.78	19.12	15.385	10.755	4.065
TEST #040	40.245	39.305	35.745	34.655	29.365	31.03	27.735	26.39	20.955	16.905	10.59	3.715
TEST #041	43.275	41.085	40.195	36.95	36.525	34.4	32.62	27.795	23.59	17.485	12.225	4.715
TEST #042	44.345	45.18	40.615	40.81	33.795	35.385	34.095	29.56	26	18.095	12.565	4.215
TEST #043	40.585	38.13	38.835	37.25	33.205	29.305	30.24	24.15	20.605	16.905	10.575	2.865
TEST #044	35.65	32.42	31.3	28.32	29.38	26.31	25.215	21.045	18.33	14.845	9.885	3.185
TEST #045	25.085	22.885	21.55	21.595	20.77	20.095	17.305	14.54	13.085	10.52	7.18	2
TEST #046	18.14	17.6	16.53	17.405	16.73	15.96	14.22	14.615	13.675	10.595	8.51	1.985
TEST #047	16.78	15.655	15.57	15.265	15.19	14.61	13.54	13.725	12.28	11.3	8.46	2.395
TEST #048	11.84	11.65	10.93	10.24	11.13	10.365	9.55	9.74	10.32	8.475	6.875	2.25
TEST #049	3.43	3.455	3.225	3.325	3.345	3.4	3.515	3.42	3.59	3.315	3.54	1.645
TEST #050	2.465	2.335	2.365	2.38	2.49	2.57	2.78	2.405	2.705	2.86	4.215	4.825
TEST #051	4.955	5.155	4.78	5.015	4.68	4.745	5.14	5.355	5.09	5.58	5.585	6.355
TEST #052	9.66	9.07	9.245	9.4	9.645	9.585	9.43	9.43	9.155	9.28	9.6	8.11
TEST #053	12.46	12.5	12.62	12.885	12.275	11.805	11.415	11.665	10.87	10.745	9.77	4.56
TEST #054	29.67	28.575	29.325	26.855	26.68	25.575	24.87	23.37	21.205	18.49	14.495	4.205
TEST #055	39.45	38.76	35.435	33.555	32.715	31.205	28.605	24.795	21.875	17.93	11.88	3.44
TEST #056	45.23	46.49	42.54	38.98	39.645	34.45	32.775	27.415	24.845	18.235	12.075	2.215
TEST #057	39.71	39.375	37.865	35.725	32.56	29.88	25.82	24.31	22.81	15.515	8.825	1.86
TEST #058	26.15	25.48	23.58	24.265	21.35	20.21	17.975	12.97	12.235	8.475	7.39	1.66
TEST #059	35.57	33.485	34.485	27.585	27.165	25.895	22.675	21.41	19.655	12.355	8.295	2.015
TEST #060	28.045	29.725	29.42	25.965	22.54	22.75	17.82	16.31	15.5	11.64	7.095	1.52
TEST #061	19.46	18.805	17.98	16.355	16.39	13.985	13.13	11.8	10.47	8.065	6.45	1.71
TEST #062	21.21	22.355	20.483	20.88	17.083	15.345	14.207	13.64	10.85	7.39	5.75	1.04
TEST #063	21.48	20.677	19.235	18.7	17.53	15.655	13.213	11.793	9.72	8.42	4.88	0.96
TEST #064	18.81	20.395	16.665	16.08	16.71	12.88	11.445	10.505	9.905	7.745	5.87	0.9
TEST #065	17.105	16.215	15.745	13.815	14.315	12.605	9.635	9.54	8.97	7.815	5.74	0.825
TEST #066	12.13	12.695	12.01	11.815	11.29	9.66	8.79	8.895	7.45	5.76	5.44	0.505
TEST #067	38.905	37.955	37.56	37.81	33.07	31.615	28.007	24.615	19.06	15.04	10.86	1.585
TEST #068	49.67	48.705	43.485	40.745	38.48	39.17	34.845	28.71	23.375	17.38	11.235	2.37
TEST #069	54.653	51.635	46.290	45.453	43.470	42.220	37.790	32.683	27.243	18.400	10.795	1.095

TABLE 3 - AVERAGE VOID FRACTIONS IN 20-cm DIAMETER PIPE

TEST NUMBER	SUPERFICIAL GAS VELOCITY	SUPERFICIAL LIQUID VELOCITY	OPTICAL PROBE VOID FRACTION	TEST SECTION PRESSURE DROP	PRESSURE DROP VOID FRACTION	FLOW REGIME
-	[m/s]	[m/s]	[%]	[mH2O]	[%]	-
TEST #001	0.021	0.143	6.475	0.056	5.656	BUBBLY
TEST #002	0.030	0.164	7.331	0.069	6.970	BUBBLY
TEST #003	0.041	0.193	9.527	0.089	8.992	BUBBLY
TEST #004	0.043	0.196	9.476	0.091	9.194	BUBBLY
TEST #005	0.055	0.219	11.400	0.109	11.014	BUBBLY
TEST #006	0.069	0.239	12.785	0.127	12.821	BUBBLY
TEST #007	0.081	0.258	14.589	0.143	14.437	BUBBLY
TEST #008	0.096	0.269	16.452	0.157	15.867	BUBBLY
TEST #009	0.087	0.259	15.287	0.149	15.057	BUBBLY
TEST #010	0.110	0.281	17.758	0.166	16.796	BUBBLY
TEST #011	0.118	0.288	18.381	0.174	17.570	BUBBLY
TEST #012	0.129	0.295	19.130	0.178	18.004	BUBBLY
TEST #013	0.135	0.298	19.580	0.181	18.317	BUBBLY UNSTABLE
TEST #014	0.152	0.304	20.886	0.182	18.422	BUBBLY UNSTABLE
TEST #015	0.164	0.309	21.947	0.184	18.608	BUBBLY UNSTABLE
TEST #016	0.183	0.317	22.731	0.190	19.218	BUBBLY-CHURN
TEST #017	0.290	0.354	28.292	0.233	23.625	CHURN-BUBBLY
TEST #018	0.367	0.376	33.026	0.262	26.571	CHURN
TEST #018A	0.370	0.378	32.465	0.260	26.371	CHURN
TEST #019	0.425	0.390	35.260	0.284	28.777	CHURN
TEST #020	0.227	0.332	25.450	0.208	21.084	BUBBLY-CHURN
TEST #021	0.467	0.401	37.801	0.294	29.827	CHURN
TEST #022	0.518	0.411	39.283	0.311	31.555	CHURN
TEST #023	0.585	0.422	42.307	0.329	33.353	CHURN
TEST #024	0.656	0.437	45.578	0.356	36.093	CHURN
TEST #025	0.665	0.120	48.833	0.432	43.649	CHURN
TEST #026	0.588	0.117	45.458	0.404	40.819	CHURN
TEST #027	0.499	0.117	41.536	0.366	36.979	CHURN
TEST #028	0.348	0.119	34.106	0.305	30.847	CHURN
TEST #029	0.182	0.116	24.440	0.219	22.148	BUBBLY-SLUG
TEST #030	0.123	0.117	19.789	0.175	17.699	BUBBLY-SLUG
TEST #031	0.088	0.117	17.340	0.157	15.879	BUBBLY UNSTABLE
TEST #032	0.058	0.134	13.683	0.139	14.061	BUBBLY
TEST #033	0.030	0.131	7.991	0.073	7.390	BUBBLY
TEST #034	0.028	0.534	2.734	0.028	2.961	BUBBLY
TEST #035	0.065	0.533	7.328	0.078	8.016	BUBBLY
TEST #036	0.112	0.523	13.819	0.128	13.069	BUBBLY
TEST #037	0.140	0.517	17.002	0.154	15.697	BUBBLY
TEST #038	0.239	0.531	24.158	0.199	20.245	BUBBLY UNSTABLE
TEST #039	0.426	0.531	34.657	0.266	27.035	CHURN
TEST #040	0.556	0.528	40.220	0.318	32.299	CHURN
TEST #041	0.674	0.528	45.039	0.347	35.243	CHURN
TEST #042	0.662	0.388	47.300	0.376	38.045	CHURN
TEST #043	0.564	0.397	41.996	0.328	33.202	CHURN
TEST #044	0.424	0.397	35.802	0.282	28.579	CHURN
TEST #045	0.245	0.386	25.615	0.205	20.784	BUBBLY-CHURN
TEST #046	0.132	0.390	18.285	0.164	16.635	BUBBLY
TEST #047	0.115	0.386	16.136	0.151	15.335	BUBBLY
TEST #048	0.070	0.382	11.389	0.107	10.885	BUBBLY
TEST #049	0.027	0.380	3.657	0.039	4.012	BUBBLY
TEST #050	0.032	0.745	2.436	0.027	2.972	BUBBLY
TEST #051	0.060	0.755	5.158	0.053	5.608	BUBBLY
TEST #052	0.110	0.755	9.641	0.099	10.251	BUBBLY
TEST #053	0.134	0.750	12.579	0.126	12.977	BUBBLY
TEST #054	0.365	0.752	30.177	0.255	26.099	CHURN-BUBBLY
TEST #055	0.600	0.745	39.772	0.298	30.433	CHURN
TEST #056	0.671	0.217	49.073	0.410	41.428	CHURN
TEST #057	0.509	0.212	40.833	0.363	36.749	CHURN
TEST #058	0.244	0.211	27.916	0.241	24.425	CHURN-BUBBLY
TEST #059	0.369	0.032	36.191	0.349	35.342	CHURN
TEST #060	0.244	0.006	30.774	0.292	29.565	CHURN-SLUG
TEST #061	0.131	0.210	19.702	0.175	17.739	BUBBLY UNSTABLE
TEST #062	0.138	0.000	22.604	0.215	21.768	BUBBLY-SLUG
TEST #063	0.123	0.000	22.082	0.200	20.250	BUBBLY-SLUG
TEST #064	0.096	0.000	19.386	0.180	18.206	BUBBLY UNSTABLE
TEST #065	0.075	0.000	17.032	0.159	16.099	BUBBLY UNSTABLE
TEST #066	0.033	0.000	12.202	0.134	13.581	BUBBLY
TEST #067	0.495	0.000	42.495	0.408	41.266	CHURN
TEST #068	0.663	0.000	49.681	0.464	46.835	CHURN
TEST #069	0.788	0.000	55.419	0.512	51.784	CHURN